Identification of novel components that connect cellulose synthases to the cytoskeleton

Dipl. Biochem. Martin Bringmann

February 28, 2012

Kumulative Dissertation zur Erlangung des akademischen Grades **Doctor rerum naturalium (Dr. rer. nat.)** im Fach Biologie

eingereicht an der
Mathematisch- Naturwissenschaftlichen Fakultät der
Universität Potsdam

Published online at the
Institutional Repository of the University of Potsdam:
URL http://opus.kobv.de/ubp/volltexte/2012/6147/
URN urn:nbn:de:kobv:517-opus-61478
http://nbn-resolving.de/urn:nbn:de:kobv:517-opus-61478

This thesis was prepared at the

Max Planck Institute of Molecular Plant Physiology
Am Mühlenberg 1
14476 Potsdam - Golm

in the independent research group "Plant Cell Walls" of Dr. Staffan Persson between September 2008 and February 2012.

Declaration

I hereby declare that the work presented in this thesis has been carried out by myself and does not incorporate any material previously submitted for another degree in any university. To the best of my knowledge, it does not contain any material previously written by another person, except where reference is made in the text.

Erklärung

Ich erkläre hiermit, die für diese Dissertationsschrift angefertigten Arbeiten selbst ausgeführt zu haben. Die Dissertationsschrift beinhaltet kein Material, das für andere Abschlüsse an dieser oder einer anderen Universität eingereicht wurde. Ich habe für diese Dissertationsschrift keine anderen als die angegebenen Hilfsmittel und Quellen verwendet.

Potsdam, February 28, 2012

Martin Bringmann

Author's Contribution

Martin Bringmann significantly contributed to design and execution of experiments, data analysis and writing of all the papers presented in section 2.

Hiermit wird bestätigt, dass der Autor dieser Dissertation, Martin Bringmann, an allen in Kapitel 2 aufgeführten Publikationen maßgeblich beteiligt war. Sein Beitrag umfasste die Entwicklung und Durchführung von Experimenten, Datenanalyse sowie das schriftliche Verfassen von Teilen der Publikationen.

Dr. Staffan Persson (PI)

Contents

Abstract **1**

Zusammenfassung **2**

1 Introduction **3**
1.1 The Plant Cell Wall . . . 3
1.1.1 Composition of Primary Cell Walls . . . 3
1.2 Cellulose is synthesized by cellulose synthase complexes (CSCs) . . 5
1.2.1 Cellulose is synthesized from uridine diphosphate (UDP)-glucose precursors . . . 5
1.2.2 CESAs are shuttled from the Golgi to the plasma membrane 6
1.2.3 The CESA family . . . 8
1.3 The plant cytoskeleton . . . 9
1.3.1 The actin cytoskeleton . . . 9
1.3.2 Microtubules . . . 10
1.3.2.1 Structure and dynamics . . . 11
1.3.2.2 Microtubule associated proteins (MAPs) . . . 13
1.4 Advances in microscopy techniques reveal microtubule-defined tracking of CESAs . . . 15
1.5 Co-expression and forward genetic screens as tools to identify genes involved in cellulose synthesis . . . 18
1.5.1 Prediction of gene function through co-expression analysis . 18
1.5.2 Identification of new genes involved in cellulose production through genetic screens . . . 19
1.6 Aim of this work . . . 19

2 Original articles published during PhD **20**
Transcriptional Wiring of Cell Wall-Related Genes in *Arabidopsis* . . . 21
Identification of a cellulose synthase-associated protein required for cellulose biosynthesis . . . 31
POM-POM2/CELLULOSE SYNTHASE INTERACTING1 Is Essential for the Functional Association of Cellulose Synthase and Microtubules in *Arabidopsis* . . . 43

3 Discussion **70**
3.1 Fifty years of alignment hypothesis – new players reveal mechanism 70
3.2 Identification of candidate genes that influence cellulose synthesis . 71
3.2.1 Co-expression analysis as a tool for candidate gene prediction 71

3.2.2 Yeast-two-hybrid screens revealed POM2/CSI1 as interaction partner of the primary CESAs 72
3.2.3 Genetic screens identified *pom2/csi1* as root expansion defective mutant 72
3.3 POM2/CSI1 possesses a molecular structure that renders it an integrative structural protein 73
3.4 Molecular characterization of POM2/CSI1 75
3.4.1 POM2/CSI1's role in CESA delivery to the plasma membrane 75
3.4.2 POM2/CSI1 is required for alignment of microtubules and CESAs and enhances CESA activity 75
3.4.2.1 POM2/CSI1 is co-localized with the CESAs in the cell cortex but not at the Golgi 76
3.4.2.2 POM2 bridges microtubules and CESAs 77
3.4.2.3 POM2/CSI1 might be involved in activation of the CESAs 78
3.4.3 *pom2/csi1* mutants have twisted organs 80
3.5 Contribution of this thesis to society and global development . . . 81
3.6 Conclusion and future research 82

Acknowledgements **84**

List of Figures **85**

Abbreviations **86**

References **88**

Abstract

Cellulose is the most abundant biopolymer on earth and the main load-bearing structure in plant cell walls. Cellulose microfibrils are laid down in a tight parallel array, surrounding plant cells like a corset. Orientation of microfibrils determines the direction of growth by directing turgor pressure to points of expansion (Somerville *et al.*, 2004). Hence, cellulose deficient mutants usually show cell and organ swelling due to disturbed anisotropic cell expansion (reviewed in Endler and Persson, 2011).

How do cellulose microfibrils gain their parallel orientation? First experiments in the 1960s suggested, that cortical microtubules aid the cellulose synthases on their way around the cell (Green, 1962; Ledbetter and Porter, 1963). This was proofed in 2006 through life cell imaging (Paredez *et al.*, 2006). However, how this guidance was facilitated, remained unknown.

Through a combinatory approach, including forward and reverse genetics together with advanced co-expression analysis, we identified *pom2* as a cellulose deficient mutant. Map- based cloning revealed that the gene locus of *POM2* corresponded to *CELLULOSE SYNTHASE INTERACTING 1 (CSI1)*. Intriguingly, we previously found the CSI1 protein to interact with the putative cytosolic part of the primary cellulose synthases in a yeast-two-hybrid screen (Gu *et al.*, 2010).

Exhaustive cell biological analysis of the POM2/CSI1 protein allowed to determine its cellular function. Using spinning disc confocal microscopy, we could show that in the absence of POM2/CSI1, cellulose synthase complexes lose their microtubule-dependent trajectories in the plasma membrane. The loss of POM2/CSI1, however does not influence microtubule- dependent delivery of cellulose synthases (Bringmann *et al.*, 2012). Consequently, POM2/CSI1 acts as a bridging protein between active cellulose synthases and cortical microtubules.

This thesis summarizes three publications of the author, regarding the identification of proteins that connect cellulose synthases to the cytoskeleton. This involves the development of bioinformatics tools allowing candidate gene prediction through co-expression studies (Mutwil *et al.*, 2009), identification of candidate genes through interaction studies (Gu *et al.*, 2010), and determination of the cellular function of the candidate gene (Bringmann *et al.*, 2012).

Identifikation neuer Proteine als Bindeglieder zwischen den Zellulosesynthasen und dem Zytoskelett

Martin Bringmann, Max Planck Institut für molekulare Pflanzenphysiologie

Zellulose ist das abundanteste Biopolymer der Erde und verleiht pflanzlichen Zellwänden ihre enorme Tragkraft. Mit der Reißfestigkeit von Stahl umwickeln Zellulosefibrillen pflanzliche Zellwände wie ein Korsett. Die Orientierung der Zellulosefibrillen bestimmt zugleich die Wachstumsrichtung, indem sie den Zellinnendruck (Turgor) in die entsprechende Ausdehnungsrichtung dirigiert (Somerville *et al.*, 2004). Folglich zeigen Mutanten mit gestörter Zellulosesynthese oft geschwollene Organe und Zellen, die sich nicht mehr gerichtet ausdehnen können (zusammengefasst von Endler und Persson, 2011).

Wie aber erhalten die Zellulosefibrillen ihre parallele Orientierung? Erste Experimente aus den 1960ern führten zur Vermutung, kortikale Mikrotubuli leiten die Zellulosesynthasen auf ringförmigen Bahnen um die Zellen herum (Green, 1962; Ledbetter and Porter, 1963). Diese Theorie wurde 2006 mit Hilfe moderner mikroskopischer Methoden bestätigt (Paredez *et al.*, 2006). Wie jedoch dieser Leitmechanismus funktioniert, blieb bisher unentdeckt.

Durch die Kombination verschiedener genetischer und bioinformatischer Methoden, konnten wir *pom2* als Zellulose defiziente Mutante identifizieren. Die Ermittlung des Genlocus durch Map-based cloning zeigte, dass es sich bei *POM2* um *CSI1* handelt, ein Gen, dessen korrespondierendes Protein, wie vorher von uns gezeigt, mit dem zytosolischen Teil der primären Zellulosesynthasen interagiert (Gu *et al.*, 2010).

Durch ausführliche zellbiologische Charakterisierung von POM2/CSI1 konnten wir seine zelluläre Funktion entschlüsseln. Mit Hilfe konfokaler Spinning-Disc-Mikroskopie konnten wir zeigen, dass in Abwesenheit von POM2/CSI1, Zellulosesynthasen von den Mikrotubuli- Bahnen abweichen. Der ebenfalls von den Mikrotubuli abhängige Transport der Zellulosesynthasen zur Zellmembran hingegen, war nicht beeinflusst (Bringmann *et al.*, 2012). Demzufolge ist POM2/CSI1 das gesuchte Bindeglied zwischen aktiven Zellulosesynthasen und Mikrotubuli.

In dieser Dissertationsschrift werden drei Publikationen des Autors zusammengefasst, die während der Arbeit an der Dissertiation entstanden sind. Sie beinhalten die Entwicklung bioinformatischer Methoden zur Ko-Expressionsanalyse, um Kandidatengene zu ermitteln (Mutwil *et al.*, 2009), die Identifikaton des Kandidatengens *POM2/CSI1* in einer Interaktionsstudie (Gu *et al.*, 2010), sowie die Bestimmung der zellulären Funktion des korrespondierenden Proteins POM2/CSI1 (Bringmann *et al.*, 2012).

1 Introduction

1.1 The Plant Cell Wall

The plant cell wall is a key component that distinguishes plant from animal cells. Cell walls are the extracellular matrix of plant cells, and as such they fulfil a range of functions, including maintenance of mechanical stability of the plant body, defence against biotic and abiotic stresses, support of cell shape and growth, as well as providing for cell-cell communication and apoplastic water and nutrient transport (Carpita and McCann, 2000; Sampathkumar *et al.*, 2011b).

Due to its multiple functions, the plant cell wall is required to adapt its physical features relatively rapidly. For example, during cell elongation of cylindrical hypocotyl cells, cell walls are required to be strong in lateral areas but flexible in apical areas to facilitate directed cell expansion by directing turgor pressure (Somerville *et al.*, 2004). Changes in physical parameters of cell walls can be achieved by alterations in wall composition as well as in orientation of cellulose microfibrils. To understand how essential processes, like the attainment of cell shape, long distance water transport or directed cell and organ growth, are put into effect, we need to understand the underlying mechanisms which determine the unique features of plant cell walls.

1.1.1 Composition of Primary Cell Walls

In general, there are two classes of cell walls in plants: primary and secondary cell walls. The new primary cell wall is formed during cell division in the cell plate. It surrounds newly formed cells and increases its area rapidly as the cells expand. At the interface between two neighboring cells, there is a middle lamella, which constitutes part of the primary cell wall (Matar and Catesson, 1988). Secondary cell walls are synthesized inside of the primary wall during cell differentiation. The secondary walls supply structural support for diverse cell types such as xylem vessels and differ from primary walls in their composition. This thesis focuses on primary cell walls, and the composition and features of these walls are therefore introduced in detail.

Figure 1 shows a schematic view of a typical primary cell wall in dicot species. The main load-bearing structures are cellulose (unbranched poly β-1,4-D-glucan) chains which are believed to be synthesized by hexameric cellulose synthase complexes (CSC) at the plasma membrane. Presumably 36 glucan chains are laid down in a twisting, ribbon-like cable to form a microfibril. Cellulose microfibrils are strong, insoluble structures that define wall features by their spacial orientation and crystallinity.

Cellulose microfibrils are interconnected by other polysaccharide chains, including the Hemicelluloses and perhaps also pectins. In contrast to cellulose, hemicelluloses are branched polymers. All hemicelluloses have a cellulose-like backbone, coupling different mono-saccharides, such as glucose, xylose, and mannose, by β-(1,4)-links (Hayashi, 1989). In addition, poales and a few other plant groups also hold β-(1,3-1,4)-mixed linked glucans, which are considered being hemicelluloses (Scheller and Ulvskov, 2010; Endler and Persson, 2011).

The hydrogen bonded network of cellulose microfibrils and hemicelluloses is embedded in a gel- like pectic matrix. Pectins are polymers with backbone structures enriched in galacturonic acids, or rhamnose interspersed with galacturonic acids, eventually carrying complex side chains (Mohnen, 2008).

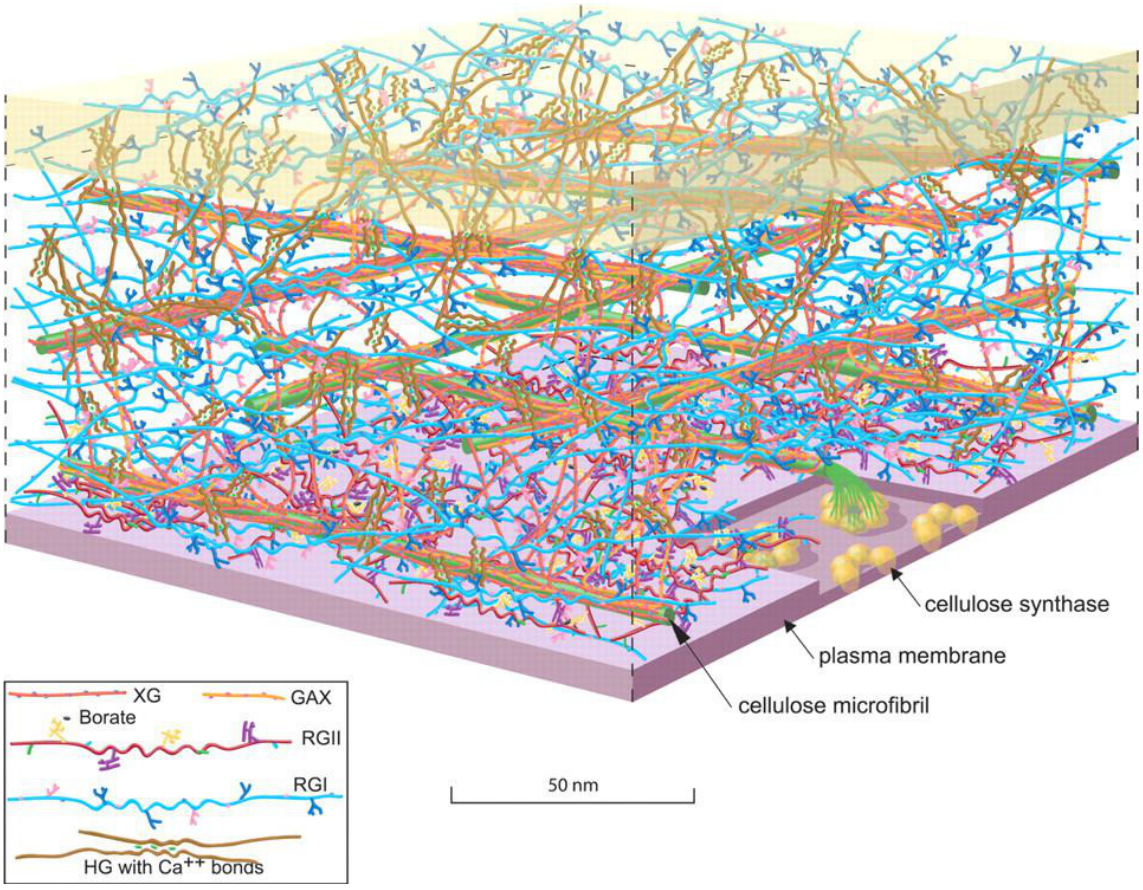

Figure 1: Scale model of a primary cell wall in an Arabidopsis leaf cell. Cellulose is produced by hexameric cellulose synthase complexes (CSCs) at the plasma membrane. Although the orientation and stoichiometric relationships are unknown it is hypothesized that the catalytic domain is cytoplasmic and that the glucan chains are extruded to the intercellular space where they form microfibrils. These microfibrils are typically cross-linked by hemicelluloses, like xyloglucan (XG) and glucoronoarabinoxylan (GAX), or by pectic polymers. The thereby formed saccharide network is embedded in an aqueous pectic matrix, composed by Rhamnogalacturonan I and II (RG I and RG II) and Homogalacturonan (HG). Image taken from Somerville *et al.* (2004).

1.2 Cellulose is synthesized by cellulose synthase complexes (CSCs)

It has been proposed that a typical cellulose microfibril is formed by 36 glucan chains with a length of 8000 (primary walls) to 15000 (secondary walls) glucose subunits (Somerville, 2006). However, the number of glucan chains that constitute the microfibril is currently under debate. Recent reports indicate for example, that 24- chained cellulose microfibrils exist in spurce wood (Fernandes *et al.*, 2011).

Based on the estimates above, it has been suggested that an individual CSC is comprised by 36 Cellulose Synthase (CESA) proteins, each producing a β-1-4-D-glucan chain. The CESAs form a hexameric rosette which spans the plasma membrane (Kimura *et al.*, 1999, for comparison see Figure 2). The intermolecular interactions between the CESAs are presumably facilitated by zinc finger domains in the N terminus of the CESAs (Joshi and Mansfield, 2007).

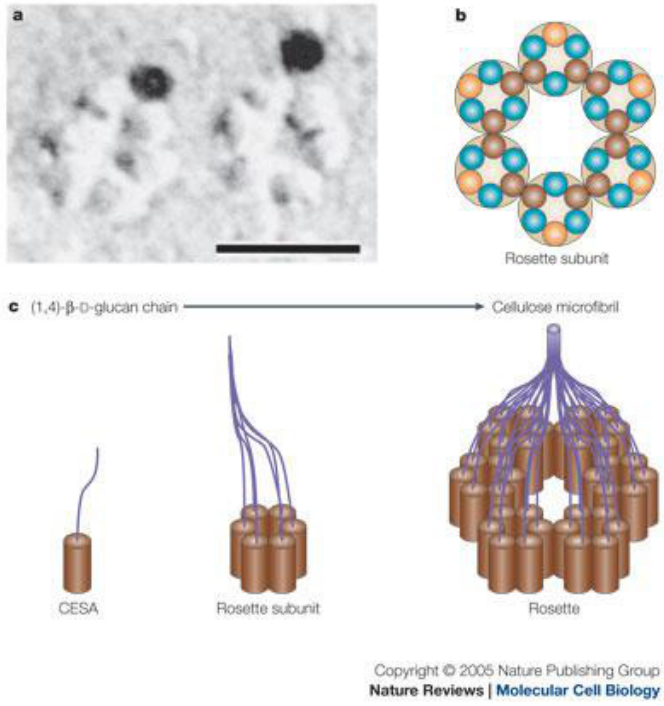

Figure 2: (a) Electron micrographs of immuno- gold- labelled CSCs that shows the hexameric structure of the rosette complex (Kimura *et al.*, 1999). The black circles represent gold nanoparticles that are attached to antibodies against CESA. Scale bar = 30 nm. **(b)** Model of a CSC. Three different CESA proteins (shown in orange, brown and green) might be organized into rosette subunits and then into a hexameric CSC (Doblin *et al.*, 2002). **(c)** Model of synthesis of a cellulose microfibril by a CSC. Each CESA protein can synthesize a single glucan chain. Image taken from (Cosgrove, 2005).

1.2.1 Cellulose is synthesized from uridine diphosphate (UDP)-glucose precursors

CSCs convert the precursor molecule UDP-glucose to macromolecular cellulose (Carpita and McCann, 2000). Recent studies showed, that detergent resistant membranes from tobacco cells hold the sufficient machinery to produce cellulose *in vitro* in the presence of 1mM UDP-glucose (Cifuentes *et al.*, 2010). UDP-glucose can be formed through two pathways. The first pathway is the cleavage of sucrose

by sucrose synthase (SUS, EC 2.4.1.13) to UDP-glucose and fructose. The second involves the active phosphorylation of glucose 1-phosphate by UDP-glucose pyrophosphorylase (UGPase, EC 2.7.7.9). Alternatively, the highly abundant hydrolyzing enzyme invertase (EC 3.2.1.26) can catalyse the cleavage of sucrose to glucose and fructose, which indirectly leads to the synthesis of UDP-glucose. This might, however, only have a regulatory effect on cellulose biosynthesis (Joshi and Mansfield, 2007). The precise mechanisms of precursor production and supply for cellulose biosynthesis are to date not clarified. However, up-regulation of SUS expression has been shown to result in increased cellulose synthesis in hybrid poplar (Coleman *et al.*, 2009). These results indicate a direct connection between sucrose supply, its breakdown, and cellulose deposition through the activity of SUS.

Still, the role of SUS in feeding starch and cellulose production with precursors is under debate. Barratt *et al.* (2009) reported, that the invertase pathway is favoured for the production of monosaccharide precursors, since quadruple mutants of *sus1/sus2/sus3/sus4*, that lacked SUS activity in any tissue except for the phloem exhibited wild-type-like growth as well as cellulose content and structure. In contrast to that, invertase double mutants *cinv1/cinv2* showed severe growth defects. This work, however, was questioned by Baroja-Fernandez *et al.* (2012), who showed, that under favourable pH conditions, SUS activity levels in leaves are 85% of wild-type in the above mentioned quadruple mutants. This in turn would be sufficient to support starch and cellulose production.

Consequently, a direct interaction between SUS and the CSC has been put forward. However, none of the SUS gene family members could be shown to be a direct or indirect interactor of the CSC, yet. Interestingly, membrane bound rosette CSCs from bean epicotyls showed cellulose production in presence of sucrose plus UDP after addition of a soluble SUS-like protein *in vitro* (Fujii *et al.*, 2010). These authors suggested a CSC model, where the actual catalytic unit for cellulose production incorporates and depends on SUS activity.

1.2.2 CESAs are shuttled from the Golgi to the plasma membrane

Being secreted proteins, the CESAs follow the secretory pathway via the endoplasmic reticulum (ER) and the Golgi apparatus before they are ultimately incorporated into the plasma membrane. CESAs are believed to be assembled into CSCs in the Golgi apparatus, where they potentially also are glycosylated (Lukowitz *et al.*, 2001; Gillmor *et al.*, 2002). After passing the trans-Golgi-network (TGN), CESAs are delivered to the plasma membrane (Geisler *et al.*, 2008). Consequently, treatments leading to reduced Golgi motility resulted in decrease of

CESA population at the plasma membrane. Gutierrez *et al.* (2009) could show that a disturbed actin cytoskeleton leads to stalled cytosplasmic steraming, and, hence, Golgi cisternae stalling. Furthermore, the double mutant *actin2 actin7*, affecting two of the three vegetative *ACTIN* isoforms, as well as treatment with the actin inhibitor Latrunculin B reduced Golgi movement. As a consequence, CESA population and cellulose production were significantly reduced compared to untreated wild type plants (Sampathkumar, 2010).

In addition to Golgi and, to some part, TGN, the CESAs may also be found associated with a currently unknown compartement. These have been termed Small CESA compartements (SmaCCs; Gutierrez *et al.*, 2009) or microtubule associated Cellulose Synthase compartements (MASCs; Crowell *et al.*, 2009). These compartements accumulate upon treatment with the cellulose synthesis inhibitor isoxaben or in response to osmotic stress. The smaCCs/MASCs associate with microtubules, and can release CESAs to the plasma membrane (Gutierrez *et al.*, 2009), indicating that they are of an exocytic nature. Still, the function of these SmaCCs/MASCs remains unclear.

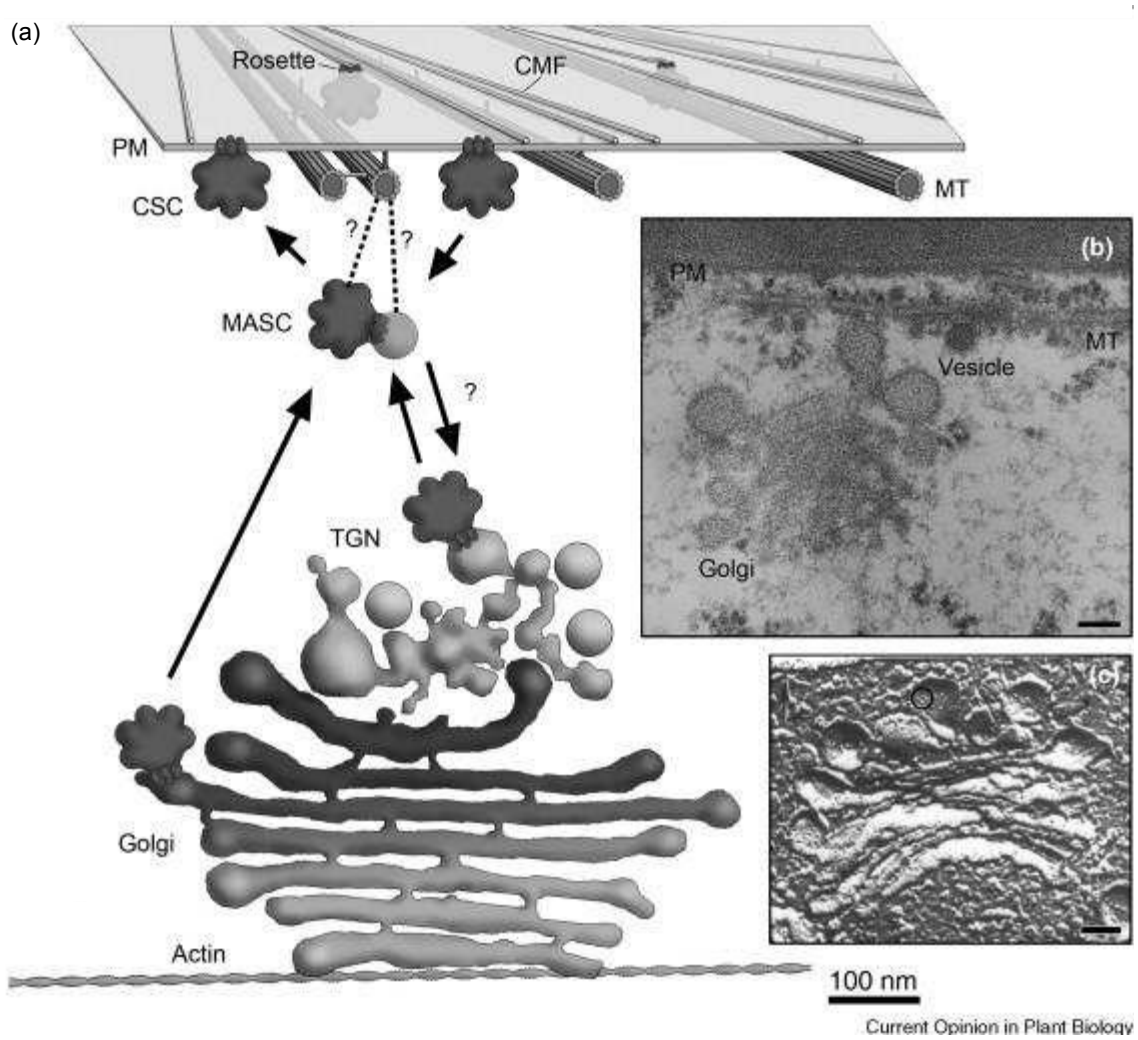

Figure 3: CESA trafficking pathways have been investigated by electron microscopy and live cell imaging. Preassembled rosettes can be detected in the ER and in the Golgi apparatus (circled in **(c)**). **(b)** Electron micrograph, that shows a Golgi body associated with a microtubule in a hypocotyl epidermis cell upon treatment with the cellulose synthesis inhibitor CGA6150315 (5 nM). **(a)** CSCs are internalized into (SmaCCs / MASCs), which are tethered to cortical microtubules via interactions with the CSC itself or with a component of SmaCC / MASC vesicles. SmaCC / MASC-like vesicles are also likely intermediates in the secretion of CSCs to the plasma membrane. Scale bars = 100 nm. Image modified from Crowell *et al.* (2010).

1.2.3 The CESA family

The *CESA* gene family was originally discovered due to sequence similarities to bacterial cellulose synthases (Pear *et al.*, 1996). It harbours ten members in *Arabidopsis* and between 9 (rice) and 18 (poplar) in all species of higher plants (Somerville, 2006; Richmond, 2000; Mutwil *et al.*, 2008a). In *Arabidopsis* at least three different CESA proteins are required for a functional CSC (Taylor *et al.*, 2000; Desprez *et al.*, 2007). Individual *CESA* genes can be involved in different aspects of cellulose synthesis. For example, in *Arabidopsis CESA 1,3* and *6* are involved in primary wall formation, whereas *CESA 4, 7* and *8* are required for the formation of secondary cell walls (Persson *et al.*, 2005; Mutwil *et al.*, 2008a). Muta-

tions in *CESA1* and *CESA3* lead to severely retarded growth phenotypes or male gametophythic letality (in full knock-outs), due to impaired cellulose production (Arioli *et al.*, 1998; Gillmor *et al.*, 2002; Beeckman *et al.*, 2002). Mutations in *CESA6*, however, merely induce deficiencies in anisotropic cell expansion (Fagard *et al.*, 2000), suggesting that the function of CESA6 can be partly replaced by redundant proteins. Indeed, three other CESAs, CESA2, 5 and 9, are very similar to CESA6. They are suggested to be capable of replacing CESA6 in the CSC (Persson *et al.*, 2007).

1.3 The plant cytoskeleton

As mentioned earlier, the plant cytoskeleton is a key component for cellulose synthesis in higher plants. Actin microfilaments/bundles and microtubules are responsible for transporting CESA-containing vesicles to the plasma membrane, and for the guidance of CESAs during cellulose synthesis, respectively. The third class of filaments, the intermediate filaments form the nuclear lamina in animals. Whether they exist in plants is to date not clearly shown (Fiserova and Goldberg, 2010).

1.3.1 The actin cytoskeleton

The term cytoskeleton implies a rigid and stable structure. However, the terms rigid and stable seem inadequate for the actin cytoskeleton. Actin microfilaments are highly dynamic and often instable. The actin cytoskeleton is characterized by rapid turnover, which allows certain cellular processes, like for instance cytoplasmic streaming, to function with high velocity. Another example is tip growth (such as in pollen tubes and root hairs), in which actin dynamics provide delivery of material required to facilitate directed tip growth. The assembly of actin filaments appears in two steps: nucleation and elongation (Pollard and Cooper, 1986). Nucleation involves monomeric actin to form trimers, which are thermodynamically unstable. These trimers form ”seeds” which can auto-polymerize to fibrillar actin involving the binding and hydrolysis of ATP (Pollard *et al.*, 2000). The onset of actin polymerization is controlled by actin binding proteins, which can inhibit or induce actin fibril formation, e.g. profilin inhibits actin nucleation and thus polymerization (Staiger and Blanchoin, 2006). Once monomeric actin has nucleated into trimers, actin polymerization happens with high velocity, depending on the concentration of actin nuclei in the cytosol.

Due to its molecular structure, an actin filament is polarized, possessing a so called barbed and a pointed end. Growth at barbed ends is up to ten times higher than growth at pointed ends. Actin filemant growth and shrinkage is primar-

ily controlled by hydrolysis of ATP at each subunit of the actin fiber. However, there are a number of regulatory proteins that control the dynamic growth at the ends of an actin fiber, such as formins which accelerate growth (Romero *et al.*, 2004). If the cytoplasmic concentration of monomeric actin falls beneath a critical concentration, actin fibers start to depolymerize. This shrinkage can also be controlled by actin binding proteins. *In vitro* experiments showed that barbed and pointed ends have different critical monomer concentrations to induce spontaneous growth or shrinkage. Concentrations above 0.1 μM induce growth for free barbed ends, above 0.7 μM globular actin are needed to induce growth at pointed ends. Concentrations of globular actin between these critical values lead to a common growth behaviour, termed treadmilling where the net length of the fiber stays the same, but monomers are constantly added at the barbed end, whereas they are released at the pointed end. In vivo, however, globular actin concentrations are much higher than the critical concentrations and growth behavior is mainly determined by actin-binding proteins (Blanchoin *et al.*, 2010; Pollard *et al.*, 2000).

Directed actin movement and growth enables cells, such as pollen tubes and root hairs, to grow in a directed fashion. This requires the delivery of secretory vesicles to the growing part of the cell. Vesicles and other kind of cargo, such as plastids, mitochondria and Golgi bodies, can be actively transported along actin filaments.

Myosins are motor proteins that are responsible for such transport processes. In animal cells, actin-myosin interactions allow muscle contraction, through a mechanism known as the sliding filament theory (Huxley, 1969). In plants, similar ATP dependent actin-myosin interactions lead to rapid transport of cargo along actin filaments (Staiger and Blanchoin, 2006).

Recent insights into actin organization and behaviour has revealed coordination between the actin cytoskeleton and the microtubules. Sampathkumar *et al.* (2011a) showed, that after disruption of the actin cytoskeleton using the actin inhibitory drug latrunculin B, de-novo formation of actin nuclei happened at the microtubules. In the absence of the microtubule array, no formation of the actin cytoskeleton was possible.

1.3.2 Microtubules

In contrast to the actin cytoskeleton, the microtubule array forms a rigid and stable structure in plant cells. Microtubules can be visualized as cables of 13 wires with a total diameter of 25 nm, which is roughly three times as wide as an actin fiber. Due to their molecular structure, microtubules are less dynamic than actin

filaments; however, their growth and shrinkage mechanisms follow the same self-assembly principle as described for actin filaments.

1.3.2.1 Structure and dynamics Microtubules are a key component of eucariotic cells. Non covalent polimerization of tubulins (cytoplasmic 55 kDa proteins) results in protofilaments. These aggregate laterally to form a hollow, cylindric microtubule. Tubulins are encoded by a multi- gene family holding six α-tubulin, nine β-tubulin and two γ-tubulin genes in *Arabidopsis* (Meagher and Williamson, 1994).Based on expression profiles, these genes appear to be associated with either vegetative or reproductive tissues. As a prerequisite for microtubule assembly, α– and β–tubulin form dimers, giving rise to a polarized microtubule where one end exposes an α–subunit (- end) and the opposite end exposes a β–subunit (+ end). Similar to actin, plus and minus ends differ in their dynamics (Waterman-Storer and Salmon, 1997). Both plus and minus ends can grow, shrink and pause; however, *in planta*, growth is typically seen only for plus ends. Minus ends, on the other hand, are generally observed to pause or shrink.

Dynamic instability is a common spatiotemporal behaviour of microtubules (Mitchison and Kirschner, 1984). It involves stochastic addition and removal of tubulin subunits leading to switches between growth, shrinkage and pausing of microtubule ends. The initiation of catastrophe (transition from growth to shrinkage) and rescue (transition from shrinkage to growth) is controlled by the Guanosine triphosphate (GTP) occupancy of tubulins. Both α and β tubulin have a GTP molecule boud as they are added to the growing microtubule. Shortly after addition of the new dimer, the GTP bound to the α–tubulin subunit becomes hydrolyzed to Guanosine diphosphate (GDP) (for comparison see Figure 4). Consequently, a GTP cap of at least one layer of heterodimers decorates the microtubule plus end. Once the rate of GTP hydrolysis has catched up with the growth rate of the micotubule, GTP is depleted from the plus end which ultimately leads to catastrophy (Caplow and Fee, 2003). The dynamic behavior of microtubules is summarized in Figure 4. Dynamic instability at the plus end and slow depolimerization at the minus end lead to hybrid treadmilling. As already described for actin, treadmilling allows polimerization-based migration of microtubules (Shaw *et al.*, 2003) and is a common mechanism for microtubule distribution.

Unlike in the animal kingdom, microtubules in cells of higher plants do not originate from a microtubule organization centre (MTOC) or a spindle pole (Vaughn and Harper, 1998). Nucleation of microtubules occurs in multiple sites throughout the whole cell cortex (Ehrhardt, 2008). After generation of new microtubules, they are transported to sites of assembly by treadmilling. Once assembled into arrays of higher structure, microtubules associate with the cell cor-

tex (Bartolini and Gundersen, 2006; Ehrhardt, 2008). Microtubule nucleation often occurs on pre-existing microtubules, in association with γ–tubulin complexes. Newly formed microtubules are released by katanin mediated severing at their minus ends (Nakamura *et al.*, 2010).

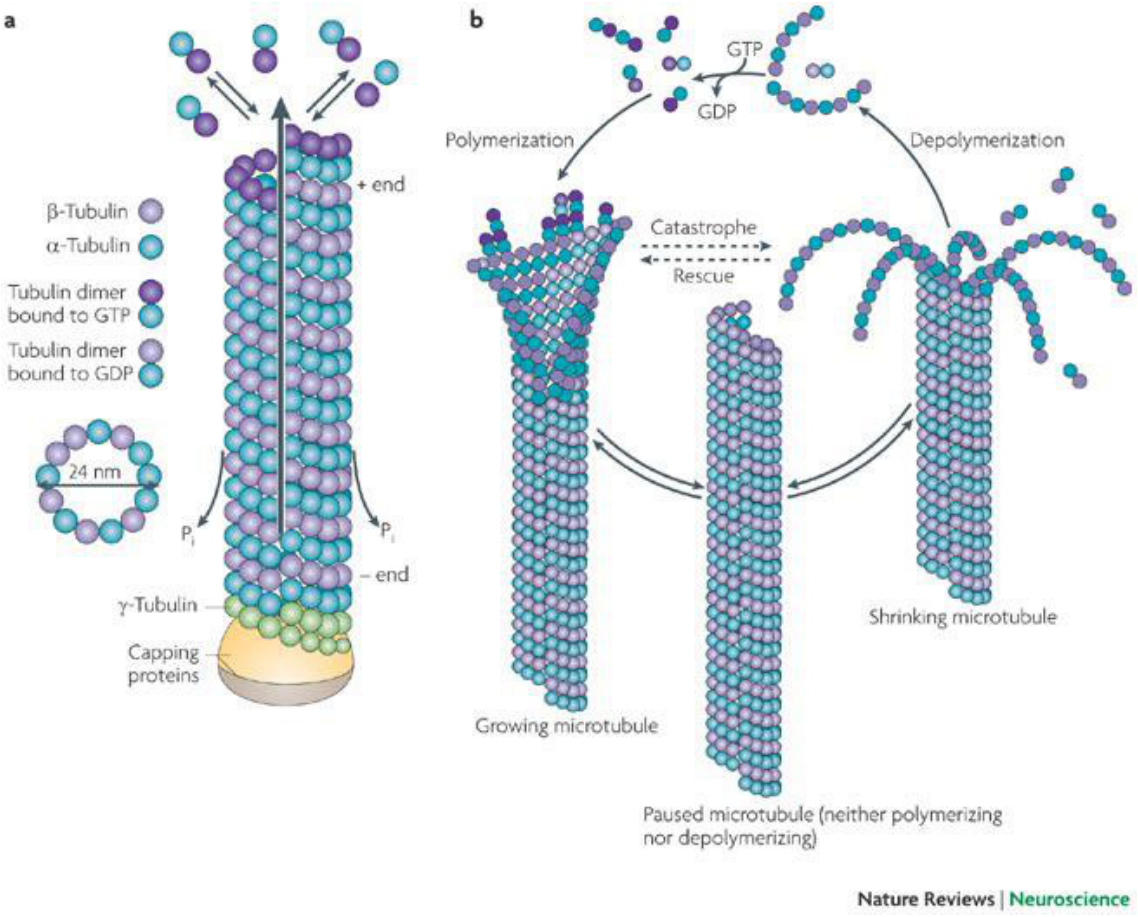

Figure 4: Microtubules are non-covalent polymers found in eukaryotic cells. They are composed of α- and β-tubulin heterodimer-subunits assembled into linear protofilaments. A single microtubule is comprised of 10 to 15 protofilaments (usually 13 in plant cells) that associate laterally to form a 24-25 nm wide hollow cylinder. The head-to-tail association of the $\alpha\beta$ subunits renders microtubules polar structures, and they have different polymerization rates at the plus and minus ends. In each microtubule, the $\alpha\beta$ heterodimers are oriented with their β-tubulin monomer pointing towards the faster-growing plus end and their α-tubulin monomer exposed at the slower-growing minus end. A third tubulin isoform, γ-tubulin, functions as a template for the correct assembly of microtubules (Nakamura *et al.*, 2010). On addition of a new dimer at the plus end, the catalytic domain of α-tubulin contacts the nucleotide exchangeable site (E-site) of the previous β-subunit and becomes ready for hydrolysis; the plus end generally has a minimum GTP cap of one tubulin layer that stabilizes the microtubule structure. When this GTP cap is stochastically lost, the protofilaments "splay" apart and the microtubule rapidly depolymerizes. Soon after polymerization, the tubulin subunits hydrolyse their bound GTP and become non-exchangeable. Thus, the microtubule lattice is predominantly composed of GDP-tubulin. During depolymerization GDP-tubulin subunits and oligomers are rapidly lost from the plus end. At the minus end, contact is made between the E site of the new dimer and the catalytic region of the last subunit at the end. Therefore, no GTP cap should be present. Image taken from Conde and Caceres (2009).

1.3.2.2 Microtubule associated proteins (MAPs) Many MAPs were first identified by co-precipitation with stabilized microtubules. Microtubules can be assembled *in vitro* from tubulin monomers. Succesive circles of microtubule assembly at elevated temperatures, incubation with cell extracts, centrifugation and disassembly of microtubules on ice lead to enrichment of MAPs in the centirifugation pellet. This system works well for animal brain tissues, since the axonal structure of nerve cells is supported by microtubules (Vallee, 1985).

Plant cells, however, have a smaller portion of microtubules and a strong background of proteins and vacuolar phenolics which makes it difficult to enrich for tubulin. Therefore, taxol stabilized neuronal tubulin was used instead to enrich plant MAPs *in vitro*. Newly found MAPs, however, had to be confirmed *in planta* (Lloyd and Hussey, 2001).

Affinity purification approaches allowed for the identification of a number of MAPs from carrot and maize cells (Cyr and Palevitz, 1989). Meanwhile, numerous MAPs were identified that partly mimic the function of their animal homologs. However, also plant specific MAPs were found. Due to their complexity, MAPs were classified according to their molecular weight. An extensively studied class of plant specific MAPs are the 65 kDa MAPs (MAP65s; see below).

The MAP65 family was shown to cross-link microtubules into larger aggregates (Lloyd and Hussey, 2001). Recent studies showed, that the MAP65 members MAP65-1 and MAP65-2 dynamically localized to sites of microtubule bundles, and enabled a microtubule templating mechanism to form the bundles. This process was essential for axial growth in etiolated *Arabidopsis* hypocotyls (Lucas *et al.*, 2011). The phragmoblast is the mitotic spindle of plants, which is a specialized microtubule array during cytokinesis. It has recently been shown that MAP65-3 is involved in antiparallel bundling of microtubules during phragmoblast formation (Ho *et al.*, 2011). MAP65-4 facilitates microtubule bundle growth in kinetochore fibres (Fache *et al.*, 2010). MAP65 members are, moreover, shown to be the main target of mitogen activated protein kinases (MAPK), which regulate cell cycle activity in plants (Komis *et al.*, 2011; Sasabe *et al.*, 2011).

The MAP70 family harbours members, that are actively involved in secondary cell wall thickening and formation of trachery elements. MAP70-1 and 5 interact with each other. Silencing of the corresponding genes through RNA interference caused microtubules and secondary thickenings to detach from the cell cortex (Pesquet *et al.*, 2010). Notably, MAP70 members are tightly transcriptionally co-regulated with the secondary CESAs (CESA4, 7 and 8) indicating putative functional association (Pesquet *et al.*, 2011). These recent results indicate

the potential for MAP70s, and other MAPs, to maintain and control microtubule arrangements during cell wall production.

Motor proteins are MAPs with motor domains. These proteins are required for directional transport of cargo along microtubules under consumption of ATP. Generally, microtubule associated motor proteins are divided into two families: kinesins and dyneins. To date, seven families of kinesins were functionally characterized in *Arabidosis* (Li *et al.*, 2011). Due to the large variety of cargo (vesicles, protein complexes and mRNA among others), kinesins are involved in numerous cellular processes that require microtubule-based transport. Examples are; transport of chromosomes during cell division, morphogenesis and signal transduction. In contrast to fungi and animals, the family of dyneins seems to be absent in the plant kingdom at least based on sequence similarities (Cai and Cresti, 2010).

Plus end trackers or +TIPs such as END BINDING 1 (EB1), CLIP ASSOCIATED PROTEIN (CLASP) and LISSENCEPHALY 1 (LIS1) appear to be ubiquitous eukaryotic proteins and are often involved in control of microtubule dynamics (Wade, 2009). Recent studies show, that AtCLASP1 is involved in microtubule guidance around cell edges (Ambrose *et al.*, 2011). Additionally, there are plant specific +TIPs like SPIRAL1 (SPR1) (Hamada, 2007). Many of these proteins are members of larger families and their function is often elusive. The *Arabidopsis* homolog of XMAP215 from *Xenopus laevis* also belongs to the class of +TIPS. It was described as MICROTUBULE ORGANIZATION 1 (MOR1) (Whittington *et al.*, 2001; Kawamura and Wasteneys, 2008). It suppresses microtubule pausing and shrinkage, and consequently supports dynamic microtubule growth. A counterpart of MOR1 is the microtubule severing protein Katanin. It can reslease newly formed microtubules which branched off from older microtubules (Nakamura *et al.*, 2010), or destroy microtubules by ATP hydrolysis (McNally and Vale, 1993).

The classes mentioned above are only examples of MAPs. There are many more proteins that bind to microtubules and potentially connect them to other cellular structures, for example to the actin cytoskeleton or to the plasma membrane (potentially facilitated by the membrane-bound phospholipase D). These proteins were extensively reviewed by Hamada (2007).

Similarities between plant and neuronal animal microtubules and their binding proteins have recently been discussed as a basis for *Arabidopsis* to become a new model organism for neuronal microtubule research (Gardiner and Marc, 2011). On the other hand, MAPs that are exclusively found in plants have a great potential to provide links between the microtubule cytoskeleton and plant specific processes, such as cellulose synthesis. Therefore, the following section will

elucidate the close interplay between cortical microtubules and cellulose synthesis in *Arabidopsis*.

1.4 Advances in microscopy techniques reveal microtubule-defined tracking of CESAs

While composition of cell walls can be assessed with the techniques of analytical chemistry, such analyses alone will not disentangle the range of molecular mechanisms that lead to the formation of a complex compartment such as the plant cell wall. Major progress with respect to cellulose synthesis mechanisms has instead been made using microscopy-based methods.

Already in the 1960s, polarization and electron microscopy were used to investigate cells of the green alga *Nitella* and their surrounding walls. Paul Green (1962) observed that cellulose microfibrils form a transverse array in elongating cells. Moreover, microfibril orientation appeared defined by proteins in the cell cortex, which were sensitive to the spindle fiber drug colchicine. Electron micrographs later confirmed that these fiber-like structures were actually microtubules, arranged in a parallel array in close vicinity to the plasma membrane (Ledbetter and Porter, 1963). Development of freeze- fracture techniques combined with electron microscopy led to visualization of the transmembrane, rosette-shaped CSCs (Mueller and Brown, 1980). These studies led the hypothesis, that cortical microtubules are tracks used by CSCs to synthesize a parallel array of cellulose microfibrils.

Electron microscopy is indeed a powerful tool to investigate subcellular structures. However, its limitation to fixed tissues is a major drawback when it comes to analyze dynamic processes. It took 44 years since Paul Greens early discoveries, until the spatiotemporal behavior of the CESAs and microtubules could be shown in a living cell.

The key technology to this breakthrough was live cell imaging, employing state of the art spinning disc confocal microscopes, which enabled Paredez *et al.* (2006) to visualize fusions of a yellow fluorescent protein (YFP) and CESA6 (CESA6:YFP) together with cyan fluorescent (CFP) protein labeled α-tubulin 1 (CFP:TUA1) in the same cell. Paredez and co-workers could determine the mean velocity of bi-directionally moving CESAs to 330 nm/min. Treatments with the microtubule inhibitor oryzalin led to changes in the distribution and patterning of moving CESAs, indicating a direct mechanism of CESA guidance by cortical microtubules. Since then the understanding of cellulose synthesis has experienced a fundamental increase on a mechanistic level.

Using the techniques of Paredez and co- workers as well as fluorescence re-

covery after photobleaching (FRAP), questions of CESA delivery could also be tackled. Gutierrez *et al.* (2009) and Crowell *et al.* (2009) could show that insertion events of CESAs to the plasma membrane happen at distinct loci in close vicinity to microtubules. Also CESA-containing vesicles, termed SmaCCs or MASCS (see section 1.2.2) were associated to microtubules. Furthermore, by point directed mutagenesis, Chen *et al.* (2010) could show, that bidirectional movement of CESAs depends on their phosphorylation status. Functional CESA5:GFP lines gave further insights in mechanisms of cellulose synthesis. Phosphorylation of CESA5 in combination with the activation of lightsensing phytochromes, revealed fine tuned mechanisms for CESA velocities in the membrane (Bischoff *et al.*, 2011) These studies were possible through live cell imaging and spinning disc microscopy. However, to identify proteins that link CESAs to other cellular processes, for example to the microtubules, such cutting edge microscopy must be combined with traditional forward genetic screens, biochemistry and/or co expression approaches.

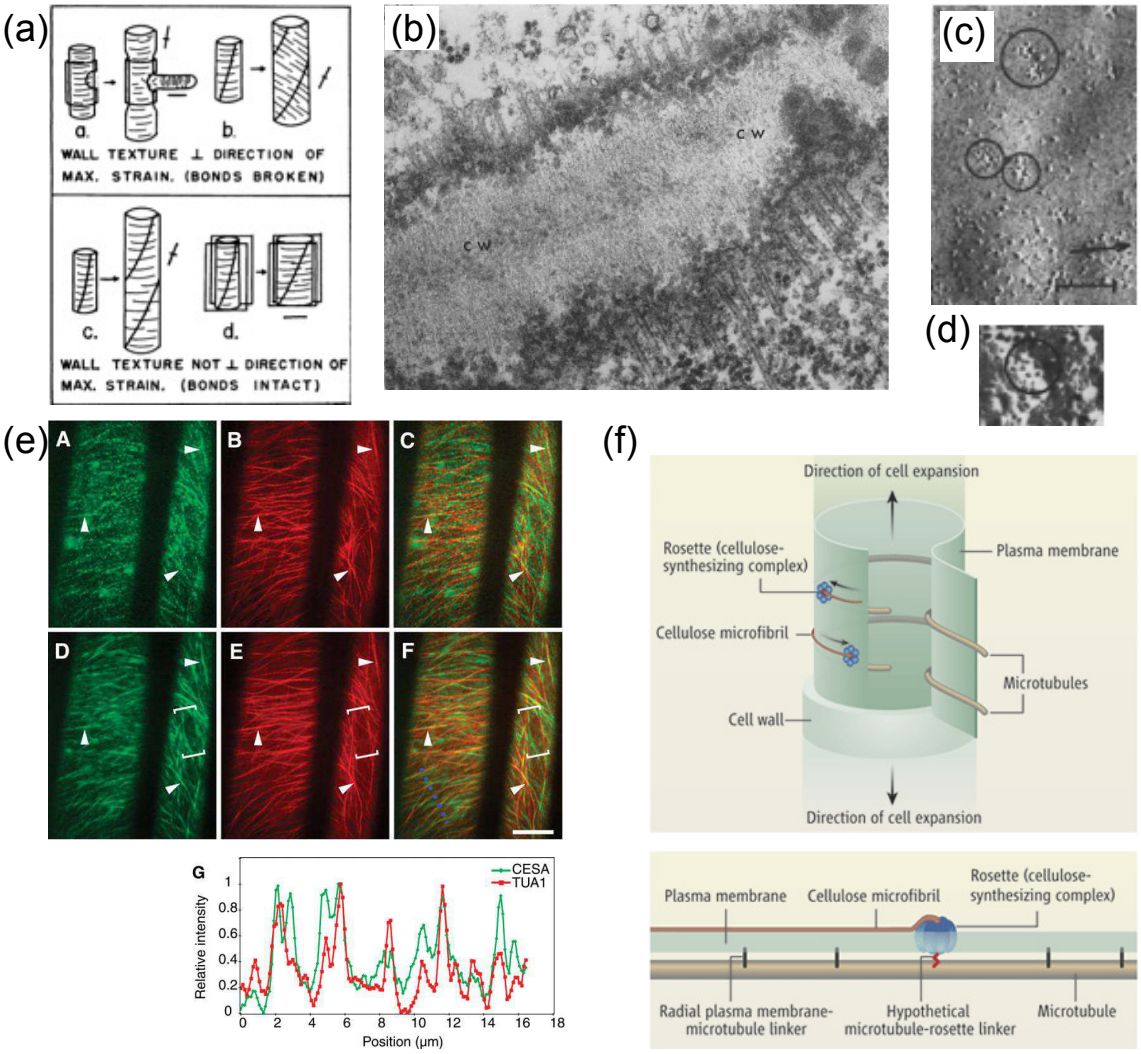

Figure 5: Advances in microscopy techniques revealed structural alignment of CESAs and mictotubules at the cell cortex. **(a)** The first model suggesting that cellulose is layed down around the cell in a parallel grid, defined by spindle fiber-like proteins was put forward by Green (1962). Due to lateral enforcement of the cell, turgor pressure can be directed to sites of expansion, which is the basis for anisotropic growth. **(b)** Spindle-like fibers, as described by Green (1962), were visualized as microtubules at the cell cortex employing electron microscopy (Ledbetter and Porter, 1963, cw = cell wall). **(c)** Mueller and Brown (1980) were the first to visualize CESAs in freeze-fracture electron micrographs of maize root cells. **(d)** Hexameric structure of the CESA rosette complex. **(e)** A breakthrough in the understanding of CESA and microtubule interactions was achieved by Paredez *et al.* (2006). For the first time, CESAs and microtubules could be co-localized in living *Arabidopsis* hypocotyl cells using the fluorescent fusion proteins YFP:CESA6 and CFP:TUA1. CESAs (A) are clearly visible as dots decorating the mictrotubules (B) when both channels are merged (C). (D to F) show time averages of (A, B and C). Over time, tracking CESAs appear as trajectories, which coincide with underlying microtubules. (G) shows a plot of fluorescence intensities along the cyan line in (F). Notably, the fluorescence intensity patterns for CESA and TUA1 show a similar pattern. **(f)** shows the current model of CESA-mictotubule alignment (Lloyd, 2006). More than 40 years after Paul Green's first model, a direct guiding mechanism for CESAs facilitated by microtubules has been established. However, the hypothetical linking elements between the CESAs and the microtubules have not yet been found.

1.5 Co-expression and forward genetic screens as tools to identify genes involved in cellulose synthesis

1.5.1 Prediction of gene function through co-expression analysis

The transcriptome is the collection of all messenger RNA (mRNA) molecules in a cell, tissue or organ. The transcriptional profile of a particular gene, with respect to tissue specificity or environmental condition, holds information about the processes it might function in. Although the mRNA abundance of a gene covers only one step in the cascade of events from the genetic code to the functional protein, and disregards translational efficiency or post-translational modifications, DNA microarrays (i.e. AtGenExpress) have found vast use in monitoring regulatory changes (Schmid *et al.*, 2005; Kilian *et al.*, 2007; Goda *et al.*, 2008).

Functionally related genes often show coordinated expression among different tissues or environmental conditions. Two genes are deemed co-expressed if their expression profiles are significantly correlated to each other (Yu *et al.*, 2003). One assumption that has been proven useful for many biological processes is that co-expressed genes are involved in related biological processes. Regardless of the large gap between transcription and function, co-expression analysis has been successfully applied to functionally characterize previously unknown genes from yeast (Yu *et al.*, 2003) and human (Lee *et al.*, 2004).

In *Arabidopsis* co-expression analysis has been used to (i) find novel genes involved in various biological processes and (ii) suggest biological processes an unknown gene might be involved in (Usadel *et al.*, 2009). One example for the successful application of co-expression analysis is the formation of secondary cell walls (Persson *et al.*, 2005; Brown *et al.*, 2005). These studies performed co-expression analysis using publicly available expression data and identified new candidate genes responsible for secondary cell wall formation. Using reverse genetics, the authors could confirm that mutations in several of these genes showed typical secondary cell wall related phenotypes.

Co-expression relationships can be visualized in graphs or tables. However, the development of new clustering algorithms have led to a more user-friendly visualization of these relationships (Mutwil *et al.*, 2010). Such network tools can be combined with basic local alignment search tool (BLAST) analysis in order to find "true" gene onthologs across model organisms like *Arabidopsis* and barley (Mutwil *et al.*, 2008b). Through comparisons of network structures, cross species and cross kingdom analyses have been made possible. These approaches have made gene function prediction more robust and effective then prediction from only one species (Mutwil *et al.*, 2011).

It therefore seems a valid strategy to search for genes associated with cellulose

synthesis using various tools of co-expression. Another approach that has led to successful identification of new genes in developmental and metabolic processes are genetic screens.

1.5.2 Identification of new genes involved in cellulose production through genetic screens

The basic principle of a forward genetic screen involves a global mutation of a seed batch; commonly used techniques are treatments with ethyl methane sulfonate (EMS) or fast neutron irradiation. The mutant population is then screened for common phenotypes for the trait of interest (i.e. organ swelling as a common phenotype for cellulose deficiency). Finally, after several back-crossing cycles, the mutated genes are identified either through map- based cloning techniques or tiling arrays (e.g. Bringmann *et al.*, 2012; Matsui *et al.*, 2010).

Several components that are important for cell expansion have been identified through genetic screens. Identification of the corresponding genes revealed many genes that are associated with cellulose synthesis. Among them are POM-POM1 (POM1)/CHITINASE- LIKE 1 (CTL1), KORRIGAN (KOR)/RADIALY SWOLLEN 2 (RSW2), COBRA (COB), KOBITO (KOB1)/ELONGATION DEFECTIVE 1 (ELD1), and the RSW1 / CESA1, CONSTITUTIVE EXPRESSION OF VSP 1 (CEV1)/ ECTOPIC LIGNIFICATION 1 (ELI1)/RSW5/CESA3 and PROCUSTE 1 (PRC1)/CESA6 (Hauser *et al.*, 1995; Arioli *et al.*, 1998; Nicol *et al.*, 1998; Fagard *et al.*, 2000; Schindelman *et al.*, 2001; Lane *et al.*, 2001; Pagant *et al.*, 2002; Wang *et al.*, 2006). Mutations in any of these genes result in epidermal cell swelling, restricted root and hypocotyl elongation, and reduced cellulose content. These genes are not necessarily parts of the CSC; however, their function seems to be crucial for cellulose synthesis.

1.6 Aim of this work

The major aim of this thesis was to find and characterize proteins that may connect the primary CESAs and elements of the cytoskeleton. The latter includes both the actin- and the microtubule cytoskeleton. Since there is a tight spatiotemporal correlation between cortical microtubules (and potentially actin filaments) and the CESAs, it is hypothesized that structural linker proteins exist that connect the CESAs to the cytoskeleton, and perhaps facilitate the movement of the CSCs.

Based on the reasoning above, a combined approach of co-expression analysis and forward genetic screening should lead to the identification of tentative candidate genes/proteins. The candidate proteins should then subsequently be characterized in terms of cellular localization using fluorescent tags, mutant analysis

using reverse genetic approaches, and a range of biochemical methods (involving induced phenotypes via drug treatments and protein-protein interaction analyses).

Established marker lines for the cytoskeleton and the CESAs should be used to analyze their concerted behavior, both in wild-type and in mutant backgrounds, employing spinning disc confocal microscopy. Ideally, new insights into the elusive alignment hypothesis of the CESAs and microtubules should be obtained.

2 Original articles published during PhD

Transcriptional Wiring of Cell Wall-Related Genes in *Arabidopsis*

Authors	Marek Mutwil, Colin Ruprecht, Federico M. Giorgi, **Martin Bringmann**, Björn Usadel, Staffan Persson
Journal	Molecular Plant
Date of Publication	September 2009

Identification of a cellulose synthase-associated protein required for cellulose biosynthesis

Authors	Ying Gu, Nick Kaplinsky, **Martin Bringmann**, Alex Cobb, Andrew Carroll, Arun Sampathkumar, Tobias I. Baskin, Staffan Persson, Chris R. Somerville
Journal	Proceedings of the National Academy of Sciences of the USA
Date of Publication	May 2010

POM-POM2/CELLULOSE SYNTHASE INTERACTING1 Is Essential for the Functional Association of Cellulose Synthase and Microtubules in *Arabidopsis*

Authors	**Martin Bringmann**, Eryang Li, Arun Sampathkumar, Tomas Kocabek, Marie-Theres Hauser, Staffan Persson
Journal	Plant Cell
Date of Publication	February 2012

Supplementary movies to the papers can be found on the CD attached to the thesis.

Molecular Plant • Volume 2 • Number 5 • Pages 1015–1024 • September 2009 RESEARCH ARTICLE

Transcriptional Wiring of Cell Wall-Related Genes in *Arabidopsis*

Marek Mutwil, Colin Ruprecht, Federico M. Giorgi, Martin Bringmann, Björn Usadel and **Staffan Persson**[1]

Max-Planck-Institute for Molecular Plant Physiology, Am Mühlenberg 1, 14476 Potsdam, Germany

ABSTRACT Transcriptional coordination, or co-expression, of genes may signify functional relatedness of the corresponding proteins. For example, several genes involved in secondary cell wall cellulose biosynthesis are co-expressed with genes engaged in the synthesis of xylan, which is a major component of the secondary cell wall. To extend these types of analyses, we investigated the co-expression relationships of all Carbohydrate-Active enZYmes (CAZy)-related genes for *Arabidopsis thaliana*. Thus, the intention was to transcriptionally link different cell wall-related processes to each other, and also to other biological functions. To facilitate easy manual inspection, we have displayed these interactions as networks and matrices, and created a web-based interface (http://aranet.mpimp-golm.mpg.de/corecarb) containing downloadable files for all the transcriptional associations.

Key words: Cell walls; bioinformatics; *Arabidopsis*; co-expression.

INTRODUCTION

The past 10 years have seen an immense increase in publicly available biological information, including genome sequences, expression analyses, protein interaction data, and metabolite profiling (Schena et al., 1995; Li et al., 2004; Baerenfaller et al., 2008). A major challenge is to utilize, and integrate, the data to understand fundamental features of living organisms (Kitano, 2002). For example, Zhang et al. (2005) constructed a biological network for yeast based on five different types of interactions, including gene expression, protein interactions, and genetic interactions, and explored this network to identify common structures in the network that may explain the design principle for the network. Similar undertakings have not yet been attempted in plants, largely due to the lack of sufficient amounts of data. However, recently Hirai et al. (2007) integrated co-expression analysis and metabolite profiling to reveal novel components in secondary metabolism. Analogously, Geisler-Lee et al. (2007) produced a web-based predictive tool that uses co-expression and orthologous protein–protein interaction data from various species to predict novel, putative protein–protein interactions in *Arabidopsis thaliana*. While similar studies currently are emerging for plants, the most commonly used metric are microarray-based co-expression analyses (Aoki et al., 2007).

Co-expressed gene pairs may be functionally related (Stuart et al., 2003; Ihmels et al., 2004; Aoki et al., 2007 and references within). The relative success of this approach has resulted in several web-based co-expression tools, including CressExpress (Srinivasasainagendra et al., 2008), ATTED-II (Obayashi et al., 2009), ASIDB (Rawat et al., 2008), Genevestigator (Zimmermann et al., 2004), GeneCAT (Mutwil et al., 2008), CSB.DB (Steinhauser et al., 2004), and Expression Angler of the Bio-Array Resource (BAR; Toufighi et al., 2005). Perhaps the best explored co-expression relationships in *Arabidopsis* are the secondary cell wall cellulose synthase (*CESA*) genes (Persson et al., 2005; Brown et al., 2005). These studies used the three secondary wall *CESA* genes as baits to identify other genes that exhibited similar expression behaviors. Several of these genes encode proteins that are associated with the production of xylan, which is another major polymer of the secondary cell wall (Bauer et al., 2006; Peña et al., 2007; Persson et al., 2007a; Brown et al., 2007).

As indicated, both cellulose and xylan are components of the plant cell wall, which is largely composed of complex polysaccharides, and heavily glycosylated proteins, and determines the shape and structure of the plant body (Somerville et al., 2004). The polysaccharides are, with the exception of cellulose, synthesized in the Golgi apparatus, and assembled into larger structures after being delivered to the cell surface (Geisler et al., 2008). It is anticipated that the synthesis and modifications of different polymers are maintained in a coordinated fashion to assure an organized cell wall architecture (Geisler et al., 2008). While such coordination most likely is sustained by specific enzyme activity and selective vesicle shuttling, other

[1] To whom correspondence should be addressed. E-mail Persson@mpimp-golm.mpg.de, fax +49-331-567-898149, tel. +49-331-567-8149.

doi: 10.1093/mp/ssp055, Advance Access publication 30 July 2009
Received 14 May 2009; accepted 3 July 2009

cellular activities may also point towards synchronization of polymer formation. For example, several genes corresponding to enzymes involved in cellulose, xylan, and lignin production are transcriptionally coordinated (Persson et al., 2005; Brown et al., 2005). Similarly, Cocuron et al. (2007) showed that the synthesis of the glucan backbone in xyloglucan most likely is synthesized by a member of the cellulose synthase-like (CSL) family C, and that the corresponding gene was co-expressed with a xylosyltransferase also involved in xyloglucan synthesis. Co-expression analyses may therefore reveal functionally linked gene pairs, and also put biological processes in functional context to each other.

Enzymes that are linked to synthesis and modifications of cell wall polysaccharides, and glycan chains associated with cell wall proteins, can be found in the Carbohydrate-Active enZYmes (CAZy) database (www.cazy.org). CAZy holds information concerning sequences, putative biochemical activities, and classifications for carbohydrate-related enzymes from a range of different organisms (Cantarel et al., 2009). To explore potential functional relationships between carbohydrate-synthesizing proteins, we investigated the degree of co-expression of the corresponding genes, using CAZy as platform. We chose to focus on *Arabidopsis* in this study, as this model plant holds good gene predictions, and has produced abundant high-quality microarray data required for co-expression analysis.

RESULTS AND DISCUSSION

Division of CAZymes Based on Visual Inspection of Phylogenetic Trees

The CAZy database (www.cazy.org/) currently holds approximately 300 super-families divided into glycosyl hydrolases (GHs), glycosyl transferases (GTs), polysaccharide lyases (PLs), carbohydrate-binding modules (CBMs), and carbohydrate estrases (CEs; Cantarel et al., 2009). Any given protein is identified as belonging to a certain CAZy super-family based on sequence commonalities, and on its modular structure (Cantarel et al., 2009). While this approach provides a useful classification, it may also group enzymes that are synthesis-related, but produce different linkages that are associated with different polysaccharides. To increase the resolution of the individual super-families, we constructed phylogenetic trees containing all assigned *Arabidopsis* enzymes for each CAZy super-family, respectively. For example, the CAZy super-family GT2 contains 42 *Arabidopsis* proteins (Figure 1A). These enzymes are referred to as the Cellulose Synthase-like (CSL) super-family, and are believed to synthesize the backbones for cellulose and hemicelluloses, e.g. β-1,4-glucan linkages, during cell wall formation (Richmond, 2000). Several studies support the idea that certain sub-families of the GT2s are involved in the synthesis of different polymers. For example, while the 10 CESAs in *Arabidopsis* are believed to synthesize cellulose microfibrils (GT2-1s in Figure 1A; Arioli et al., 1998; Kimura et al., 1999; Paredez et al., 2006), the nine CSLAs (GT2-8s in Figure 1A) appear to synthesize the backbone of the hemicellulose mannan (Liepman et al., 2005; Dhugga et al., 2004). While the members of these two families produce structurally related linkages, these linkages may be part of different polysaccharides. We argued that the functional context, and therefore perhaps also the co-expressed context, for the gene products in these families may differ. To minimize functional overlaps of members in the CAZy super-families, we visually inspected each of the phylogenetic trees, and divided the super-families into putative families based on prominent clades (Figure 1A; http://aranet.mpimp-golm.mpg.de/corecarb). We subsequently used these families for the co-expression analyses.

Transcriptional Associations between Different CAZy-Related Families in *Arabidopsis*

We explored the transcriptional associations between CAZy genes in *Arabidopsis* by using publicly available microarray data. Using the data, we constructed mutual rank-based correlation matrices for all the genes that corresponded to the CAZy proteins (Mutwil et al., 2008). We visualized connections below a certain mutual rank as networks, as such representations can display multiple gene associations, which is rather difficult to display in co-expression matrices. While various studies have used distinct Pearson *r*-value cut-offs to define significant levels of co-expression (e.g. van Noort et al., 2004), several recent reports have utilized mutual rank-based cut-offs (Mutwil et al., 2008; Obayashi et al., 2009). These values indicate whether the mutual co-expression rank of two genes is below a certain level. For example, if gene A is ranked as the seventh highest co-expressed gene with gene B, and gene B is the eleventh gene in the co-expression list for gene A, then their mutual rank corresponds to nine. Although this approach may exclude connections for genes that are well connected, it may also reveal biological information that is lost using a strict *r*-value cut-off. For example, several gene products have been indirectly connected to cellulose synthesis, including the GPI-anchored protein COBRA (COB; Roudier et al., 2005), and the chitinase-like protein POM1/CTL1 (Hauser et al., 1995; Mouille et al., 2003). However, a cut-off *r*-value of 0.8 did not associate these genes when using the primary *CESA* gene *CESA6* as bait gene (*r*-values 0.77 and 0.75, respectively, using GeneCAT; Mutwil et al., 2008). On the contrary, using a mutual rank-based cut-off of 30 readily links the *CESA6* gene with these genes (mutual ranks 4 and 9, respectively, using GeneCat; Mutwil et al., 2008). We chose a mutual rank cut-off of 30 to generate a co-expression network for all the genes associated with the different putative CAZy families, and then investigated whether certain families were connected more often than expected by chance ($p \leqslant 0.05$). For example, if several genes in one CAZy family are co-expressed to several genes in another family, and if these relationships occur more frequently then expected by chance, we propose that genes belonging to these families are co-expressed. We estimated the relationships by sampling the co-expressed node (gene)

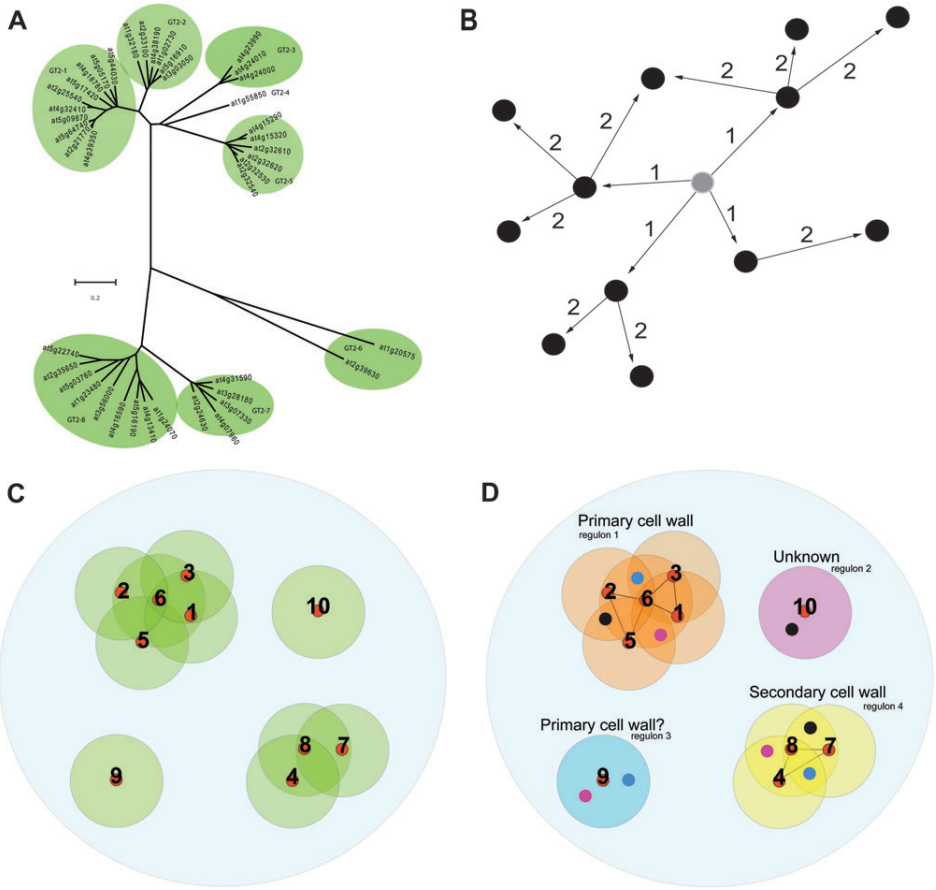

Figure 1. Work-flow of the gene family association method using the *CESA* family as example.

(A) Sub-division of the GT2 CAZy super-family. Clades, corresponding to families in the paper, in the unrooted tree are marked by green ovals, and tagged as GT2-1, GT2-2, etc.

(B) Defining co-expressed network vicinity. The co-expressed network vicinity is extracted by taking *n* steps out from a node (gene) of interest, which is indicated in grey. $n = 2$ is used in this paper.

(C, D) Description of the method used for detection of family associations using the GT2-1 clade (*CESAs*) as a case study. (C) Primary cell wall cellulose synthesizing *CESA1*, *2*, *3*, *5*, and *6*, and secondary cell wall *CESA4*, *7*, and *8* are within each other's co-expressed network vicinity, respectively. These vicinities therefore form distinct regulons in the co-expression network. *CESA9* and *CESA10* are separated from the primary and secondary cell wall regulons, and thus constitute separate regulons. (D) Examples of Pfam-associated genes co-expressed with the four GT2-1 regulons. Blue dots depict *COB* family members present in the primary, secondary, and *CESA9* regulon. Black and purple dots represent protein tyrosine kinase and *DUF246* family members, respectively.

vicinities for each individual gene ($n = 2$), namely nodes that are found within two steps from the bait gene, in the mutual rank-based network (Figure 1B; Mutwil et al., submitted elsewhere), and subsequently counted the co-occurrence of different CAZy family members.

However, such relationships may become skewed if two or more genes from the same CAZy family are in the same co-expressed node vicinity. For instance, if two or more such genes are linked in a co-expression network, a large extent of the sampled area will be covered two times (Figure 1C). This is clear if we look at the *CESA* family in which *CESA1*, *2*, *3*, *5*, and *6*, and *CESA4*, *7*, and *8* are in each other's node vicinities, respectively (Figure 1C). To avoid this type of skewed enrichment, we considered overlapping areas only once; in other words, if two of the genes from one family are within two steps' distance from one another, we assign them to a regulon. For example, *CESA1*, *2*, *3*, *5*, and *6* are all within two steps away from one another and were therefore assigned to one regulon (Figure 1D). The co-expression relationships between CAZy families, and between individual genes in these families, are available from http://aranet.mpimp-golm.mpg.de/corecarb.

Construction of a CAZy-Based Co-Expression Network

We depicted the co-expression relationships for the different CAZy families as a network structure, in which individual families represent nodes, and connections (edges) between the nodes represent significant co-expression (Figure 2A; http://aranet.mpimp.golm-mpg.de/corecarb). From this network, it is evident that, for example, the *CESAs* tend to be transcriptionally connected to members in family GT8-2 and in GT47-2

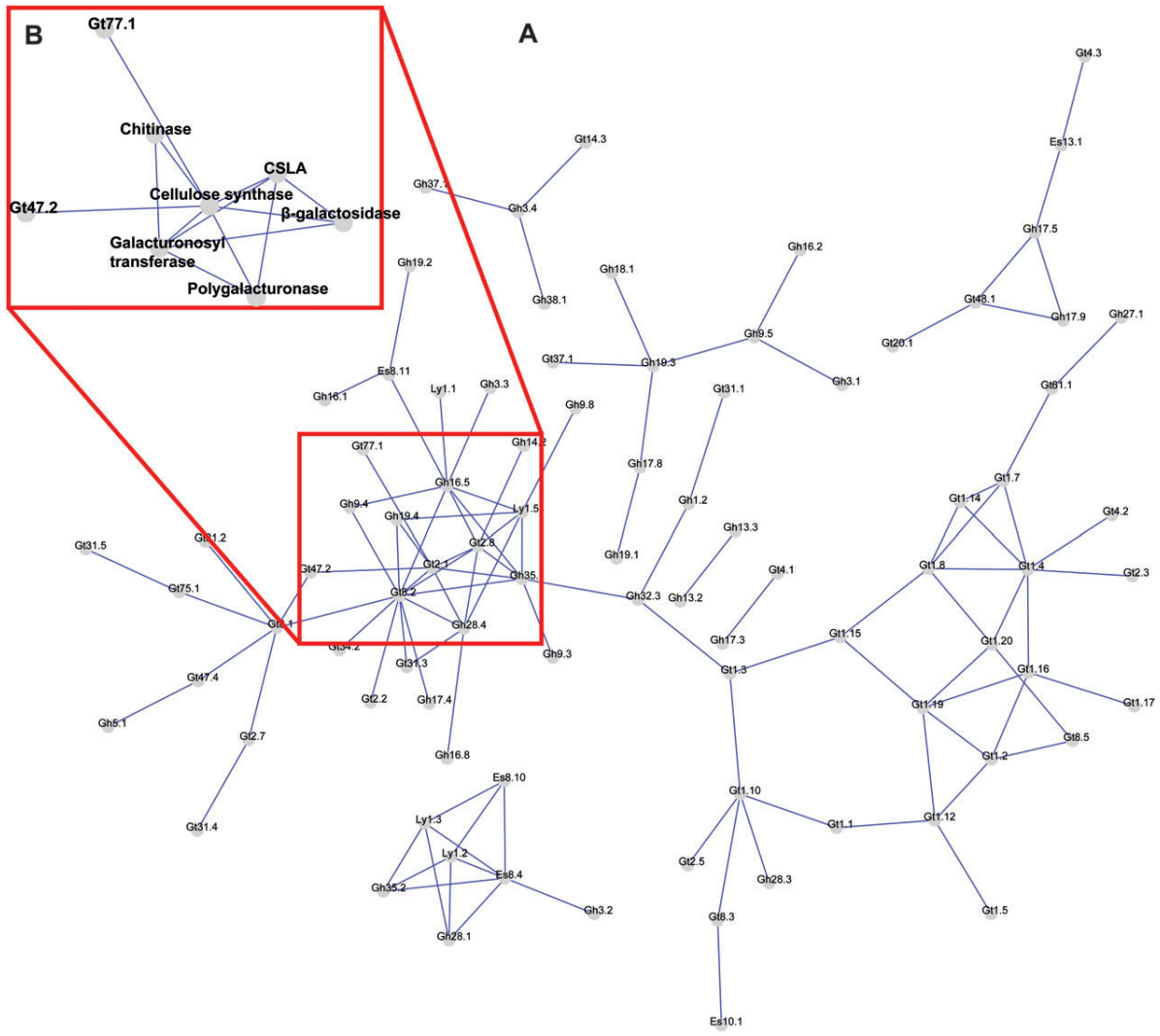

Figure 2. Co-Expression Network between Different CAZy Families.

(A) The different CAZy families inferred in this paper are represented by nodes, while significant transcriptional associations between any two families are represented by lines, or edges, connecting the nodes.

(B) Blow-up of the network surrounding the GT2-1 (*CESA*) family.

(Table 1 and Figure 2). The GT47 gene (*At1g27440*) that is co-expressed with the secondary *CESA* regulon corresponds to *IRegular Xylem 10 (IRX10;* Brown et al., 2007, 2009), and is necessary for the synthesis of xylan during secondary cell wall production. While the *GT8-2* gene that is indicated as co-expressed with the secondary *CESA* regulon in Table 1 so far has not been reported to be involved in secondary cell wall synthesis, another *GT8* gene that is associated with the *GT8-1* family (*IRX8*; At5g54690) is also closely co-expressed with the secondary *CESAs* (Persson et al., 2005; Brown et al., 2005; http://aranet.mpimp-golm.mpg.de/aranet). It is currently hypothesized that the function of this gene is associated with initiation or capping of the polymer, or perhaps with cross-linking of the xylan polymer to other cell wall polymers (Peña et al., 2007; Persson et al., 2007a). The IRX10 gene product, on the other hand, appears to be associated with the elongation of the xylan backbone (Brown et al., 2009).

Similarly, at least four GT8s from the same family (GT8-2) are present in close vicinity to the primary cell wall *CESAs* (Table 1). While xylan is not present to any larger extent in the primary cell wall, at least one of the GT8s has been shown to have galacturonosyltransferase activity (GAUT1; Sterling et al., 2006) presumably associated with the production of the pectic polymer homogalacturonan (HG). The GT8-2 family has been referred to as the GAUT-like clade (Sterling et al., 2006), and, if the four GT8-2s that are co-expressed with the primary wall CESAs also hold similar activities, it appears likely that they are involved in the synthesis of HG, which is prevalent during primary wall formation.

Table 1. Putative CAZy families, and family members, displaying co-regulation with the different *CESA* regulons.

CAZy family	CAZy description*	*CESA* regulon 1	*CESA* regulon 2	*CESA* regulon 3	*CESA* regulon 4
gh28-4	Glycosyl hydrolase 28-4	*At3g06770*	–	–	*At1g19170*
gt47-2	Glycosyl transferase 47-2	*At5g61840*	–	–	*At1g27440*
gt8-2	Glycosyl transferase 8-2	*At1g13250 At1g24170 At4g02130 At3g62660*	–	–	*At1g19300*
gh19-4	Glycosyl hydrolase 19-4	*At1g05850*	–	–	*At3g16920*
gt77-1	Glycosyl transferase 77-1	*At1g19360*	–	*At1g75110*	–

***** The description of the CAZy families can be obtained at http://aranet.mpimp.golm-mpg.de/CoreCarb.

Associations of the Putative CAZy Families with Other Families (Pfams) in the Genome

While it may be useful to depict the transcriptional coordination between genes associated with the different CAZy families, it may also be of interest to explore the co-expression relationships between these genes and all the genes present on the ATH1 chip. Such analysis could reveal novel gene partners necessary for synthesis of specific polysaccharides. To do this, we took a similar approach as for detecting associations between the CAZy-based families. We grouped all genes present on the ATH1 chip into families according to the Pfam classification (Finn et al., 2008; http://pfam.sanger.ac.uk/). Similar to the CAZy family network, we used a mutual rank cut-off of 30, and considered all genes in the matrix that had a rank value below this value as co-expressed (http://aranet.mpimp.golm-mpg.de/corecarb). We subsequently analyzed whether genes of a certain Pfam co-occurred with genes of a certain CAZy family more than expected by chance ($p \leqslant 0.05$). Based on these relationships, we created lists for each putative CAZy family, displaying the connections between the CAZy families and *Arabidopsis* Pfams (http://aranet.mpimp-golm.mpg.de/corecarb).

To illustrate the example above, we chose to focus on the co-expression between genes in the *CESA* family and different Pfam genes (Table 2). Interestingly, *COBRA*-related genes, which are not yet associated with any comprehensible biological function, are associated with three of the four *CESA* node regulons (Figure 1D and Table 2). *COBRA1* is closely co-expressed with the primary wall *CESAs*, and results in reduced cellulose content and cell expansion deficiencies when mutated (Roudier et al., 2005). Analogously, the *COBRA-like 4* gene is essential for secondary cell wall integrity, and is closely co-expressed with the secondary *CESA* genes (Brown et al., 2005). These two genes therefore appear to play essential roles during primary and secondary cell wall biosynthesis. In addition, *COBRA-like 6* (*COBL6*; *At1g09790*) is co-expressed with *CESA9* (Table 3), which is only expressed in mature pollen, and in seeds (data not shown). Considering that CESA9 appears to be functionally similar to another primary wall CESA, CESA6 (Persson et al., 2007b), the *COBL6* may constitute an interesting candidate to further explore the functions of the COBRAs.

Another interesting gene family that is transcriptionally connected to two of the four *CESA* node vicinities is the 'multi-copper oxidase-related' family (Table 2). Several such genes are co-expressed with the secondary wall-related *CESAs*, and are referred to as diphenol oxidases or laccases (Table 3). These include at least one gene that is essential for secondary cell wall deposition, *IRX12* (*At2g38080;* Brown et al., 2005). At least five additional laccases are found in the close vicinity of the secondary wall *CESAs*, and are perhaps therefore likely to mask phenotypic traits in the absence of one of the other laccase-related genes. Another multi-copper-related gene is co-expressed with the primary wall *CESAs* (Table 3). This gene corresponds to *SKU5* (*At4g12420;* Sedbrook et al., 2002), which encodes a glycosyl phosphatidylinositol-anchored glycoprotein that is involved in directional growth processes (Sedbrook et al., 2002). In addition, at least three *SKU5-like* genes, including *SKS4* (*At4g22010*), *SKS5* (*At1g76160*), and *SKS6* (*At1g41830*) are in close vicinity to the primary *CESA* regulon (data not shown). These genes are closely related to each other, and the corresponding proteins may therefore be likely to perform similar functions, perhaps in concert with SKU5.

Some other Pfams that may be interesting to investigate are the 'Protein kinase domain' and 'Protein tyrosine kinase' families (Table 3). A multitude of such genes are co-regulated with the primary wall *CESA* regulon (Table 3). While most of these are Receptor-like kinases (RLKs) of unknown function, several of them have been associated with cell elongation. For example, *THESEUS1* (*THE1; At5g54380*), which suppresses the mutant phenotype *prc1-1* (affecting the primary CESA, *CESA6*) when mutated, has recently been suggested to be involved in sensing primary cell wall integrity (Hématy et al., 2007). In addition, another RLK *FEI1* (*At1g31420;* Xu et al., 2008) is necessary for primary wall deposition and for root elongation, and is also co-expressed with the primary *CESAs* (Table 3). Several of the other RLKs associated with the primary *CESA* regulon may therefore be relevant targets for further insight into cell wall signaling. Furthermore, multiple genes with the same Pfams are also co-expressed with the secondary *CESA* regulon, and may perhaps therefore be associated with regulation of secondary wall polymer synthesis.

In summary, we have investigated co-expression relationships for the different CAZy families. This approach exposes both gene correlations on an individual gene level, and also provides insight into how multiple members of the different families are transcriptionally linked. In addition, we extended

Table 2. Pfams co-expressed with two or more of the *CESA*-related regulons.

PfamID*	Pfam symbol	Description	Present in # of regulons:
pfam07714	Pkinase_Tyr	Protein tyrosine kinase.	3
pfam04833	COBRA	COBRA-like protein. Family of plant proteins are designated COBRA-like (COBL) proteins. The 12 Arabidopsis members of the family are all GPI-liked. Some members of this family are annotated as phytochelatin synthase.	3
pfam03138	DUF246	Plant protein family. The function of this family of plant proteins is not known.	3
pfam02298	Cu_bind_like	Plastocyanin-like domain. This family represents a domain found in flowering plants related to the copper binding protein plastocyanin.	3
pfam00010	HLH	Helix-loop-helix DNA-binding domain.	3
pfam07732	Cu-oxidase_3	Multicopper oxidase. This entry contains many divergent copper oxidase-like domains that are not recognised by the pfam00394 model.	2
pfam06749	DUF1218	Protein of unknown function (DUF1218). This family contains hypothetical plant proteins of unknown function. Family members contain a number of conserved cysteine residues.	2
pfam06346	Drf_FH1	Formin Homology Region 1. This region is found in some of the Diaphanous related formins (Drfs).	2
pfam05911	DUF869	Plant protein of unknown function (DUF869). This family consists of a number of sequences found in Arabidopsis thaliana, Oryza sativa and Lycopersicon esculentum (Tomato).	2
pfam05109	Herpes_BLLF1	Herpes virus major outer envelope glycoprotein (BLLF1). This family consists of the BLLF1 viral late glycoprotein, also termed gp350/220.	2
pfam04669	DUF579	Protein of unknown function (DUF579).	2
pfam03999	MAP65_ASE1	Microtubule associated protein (MAP65/ASE1 family).	2
pfam03005	DUF231	Arabidopsis proteins of unknown function.	2
pfam02469	Fasciclin	Fasciclin domain. This extracellular domain is found repeated four times in grasshopper fasciclin I as well as in proteins from mammals, sea urchins, plants, yeast and bacteria.	2
pfam02463	SMC_N	RecF/RecN/SMC N terminal domain. This domain is found at the N terminus of SMC proteins. The SMC (structural maintenance of chromosomes) superfamily proteins have ATP-binding domains at the N- and C-termini, and two extended coiled-coil domains separated by a hinge in the middle.	2
pfam02309	AUX_IAA	AUX/IAA family. Transcription of the AUX/IAA family of genes is rapidly induced by the plant hormone auxin. Some members of this family are longer and contain an N terminal DNA binding domain.	2
pfam01565	FAD_binding_4	FAD binding domain. This family consists of various enzymes that use FAD as a co-factor, most of the enzymes are similar to oxygen oxidoreductase.	2
pfam00642	zf-CCCH	Zinc finger C-x8-C-x5-C-x3-H type (and similar).	2
pfam00620	RhoGAP	RhoGAP domain. GTPase activator proteins towards Rho/Rac/Cdc42-like small GTPases.	2
pfam00612	IQ	IQ calmodulin-binding motif. Calmodulin-binding motif.	2
pfam00561	Abhydrolase_1	alpha/beta hydrolase fold. This catalytic domain is found in a very wide range of enzymes.	2
pfam00234	Tryp_alpha_amyl	Protease inhibitor/seed storage/LTP family. This family is composed of trypsin-alpha amylase inhibitors, seed storage proteins and lipid transfer proteins from plants.	2
pfam00190	Cupin_1	Cupin. This family represents the conserved barrel domain of the 'cupin' superfamily ('cupa' is the Latin term for a small barrel). This family contains 11S and 7S plant seed storage proteins, and germins.	2
pfam00120	Gln-synt_C	Glutamine synthetase, catalytic domain.	2
pfam00071	Ras	Ras family. Includes sub-families Ras, Rab, Rac, Ral, Ran, Rap Ypt1 and more. Shares P-loop motif with GTP_EFTU, arf and myosin_head. See pfam00009 pfam00025, pfam00063. As regards Rab GTPases, these are important regulators of vesicle formation, motility and fusion.	2
pfam00069	Pkinase	Protein kinase domain.	2
pfam00026	Asp	Eukaryotic aspartyl protease. Aspartyl (acid) proteases include pepsins, cathepsins, and renins.	2

* PfamID indicates the identification code from the Pfam database.

Table 3. Individual Pfam genes associated with the different *CESA* regulons.

Pfam	Pfam description	*CESA* regulon 1	*CESA* regulon 2	*CESA* regulaon 3	*CESA* regulon 4
pfam07732	Multicopper oxidase.	*At4g12420*	–	–	*At5g01190 At2g38080 At5g05390 At5g03260 At2g29130 At5g60020*
pfam00010	Helix-loop-helix DNA-binding domain.	*At2g31730*	*At4g09820*	–	*At5g48560*
pfam00612	IQ calmodulin-binding motif. Calmodulin-binding motif.	*At5g03040*	–	–	*At3g59690 At3g15050*
pfam04833	COBRA–like protein. Family of plant proteins are designated COBRA–like (COBL) proteins.	*At5g60920*	–	*At1g09790*	*At5g15630*
pfam03138	Plant protein family. The function of this family of plant proteins is not known.	*At3g02250 At5g15740 At3g21190*	–	*At1g20550*	*At1g29200*
pfam00026	Eukaryotic aspartyl protease. Aspartyl (acid) proteases include pepsins, cathepsins, and renins.	*At3g54400 At3g52500*	–	–	*At2g03200*
pfam01565	FAD binding domain. This family consists of various enzymes that use FAD as a co-factor, most of the enzymes are similar to oxygen oxidoreductase.	*At3g19820*	–	–	*At2g46760*
pfam00120	Glutamine synthetase, catalytic domain.	*At1g66200*	–	*At1g48470*	-
pfam06346	Formin Homology Region 1.	*At2g14890*	*At3g24250*	–	–
pfam06749	Protein of unknown function (DUF1218).	*At1g13380 At3g15480*	–	-	*At1g31720 At4g27435*
pfam02309	AUX/IAA family. Transcription of the AUX/IAA family of genes is rapidly induced by the plant hormone auxin.	*At3g04730 At3g23050*	*At3g17600*	–	–
pfam00069	Protein kinase domain.	*At3g51850 At1g31420 At1g28440 At1g56720 At3g02880 At2g30980 At1g53730 At3g14350 At4g23650 At4g35310 At1g01540 At3g23000 At5g55910 At4g18640 At1g66150 At2g01820 At1g06390 At2g26730 At5g16590 At5g18500*	–	–	*At5g48740 At1g09440 At1g24030 At1g56720 At2g40120*
pfam00190	Cupin. This family represents the conserved barrel domain of the 'cupin' superfamily.	–	*At5g39130*	–	*At3g62020*
pfam03005	Arabidopsis proteins of unknown function.	*At5g06700 At2g40150 At1g01430 At1g70230*	–	–	*At5g01360*
pfam05911	Plant protein of unknown function (DUF869).	*At1g19835*	–	–	*At3g19370*
pfam00234	Protease inhibitor/seed storage/LTP family. This family is composed of trypsin-alpha amylase inhibitors, seed storage proteins and lipid transfer proteins from plants.	*At2g13820*	*At5g38195 At2g15325 At5g09370 At5g38180*	-	–
pfam00620	RhoGAP domain. GTPase activator proteins towards Rho/Rac/Cdc42-like small GTPases.	*At3g11490*	–	–	*At1g08340*
pfam00561	alpha/beta hydrolase fold.	*At3g01690*	*At2g23580 At2g23550*	–	–

Table 3. Continued

Pfam	Pfam description	*CESA* regulon 1	*CESA* regulon 2	*CESA* regulaon 3	*CESA* regulon 4
pfam00071	Ras family. Includes sub-families Ras, Rab, Rac, Ral, Ran, Rap Ypt1 and more. Shares P-loop motif with GTP_EFTU, arf and myosin_head.	*At1g20090 At4g39990 Aat5g03520*	–	–	*At1g73640 At5g45970*
pfam00642	Zinc finger C-x8-C-x5-C-x3-H type (and similar).	–	–	*At3g48440*	*At1g66810*
pfam02463	RecF/RecN/SMC N terminal domain. This domain is found at the N terminus of SMC proteins.	*At1g22060*	–	*At3g09730*	–
pfam02298	Plastocyanin-like domain.	*At5g15350 At4g12880 At1g64640 At3g27200*	*At4g28365; At4g32490 At5g57920*	–	*At5g26330 At1g72230 At1g22480 At3g27200*
pfam02469	Fasciclin domain. This extracellular domain is found repeated four times in grasshopper fasciclin I as well as in proteins from mammals, sea urchins, plants, yeast and bacteria.	*At3g52370 At5g44130 At2g04780 At1g03870 At2g35860 At2g45470 At4g12730 At3g11700*	–	–	*At5g60490 At5g03170*
pfam05109	Herpes virus major outer envelope glycoprotein (BLLF1). This family consists of the BLLF1 viral late glycoprotein, also termed gp350/220.	*At2g42580*	*At5g45770*	–	–
pfam03999	Microtubule associated protein (MAP65/ASE1 family).	*At2g01910*	–	–	*At1g27920*
pfam04669	Protein of unknown function (DUF579).	–	*At1g71690*	–	*At5g67210 At3g50220 At1g09610*
pfam07714	Protein tyrosine kinase.	*At2g35050 At1g07650 At5g54380 At5g50000 At4g39400 At4g03390 At3g51550 At3g56050*	–	*At4g14780*	*At1g79620*

the analyses to include all genes on the ATH1 chip, and explored co-expression relationships between the different CAZy families and Pfams. All of the results are downloadable from http://aranet.mpimp-golm.mpg.de/corecarb as text, and excel files. Co-expression networks for individual genes can be mined at http://aranet.mpimp-golm.mpg.de/aranet (Mutwil et al., submitted elsewhere).

METHODS

Microarray Data

All calculations for this work were done using python and java code. The datasets are the same as used for the GeneCAT webtool (Mutwil et al. 2008). Specifically, databases for *Arabidopsis* use Affymetrix ATH1 (22 810 probe sets) *Arabidopsis* microarray datasets consisting of 1428 ATH1 microarrays, which were obtained from TAIR (www.Arabidopsis.org/). The microarray data were quality controlled by visual inspection of boxplots of raw PM data and RMA residuals of RMA normalized data, using the RMA express program. Cel files showing artifacts on RMA residual plots or visibly deviating from the majority on the PM-boxplots were removed from further analysis. In addition, we removed experiments representing very similar transcriptomic snapshots by iteratively discarding microarrays that displayed Pearson correlation $r(A,B) \geqslant 0.95$ to more than three other microarrays. From these analyses, we retained 351 microarrays, which subsequently were normalized using R package simpleAffy.

Phylogenetic Analysis of CAZy Families

Arabidopsis thaliana gene identifiers (AGI codes) for the different carbohydrate active enzymes super-families were downloaded from the CAZy database (www.cazy.com). The protein sequences of the super-families were then aligned by clustalW in the MEGA software package using standard settings (Tamura et al., 2007). The resulting alignments were then subjected to Neighbor Joining algorithm, exported as phylogenetic trees, and clades were extracted. We chose to divide the trees by visual inspection, as neither tree branch length nor BLAST score cut-off values can reliably identify groups of similar genes.

Division of *Arabidopsis thaliana* Proteins into Families using PFAM

Each probeset in the Affymetrix ATH1 microarray platform was mapped using BLAST (Altschul et al., 1990) to the

corresponding best-hit coding sequence as defined by TAIR8 (www.Arabidopsis.org/). Probesets with no gene hit or expected values higher than 0.01 were excluded from further analysis.

Using reversed position-specific BLAST (RPS-BLAST; Marchler-Bauer et al., 2002) with a cut-off expected value of 0.01, we assigned each *Arabidopsis* gene to the best-hit Pfam family (Finn et al., 2008, Pfam v23.0).

Calculating Statistical Significance of Family Associations

To obtain empirical *p*-values for the co-association of the different families, the family tags were shuffled 10 000 times. During each shuffling, the number of instances in which any two proteins could be found in each other's network vicinity ($n = 2$) was counted, and the number was divided by 10 000 to obtain the *p*-value. The co-expressed network vicinity was generated by moving two steps out from a node of interest; thus, any gene that is a direct neighbor or a neighbor of a neighbor is included in the node vicinity. Any two families associated with a *p*-value < 0.05 were called '*p*-value co-regulated'.

To obtain the number of protein families present in separate regulons of each family, members of a family were recursively grouped together if they were neighbors in a co-expression network (i.e. within two steps away from each other). The obtained regulons were then examined for presence of protein families. If any protein family was found in two or more regulons, it was called 'regulon co-regulated'. Finally, any two families were called significantly co-regulated if they were both *p*-value and regulon co-regulated.

FUNDING

This work was funded by the Max-Planck-Gesellschaft.
No conflict of interest declared.

REFERENCES

Altschul, S.F., Gish, W., Miller, W., Myers, E.W., and Lipman, D.J. (1990). Basic local alignment search tool. J. Mol. Biol. **215,** 403–410.

Aoki, K., Ogata, Y., and Shibata, D. (2007). Approaches for extracting practical information from gene co-expression networks in plant biology. Plant Cell Physiol. **48,** 381–390.

Arioli, T., et al. (1998). Molecular analysis of cellulose biosynthesis in *Arabidopsis*. Science. **279,** 717–720.

Baerenfaller, K., Grossmann, J., Grobei, M.A., Hull, R., Hirsch-Hoffmann, M., Yalovsky, S., Zimmermann, P., Grossniklaus, U., Gruissem, W., and Baginsky, S. (2008). Genome-scale proteomics reveals *Arabidopsis* thaliana gene models and proteome dynamics. Science. **320,** 938–941.

Bauer, S., Vasu, P., Persson, S., Mort, A.J., and Somerville, C.R. (2006). Development and application of a suite of polysaccharide degrading enzymes for analyzing plant cell walls. Proc. Natl Acad. Sci. U S A. **103,** 11417–11422.

Brown, D.M., Goubet, F., Wong, V.W., Goodacre, R., Stephens, E., Dupree, P., and Turner, S.R. (2007). Comparison of five xylan synthesis mutants reveals new insight into the mechanisms of xylan synthesis. Plant J. **52,** 1154–1168.

Brown, D.M., Zeef, L.A., Ellis, J., Goodacre, R., and Turner, S.R. (2005). Identification of novel genes in *Arabidopsis* involved in secondary cell wall formation using expression profiling and reverse genetics. Plant Cell. **17,** 2281–2295.

Brown, D.M., Zhang, Z., Stephens, E., Dupree, P., and Turner, S.R. (2009). Characterization of IRX10 and IRX10-like reveals an essential role in glucuronoxylan biosynthesis in *Arabidopsis*. Plant J. **57,** 732–746.

Cantarel, B.L., Coutinho, P.M., Rancurel, C., Bernard, T., Lombard, V., and Henrissat, B. (2009). The Carbohydrate-Active EnZymes database (CAZy): an expert resource for Glycogenomics. Nucleic Acids Res. **37(Database Issue),** D233–D238.

Cocuron, J.C., Lerouxel, O., Drakakaki, G., Alonso, A.P., Liepman, A.H., Keegstra, K., Raikhel, N., and Wilkerson, C.G. (2007). A gene from the cellulose synthase-like C family encodes a beta-1,4 glucan synthase. Proc. Natl Acad. Sci. U S A. **104,** 8550–8555.

Dhugga, K.S., et al. (2004). Guar seed beta-mannan synthase is a member of the cellulose synthase super gene family. Science. **303,** 363–366.

Finn, R.D., et al. (2008). The Pfam protein families database. Nucleic Acids Res. **36(Database Issue),** D281–D288.

Geisler, D.A., Sampathkumar, A., Mutwil, M., and Persson, S. (2008). Laying down the bricks: logistic aspects of cell wall biosynthesis. Curr. Opin. Plant Biol. **11,** 647–652.

Geisler-Lee, J., O'Toole, N., Ammar, R., Provart, N.J., Millar, A.H., and Geisler, M. (2007). A predicted interactome for *Arabidopsis*. Plant Physiol. **145,** 317–329.

Hauser, M.T., Morikami, A., and Benfey, P.N. (1995). Conditional root expansion mutants of *Arabidopsis*. Development. **121,** 1237–1252.

Hématy, K., Sado, P.E., Van Tuinen, A., Rochange, S., Desnos, T., Balzergue, S., Pelletier, S., Renou, J.P., and Höfte, H. (2007). A receptor-like kinase mediates the response of *Arabidopsis* cells to the inhibition of cellulose synthesis. Curr. Biol. **17,** 922–931.

Hirai, M.Y., et al. (2007). Omics-based identification of *Arabidopsis* Myb transcription factors regulating aliphatic glucosinolate biosynthesis. Proc. Natl Acad. Sci. U S A. **104,** 6478–6483.

Ihmels, J., Levy, R., and Barkai, N. (2004). Principles of transcriptional control in the metabolic network of *Saccharomyces cerevisiae*. Nat. Biotechnol. **22,** 86–92.

Kimura, S., Laosinchai, W., Itoh, T., Cui, X., Linder, C.R., and Brown, R.M.,Jr (1999). Immunogold labeling of rosette terminal cellulose-synthesizing complexes in the vascular plant *Vigna angularis*. Plant Cell. **11,** 2075–2086.

Kitano, H. (2002). Systems biology: a brief overview. Science. **295,** 1662–1664.

Li, S., et al. (2004). A map of the interactome network of the metazoan *C. elegans*. Science. **303,** 540–543.

Liepman, A.H., Wilkerson, C.G., and Keegstra, K. (2005). Expression of cellulose synthase-like (Csl) genes in insect cells reveals that CslA family members encode mannan synthases. Proc. Natl Acad. Sci. U S A. **102,** 2221–2226.

Marchler-Bauer, A., Panchenko, A.R., Shoemaker, B.A., Thiessen, P.A., Geer, L.Y., and Bryant, S.H. (2002). CDD: a database of conserved domain alignments with links to domain three-dimensional structure. Nucleic Acids Res. **30,** 281–283.

Mouille, G., Robin, S., Lecomte, M., Pagant, S., and Höfte, H. (2003). Classification and identification of *Arabidopsis* cell wall mutants using Fourier-Transform InfraRed (FT-IR) microspectroscopy. Plant J. **35,** 393–404.

Mutwil, M., Obro, J., Willats, W.G., and Persson, S. (2008). GeneCAT–novel webtools that combine BLAST and co-expression analyses. Nucleic Acids Res. **Webserver Issue**. W320–W326.

Mutwil, M., Usadel, B., Schütte, M., Loraine, A., Ebenhöh, O., and Persson, S. (submitted elsewhere) Assembly of an interactive correlation network for the *Arabidopsis* genome using a novel heuristic clustering algorithm. .

Obayashi, T., Hayashi, S., Saeki, M., Ohta, H., and Kinoshita, K. (2009). ATTED-II provides coexpressed gene networks for *Arabidopsis*. Nucleic Acids Res. **37(Database Issue),** D987–D991.

Paredez, A.R., Somerville, C.R., and Ehrhardt, D.W. (2006). Visualization of cellulose synthase demonstrates functional association with microtubules. Science. **312,** 1491–1495.

Peña, M.J., Zhong, R., Zhou, G.K., Richardson, E.A., O'Neill, M.A., Darvill, A.G., York, W.S., and Ye, Z.H. (2007). *Arabidopsis* irregular xylem8 and irregular xylem9: implications for the complexity of glucuronoxylan biosynthesis. Plant Cell. **19,** 549–563.

Persson, S., Caffall, K.H., Freshour, G., Hilley, M.T., Bauer, S., Poindexter, P., Hahn, M.G., Mohnen, D., and Somerville, C. (2007a). The *Arabidopsis* irregular xylem8 mutant is deficient in glucuronoxylan and homogalacturonan, which are essential for secondary cell wall integrity. Plant Cell. **19,** 237–255.

Persson, S., Paredez, A., Carroll, A., Palsdottir, H., Doblin, M., Poindexter, P., Khitrov, N., Auer, M., and Somerville, C.R. (2007b). Genetic evidence for three unique components in primary cell-wall cellulose synthase complexes in *Arabidopsis*. Proc. Natl Acad. Sci. U S A. **104,** 15566–15571.

Persson, S., Wei, H., Milne, J., Page, G.P., and Somerville, C.R. (2005). Identification of genes required for cellulose synthesis by regression analysis of public microarray data sets. Proc. Natl Acad. Sci. U S A. **102,** 8633–8638.

Rawat, A., Seifert, G.J., and Deng, Y. (2008). Novel implementation of conditional co-regulation by graph theory to derive co-expressed genes from microarray data. BMC Bioinformatics. 9 Suppl 9, S7.

Richmond, T. (2000). Higher plant cellulose synthases. Genome Biol. **1: reviews,** 3001.1-3001.6.

Roudier, F., et al. (2005). COBRA, an *Arabidopsis* extracellular glycosyl-phosphatidyl inositol-anchored protein, specifically controls highly anisotropic expansion through its involvement in cellulose microfibril orientation. Plant Cell. **17,** 1749–1763.

Schena, M., Shalon, D., Davis, R.W., and Brown, P.O. (1995). Quantitative monitoring of gene expression patterns with a complementary DNA microarray. Science. **270,** 467–470.

Sedbrook, J.C., Carroll, K.L., Hung, K.F., Masson, P.H., and Somerville, C.R. (2002). The *Arabidopsis* SKU5 gene encodes an extracellular glycosyl phosphatidylinositol-anchored glycoprotein involved in directional root growth. Plant Cell. **14,** 1635–1648.

Somerville, C., et al. (2004). Toward a systems approach to understanding plant cell walls. Science. **306,** 2206–2211.

Srinivasasainagendra, V., Page, G.P., Mehta, T., Coulibaly, I., and Loraine, A.E. (2008). CressExpress: a tool for large-scale mining of expression data from *Arabidopsis*. Plant Physiol. **147,** 1004–1016.

Steinhauser, D., Usadel, B., Luedemann, A., Thimm, O., and Kopka, J. (2004). CSB.DB: a comprehensive systems-biology database. Bioinformatics. **20,** 3647–3651.

Sterling, J.D., Atmodjo, M.A., Inwood, S.E., Kumar Kolli, V.S., Quigley, H.F., Hahn, M.G., and Mohnen, D. (2006). Functional identification of an *Arabidopsis* pectin biosynthetic homogalacturonan galacturonosyltransferase. Proc. Natl Acad. Sci. U S A. **103,** 5236–5241.

Stuart, J.M., Segal, E., Koller, D., and Kim, S.K. (2003). A gene-coexpression network for global discovery of conserved genetic modules. Science. **302,** 249–255.

Tamura, K., Dudley, J., Nei, M., and Kumar, S. (2007). *MEGA4*: Molecular Evolutionary Genetics Analysis (MEGA) software version 4.0. Molecular Biology and Evolution. **24,** 1596–1599.

Toufighi, K., Brady, S.M., Austin, R., Ly, E., and Provart, N.J. (2005). The Botany Array Resource: e-Northerns, expression angling, and promoter analyses. Plant J. **43,** 153–163.

van Noort, V., Snel, B., and Huynen, M.A. (2004). The yeast coexpression network has a small-world, scale-free architecture and can be explained by a simple model. EMBO Rep. **5,** 280–284.

Xu, S.L., Rahman, A., Baskin, T.I., and Kieber, J.J. (2008). Two leucine-rich repeat receptor kinases mediate signaling, linking cell wall biosynthesis and ACC synthase in *Arabidopsis*. Plant Cell. **20,** 3065–3079.

Zhang, L.V., King, O.D., Wong, S.L., Goldberg, D.S., Tong, A.H., Lesage, G., Andrews, B., Bussey, H., Boone, C., and Roth, F.P. (2005). Motifs, themes and thematic maps of an integrated Saccharomyces cerevisiae interaction network. J. Biol. **4,** 6.

Zimmermann, P., Hirsch-Hoffmann, M., Hennig, L., and Gruissem, W. (2004). GENEVESTIGATOR. *Arabidopsis* microarray database and analysis toolbox. Plant Physiol. **136,** 2621–2632.

Identification of a cellulose synthase-associated protein required for cellulose biosynthesis

Ying Gu[a,1], Nick Kaplinsky[b], Martin Bringmann[c], Alex Cobb[d], Andrew Carroll[a,e], Arun Sampathkumar[c], Tobias I. Baskin[d], Staffan Persson[c], and Chris R. Somerville[a,2]

[a]Energy Biosciences Institute, University of California, Berkeley, CA 94720; [b]Department of Biology, Swarthmore College, Swarthmore, PA 19081; [c]Max-Planck-Institute for Molecular Plant Physiology, 14476 Potsdam, Germany; [d]Biology Department, University of Massachusetts, Amherst, MA 01003; and [e]Department of Biology, Stanford University, Stanford, CA 94305

Contributed by Chris R. Somerville, May 24, 2010 (sent for review May 8, 2010)

Cellulose synthase-interactive protein 1 (CSI1) was identified in a two-hybrid screen for proteins that interact with cellulose synthase (CESA) isoforms involved in primary plant cell wall synthesis. CSI1 encodes a 2,150-amino acid protein that contains 10 predicted Armadillo repeats and a C2 domain. Mutations in *CSI1* cause defective cell elongation in hypocotyls and roots and reduce cellulose content. CSI1 is associated with CESA complexes, and *csi1* mutants affect the distribution and movement of CESA complexes in the plasma membrane.

cell walls | CESA complexes | cell expansion | microtubules | polysaccharides

Cellulose is synthesized at the plasma membrane by hexameric protein complexes with a diameter of 25–30 nm when observed by freeze-fracture electron microscopy in algae, moss, and vascular plants (1–4). The only known component of the complexes is cellulose synthase (CESA), which is represented by 10 isoforms in *Arabidopsis* (5). Genetic studies indicate at least three *Arabidopsis* CESA isoforms are required for primary cell wall synthesis (6, 7). Lesions in CESA1 (*rsw1*), CESA3 (*cev1*), or CESA6 (*prc1*) lead to a deficiency in elongation in dark-grown seedlings (8–10). Genetic and biochemical studies demonstrating interactions between CESAs led to a heteromeric model of cellulose synthesis (11, 12) in which the complexes are composed of at least three functionally nonredundant CESA isoforms. It generally is accepted that in *Arabidopsis* CESA1, CESA3, and CESA6 or CESA6-like proteins are required for functional primary cell wall complexes, whereas CESA4, CESA7, and CESA8 are required for functional secondary cell wall complexes. However, the exact number of CESA proteins contained within the complex, their stoichiometry, and their specific interactions are unknown, and no other components of the complex have been reported.

Recent advances in cell biology and microscopy allow imaging of CESA complexes in live tissues. At least two of the three primary CESAs (CESA3 and CESA6) are functional when labeled with GFP and its derivatives. Both GFP-CESA3 and YFP-CESA6 were observed at the plasma membrane as discreet particles that move along linear trajectories coincident with underlying cortical microtubules (7, 13). CESA particles move bidirectionally with an average velocity of about 350 nm/min corresponding to the addition of ~700 glucose residues per glucan chain per minute (13). CESA particle dynamics are sensitive to osmotic stress and to several drugs that affect cytoskeleton and cellulose synthesis. The observation that perturbation of microtubule polymerization by oryzalin affects the overall distribution and motility of CESA particles supports models in which the microtubules guide the deposition of cellulose. However, CESA particles appear to have an intrinsic level of organization that is evident when microtubules are completely depleted (13).

Genetic screens for mutants deficient in cellulose have implicated a number of proteins in the overall process of cellulose biosynthesis. Mutations in *KORRIGAN* (*KOR*), which encodes an endo-β-1,4-glucanase, exhibit deficiencies in cell elongation and reduced cellulose production (14). KOR-like proteins from *Brassica napus* and poplar exhibit cellulase activity in vitro. However, the exact role of cellulase in cellulose synthesis is unknown. Additional cellulose-deficient mutants include *cobra*, *kobito*, *pom1*, *rsw3*, *fragile fiber1*, and *fragile fiber2*, none of which has been assigned a clear mechanistic function in cellulose synthesis. Here we report the identification of a protein involved in cellulose synthesis that appears to be associated with primary CESA complexes. Identification of this protein opens an avenue in ongoing efforts to understand the mechanism of cellulose synthesis.

Results

Cellulose Synthase-Interactive Protein 1 Interacts with Multiple Primary CESAs. To explore whether additional proteins may be required for cellulose biosynthesis, we performed yeast two-hybrid screens to identify proteins that physically interact with CESA1, -3, and -6. Using 541 amino acids of the putative catalytic domain of CESA6 as bait, we identified a protein referred to as "cellulose synthase-interactive protein 1" (CSI1; At2g22125) (Fig. 1*A*). To confirm the interaction of CESA6 and CSI1, we subcloned the prey into a GAL4 activation domain (GAL4-AD) and fused the putative catalytic domain of CESA6 with GAL4 binding domain (GAL4-BD). Coexpression of these constructs in yeast resulted in the appearance of β-galactosidase (GUS) activity, confirming the interaction between CESA6 and CSI1. CESA1 and CESA3 also showed positive interactions with CSI1, although the CESA3 interaction appeared to be weaker than the CESA1 or CESA6 interaction (Fig. 1*B*).

CSI1 was identified previously as one of the genes that is coregulated transcriptionally with the primary *CESA*s (15). In addition to *CSI1*, several genes that affect cellulose deposition, including *COBRA* and *CTL1*/*POM1*, also are coexpressed with the *CESA* genes (Fig. 1*C*). Consistent with coexpression analysis, transgenic plants in which *GUS* was placed under the control of the 1.4-kb promoter region upstream of the *CSI1* gene exhibited a pattern of GUS activity (Fig. 1 *D*, *F*, and *H* and Fig. S1) similar to that seen with promoter:GUS fusions of primary wall *CESA* genes (Fig. 1 *E*, *G*, and *I*). In addition, the *CSI1* promoter drives GUS expression in floral tissues, rosette leaves, roots, and pollen (Fig. S1), indicating that the *CSI1* expression pattern is similar to that of *CESA*s throughout development.

Author contributions: Y.G., N.K., M.B., A. Cobb, A. Carroll, T.I.B., S.P., and C.R.S. designed research; Y.G., N.K., M.B., A. Cobb, A. Carroll, and A.S. performed research; A. Cobb contributed new reagents/analytic tools; Y.G., N.K., M.B., A. Cobb, A. Carroll, A.S., T.I.B., S.P., and C.R.S. analyzed data; and Y.G., N.K., M.B., A. Cobb, A. Carroll, A.S., T.I.B., S.P., and C.R.S. wrote the paper.

The authors declare no conflict of interest.

[1]Present address: Department of Biochemistry and Molecular Biology, Pennsylvania State University, University Park, PA 16802.

[2]To whom correspondence should be addressed. E-mail: crs@berkeley.edu.

This article contains supporting information online at www.pnas.org/lookup/suppl/doi:10.1073/pnas.1007092107/-/DCSupplemental.

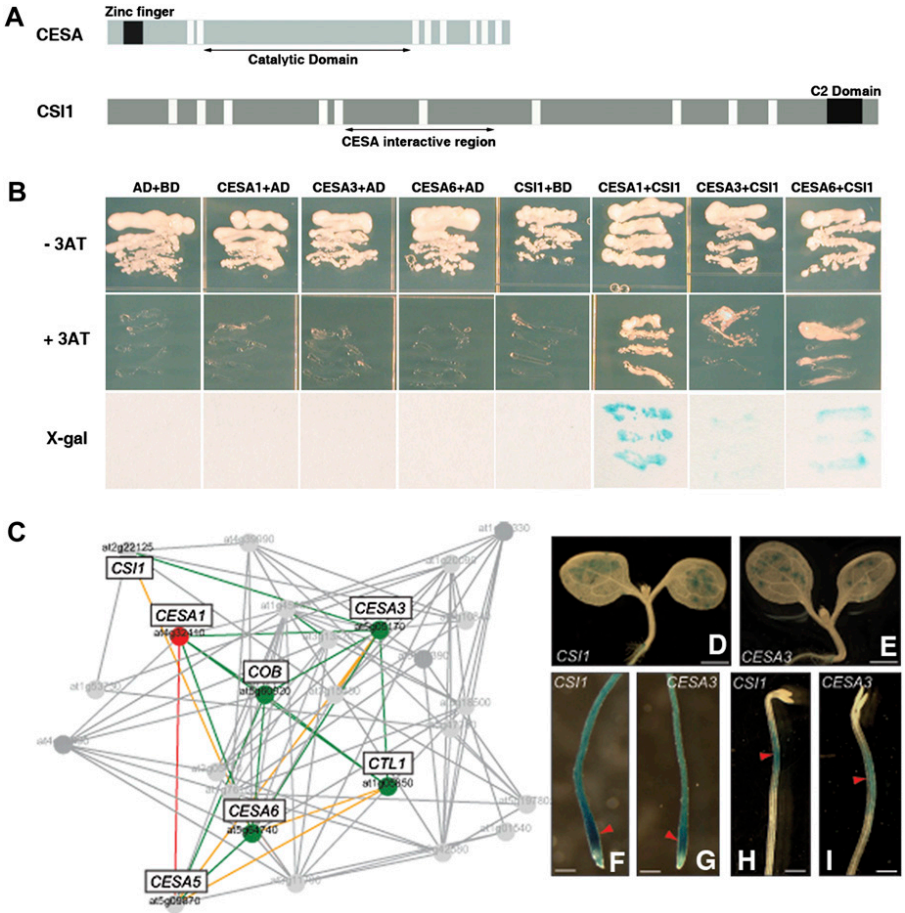

Fig. 1. Identification of CSI1. (*A*) Schematic representation of CESA and CSI1 proteins. White bars represent predicted transmembrane domains and ARM repeats in CESA and CSI1, respectively. The regions of the proteins used for the two-hybrid interaction tests are shown as arrows below the bars representing the proteins. (*B*) CSI1 interacts with three primary CESA proteins in yeast. CSI1 fused with GAL4-AD specifically interacted with the central catalytic domain of three primary CESAs fused with GAL4-BD. (*C*) Truncated coexpression network for primary wall cellulose-related genes using the AraGenNet at http://aranet.mpimp-golm.mpg.de/aranet/AraGenNet (29). Colored lines indicate strength of transcriptional coordination: green, mutual rank ≤10; orange, mutual rank ≤20; red, mutual rank ≤30. Connections of moderate interest for the study are shown in gray. Low mutual rank indicates stronger coexpression relationships. (*D–I*) Promoter GUS analysis of *CSI1::GUS* (*D*, *F*, and *H*) and *CESA3::GUS* (*E*, *G*, and *I*). GUS staining pattern is shown in light-grown seedlings (*D* and *E*) and etiolated seedlings (*F–I*). Red arrows indicate strong GUS activity. (Scale bars: 750 μm in *D* and *E* and 200 μm in *F–I*.)

***CSI1* Encodes an Armadillo Repeat-Containing Protein.** Protein sequence homology searches identified *CSI1*-related sequences in a variety of dicots, monocots, and the moss *Physomitrella patens* (Fig. S2). The *Arabidopsis* genome contains two closely related genes, which we refer to as "*CSI2*" and "*CSI3*" and which share about 55% sequence similarity with CSI1. No CSI1-like proteins were identified outside the land plants. The CSI protein contains multiple tandem copies of a degenerate protein sequence motif, the armadillo (ARM) repeat. The ARM repeat is an ≈40-aa long, tandemly repeated sequence first identified in the Drosophila segment polarity gene, *armadillo* (16). ARM repeats are found in more than 240 proteins which are predicted to share a conserved 3D structure and often participate in protein–protein interactions (17–19). CSI1 also contains a C2 domain at its C terminus. Some C2 domains have been shown to bind phospholipids in a calcium-dependent or -independent manner and are involved in targeting proteins to cell membranes (20, 21). Other C2 domains have been shown to mediate protein–protein interactions (22).

***csi1* Mutants Have Defects in Expansion.** To investigate the biological function of CSI1, we analyzed six independent homozygous transfer DNA (T-DNA) insertion lines with insertions in either exons or introns of *CSI1* from the Salk Institute Genomic Analysis Laboratory (SIGnAL) collection (Fig. 2*A*) (23). At least five of the lines probably were null alleles for *CSI1*, because no *CSI1* mRNA was detectable by RT-PCR (Fig. S3*A*). Hypocotyls in etiolated *csi1* mutants were ≈30% shorter and ≈80% wider than in wild-type plants (Fig. 2 *B*, *C*, and *E*) and elongated less rapidly than in wild-type but more quickly than in *prc1-1* (a CESA6 mutant) plants (Fig. 2*D*). The reduced hypocotyl length and increased diameter indicate that *csi1* mutants have defects in the control of anisotropic expansion (highlighted cells in Fig. 2*E*). The etiolated seedlings of *csi1* alleles had a 50% reduction in crystalline cellulose (Fig. 2*F*). Several cellulose-deficient mutants, such as *cob-6*, *ctl1*/*pom1*, and *kor1*, display similar cell elongation phenotypes (14, 24, 25).

csi1 mutants also exhibited short, and swollen, seedling roots. In 8-d-old light-grown seedlings, roots in *csi1* mutants were ≈25% shorter than in wild-type plants (Fig. S3 *B* and *C*). The roots in *csi1* mutants also exhibited epidermal cell swelling and were 80% wider than wild-type roots (Fig. S3 *D–F*). Additionally, adult *csi1* mutants were dwarfed and had shorter siliques than wild-type plants (Fig. S3*G*). To test whether the smaller siliques were caused by partial sterility, we conducted reciprocal backcrosses to wild-type plants using heterozygous plants. The progeny of these crosses clearly showed that the transmission of the *csi1* allele occurred at much lower frequency from the male gametophytes than from the female, indicating that the reduced

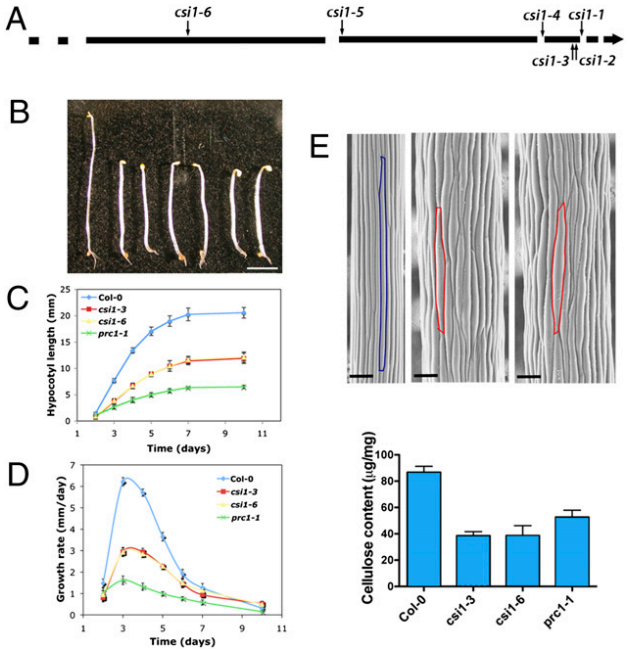

Fig. 2. CSI1 is required for normal cell expansion. (*A*) Schematic representation of six T-DNA insertion sites in *csi1*. Exons are represented by black lines, and introns are shown by breaks. (*B*) Morphology of 4-d-old dark-grown seedlings: (*Left* to *Right*) Col-0 (wild-type) and *csi1-1*, *csi1-2*, *csi1-3*, *csi1-4*, *csi1-5*, and *csi1-6* mutants. (Scale bar: 2 mm.) (*C* and *D*) Hypocotyl length (*C*) and growth rate (*D*) of dark-grown wild-type (Col-0) plants and *csi1-3*, *csi1-6*, and *prc1-1* mutants. Data were collected from the measurement of ~50 seedlings for each genotype. Error bars represent SE (absent error bars were obscured by symbols). (*E*) SEM of dark-grown hypocotyls in wild-type plants and *csi1* mutants: (*Left* to *Right*) *Arabidopsis thaliana* Columbia (Col-0), *csi1-3*, and *csi1-6* mutants. Colors outline one epidermal cell. (Scale bar: 100 μM.) (*F*) Cellulose content was reduced in *csi1* mutants. $n = 5$. Error bars represent SE.

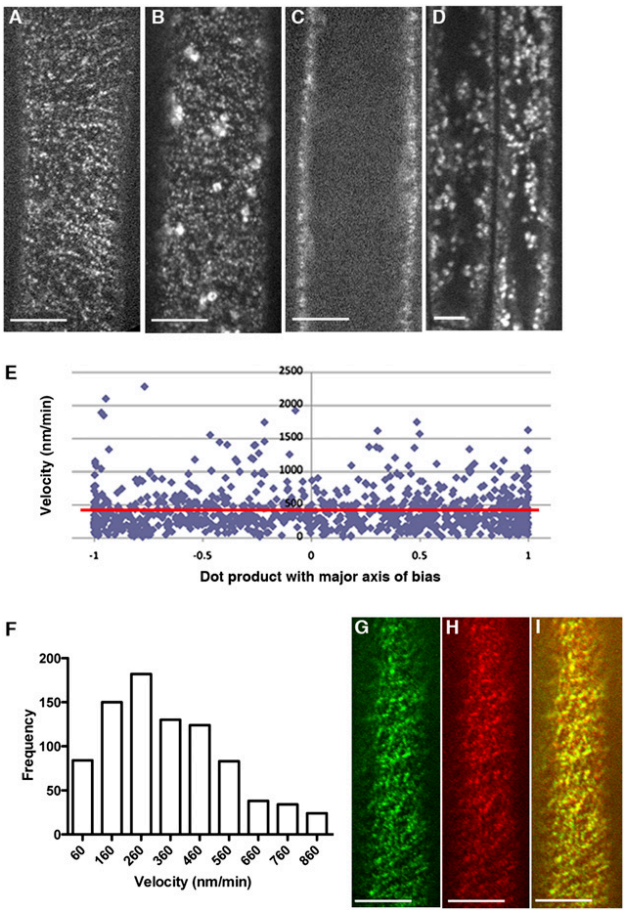

Fig. 3. CSI1 is localized to CESA-like particles in dark-grown hypocotyls cells. (*A–D*) Optical sections of epidermal cells in 3-d-old dark-grown hypocotyls expressing RFP-CSI1 (*A* and *C*) and YFP-CESA6 (*B* and *D*). Focal planes of the plasma membrane (*A* and *B*) and lower cortex (*C* and *D*) are shown. (Scale bar: 5 μm.) (*E*) Plot of RFP-CSI1 particle velocity vs. its dot product (i.e., scalar product; see *Methods*) with the direction of bias. Red line indicates the linear regression of the plot. A slope of 0 indicates no bias in direction. (*F*) Histogram of measured RFP-CSI1 particle velocities. The mean is 416 nm/min ($n = 917$). (*G–I*) Localization of GFP-CESA3 (*G*), RFP-CSI1 (*H*), and merge (*I*). (Scale bar: 5 μm.)

fertility of *csi1* mutants was caused mainly by pollen defects (Table S1). Therefore, we examined the surface structure of the mature pollen grains by SEM. Although all wild-type pollen grains displayed typical morphology, very few typical pollen grains were observed in the *csi1* alleles. Instead, the majority of the *csi1* pollen grains displayed irregular or collapsed cell wall morphologies (Fig. S3 *I* and *K*). Similar observations also have been reported for null alleles of *CESA1* and *CESA3* (6).

CSI1 Is Associated with CESA Complexes. To investigate the subcellular localization of CSI1, we generated both N- and C-terminal translational fusions of red fluorescent protein (RFP) to the CSI1 protein under the native *CSI1* promoter in the *csi1-6*–mutant background. Both N- and C-terminal constructs complemented the mutant phenotypes of reduced hypocotyl elongation and reduced expansion anisotropy, indicating that the fusion protein was functional (Fig S4). Observation of epidermal cells in dark-grown hypocotyls by spinning disk confocal microscopy revealed that RFP-CSI1 was detected as distinct particles at the plasma membrane (Fig. 3*A* and Movie S1). Similar to YFP-CESA6, RFP-CSI1 particles were organized into linear arrays. To assess whether RFP-CSI1 particles move bidirectionally like those of YFP-CESA6, directional bias was analyzed by calculating the dot product of each particle relative to the dominant axis of potential particle bias and correlating this dot product with the velocity of each particle (Fig. 3*E*). Greater differences between particle velocities going with and against the major axis result in a larger slope in a linear regression of the plot. As seen in Fig. 3*E*, RFP-CSI1 particles ($n = 917$) travel bidirectionally with no bias relative to the major axis. The average velocity of RFP-CSI1 particles in epidermal cells in dark-grown hypocotyls was 416 nm/min (range 63–860 nm/min; Fig. 3*F*). The velocity of RFP-CSI1 is similar to that reported for YFP-CESA6 (13). Unlike YFP-CESA6, which is associated with the Golgi complex in addition to the plasma membrane (Fig. 3 *B* and *D*) (13), RFP-CSI1 was not detected in the cytoplasmic compartments (Fig. 3*C*). In plants containing both GFP-CESA3 and RFP-CSI1, the RFP-CSI1 particles were substantially colocalized with GFP-CESA3 (Fig. 3 *G–I*).

Lesions in *csi1* Affect the Distribution and Motility of YFP-CESA6. To monitor the dynamics of CESA complexes in *csi1* mutants directly, we introduced a homozygous *csi1-3* allele into a YFP-CESA6 line (13). Using the YFP-CESA6 marker, CESA complexes can be observed at the plasma membrane as distinct punctuate particles that move at constant rates along linear tracks (13). Although the CESA particles in the plasma membranes of wild-type (control) epidermal cells were organized into linear arrays, the distribution of the CESA particles appeared to be disorganized in plasma membranes of the *csi1-3* background (Fig. 4*C* and Movie S2). In contrast, CESA particles in the internal cell layers were not affected in *csi1-3* mutants. We did not observe any significant differences in

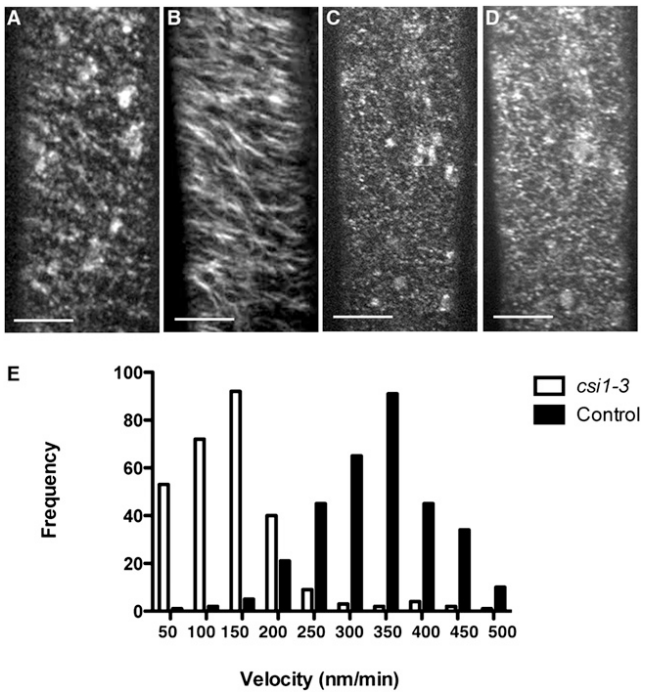

Fig. 4. YFP-CESA6 dynamics are altered in *csi1-3* mutants. YFP-CESA6 localization in dark-grown hypocotyls cells is shown in wild-type plants (*A* and *B*) and *csi1-3* mutants (*C* and *D*). (*A*) A single optical section acquired at the plane of plasma membrane in wild-type plants. (*B*) Average of 61 frames (duration: 2 min; 2-s interval) showing movement of labeled particles along linear trajectories. (*C*) Single optical section of YFP-CESA6 in *csi1-3* mutant. (*D*) Average of 61 frames (duration: 2 min; 2-s interval) in *csi1-3* mutant. (Scale bars: 5 μm.) (*E*) Histogram of measured particle velocities. The mean velocity is 365 nm/min in control plants (n = 318) and 132 nm/min in *csi1-3* mutants (n = 225).

the distribution or motility of CESA particles associated with the Golgi complex in *csi1-3* mutants compared with control lines (Golgi in the *csi1-3* mutants moved at 6021 ± 405 nm/min vs. 5214 ± 982 nm/min in wild-type plants). In control cells, CESA particles associated with the plasma membrane migrated with an average velocity of 365 ± 45 nm/min (n = 318). In *csi1-3* mutants, however, the average velocity of CESA particles was reduced to 132 ± 52 nm/min (n = 225; Fig. 4*E*). These observations are reflected clearly in time-averaged projections of the CESA particles (Fig. 4 *B* and *D*). In control cells, motile particles form linear trajectories along the axes of the particle arrays. Although CESA particles still move bidirectionally in *csi1-3* mutants (as assessed by Imaris software), linear tracks in time-averaged images were much shorter.

Uniformity of Cellulose Microfibrils Is Affected in *csi1* Mutants. To investigate effects of the *csi* mutations on the arrangement of cellulose microfibrils, we observed the longitudinal cell walls of wild-type and *csi1-1* roots using circularly polarized light enhanced with the universal compensator (26). Polarized light can be used to assay the abundance and orientation of cellulose microfibrils because of their partial crystallinity. Overall, the cell walls appeared similar in both genotypes (Fig. 5 *A* and *B*). To determine whether there was a quantitative difference in microfibril abundance or orientation, we quantified the retardance of the cell walls and the azimuth of the crystalline elements. The average retardance was about 1 nm, similar to that reported previously for *Arabidopsis* cell walls (27), and there was no significant difference between the genotypes in the three delineated zones of the root (Fig. 5*C*). Similarly, in the three root zones of both genotypes, the azimuths averaged to 90° transverse to the long axis of the root. However, for the elongation and mature zones, the variability among azimuth measurements made in individual roots was significantly greater in *csi1-1* mutants than in wild-type roots, suggesting that microfibril alignment in these cell walls had become less uniform.

Discussion

The CSI1 protein is the first non-CESA protein associated with CESA complexes. Several lines of evidence led us to hypothesize that CSI1 exerts a direct effect on cellulose synthesis through its association with CESA complexes. First, CSI1 physically interacts with multiple primary CESAs in yeast two-hybrid assays, and CSI1 is transcriptionally coregulated with several of the *CESA* genes involved in primary cell wall synthesis, but there was no obvious association with CESAs involved in secondary cell wall synthesis. Additionally, CSI1 colocalizes with primary CESA complexes, and *csi1* mutations affect the distribution and movement of CESA complexes, resulting in strongly reduced rates of CESA complex movement. If we assume that the length of cellulose microfibrils is affected by the velocity and lifetimes of CESA particles, the cellulose deficiency and the associated swelling phenotype can be attributed to the effect of the *csi1* mutations on the activity of the CESA complexes. Additionally, the *csi1* mutations appeared to decrease the degree to which cellulose microfibrils are coaligned. Polarized light is sensitive to the azimuth at which the optical axis of the crystalline sample is oriented. In both *csi1* mutants and wild-type roots the average azimuth of cellulose microfibrils was transverse to the long axis of the root. However, the SD of the azimuth measurements was larger in *csi1* mutants than in wild-type roots. In other words, microfibril alignment, on a scale greater than that of a wavelength, is noisier in *csi1* mutants than in wild-type roots. A similar reduction in the uniformity of microfibril alignment across the root has been reported for treatment with low concentrations of the microtubule inhibitor oryzalin (27). The decrease in cellulose organization in *csi1* mutants indicates that CSI1 may participate in the mechanisms responsible for organizing the deployment of cellulose microfibrils in primary walls.

CSI1 belongs to a family of highly conserved land plant-specific proteins. CSI1 contains multiple predicted ARM repeats and a single C2 domain. Three-dimensional structures of previously characterized ARM repeats comprise three α helices. For example, yeast importin-α contains a central region of 442 aa that contains 10 ARM repeats of 42 aa, forming a right-handed superhelix of helices that creates a surface for protein–protein interactions (18). By comparison, CSI1 has 10 predicted ARM repeats distributed unevenly across the entire protein (2,151 aa). We are not able to draw direct structural comparisons between CSI1 and other proteins containing ARM repeats.

Methods

Plant Materials and Growth Conditions. *Arabidopsis thaliana* Columbia (Col-0) seeds were sterilized and germinated on Murashinge and Skoog plates (1/2 × MS salts, 0.8% agar, 0.05% monohydrate 2-(N-Morpholino) ethanesulfonic acid, pH 5.7). Seedlings were grown vertically on the agar at 22 °C in darkness for 3 d before imaging. For soil-grown plants, seedlings were germinated on MS plates containing 1% sucrose and then were transferred to pots in a greenhouse at 22 °C under 16-h light and 8-h dark.

Yeast Two-Hybrid Assay. The yeast two-hybrid screen was carried out by Hybrigenics. CSI1 was identified as a CESA6-interactive protein. To confirm the interaction between CSI1 and CESA6, we subcloned the prey fragment into pACTII (28). The catalytic domains of CESA1, CESA3, and CESA6 were cloned into pAS1-CYH2 (28) using primers indicated in Table S2. The resulting constructs were cotransformed into yeast strain Y190 as pairs (Fig. 1*B*). Transformants were selected on SC-Trp-Leu-His plates. Positive interactions were tested by their ability to grow on SC-Trp-Leu-His plates

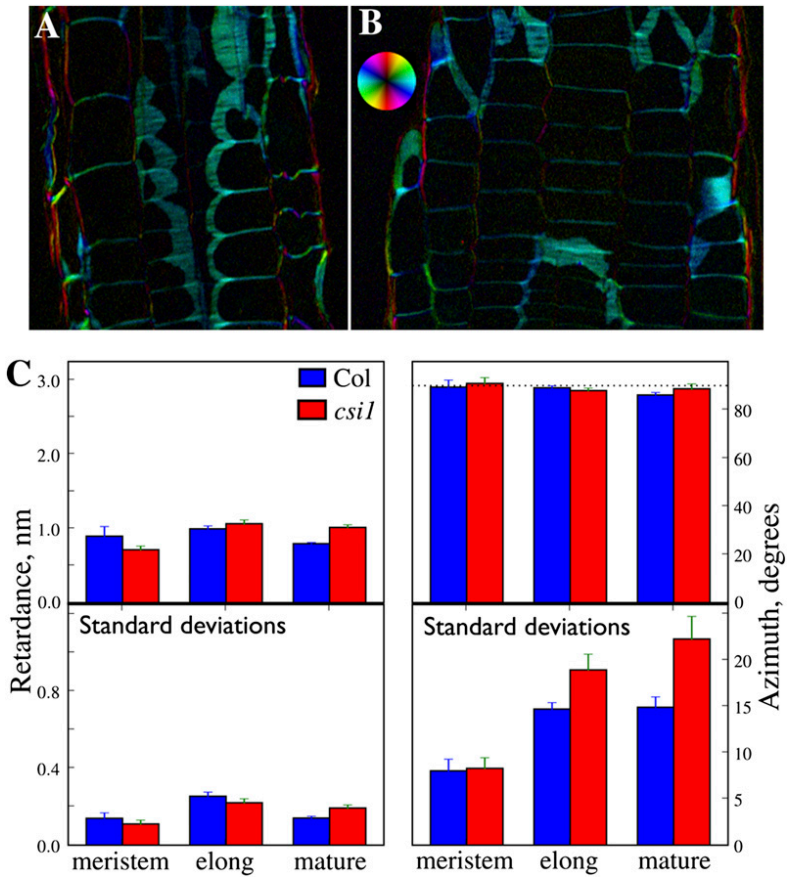

Fig. 5. Polarized light analysis of *csi1* mutants. (*A* and *B*) Polarized-light micrographs of (*A*) wild-type and (*B*) *csi1-1*-mutant roots. Images are of longitudinal-tangential sections through cortex and epidermis. Intensity is proportional to retardance, and color represents optical axis (azimuth) of the crystalline elements, as shown by the color wheel. Note the similar intensity and color for the two genotypes. (*C*) Quantification of retardance and azimuth (90° is transverse to the root's long axis). Top panels show means ± SEM ($n = 3$ roots); bottom panels show the average SD ($n \sim 200$ measurements) ± SEM for each of the roots. Note the larger SDs for *csi1-1* mutants in the elongation and mature zones.

supplemented with 100 mM 3-aminotriazole (Sigma) and for GUS activity using a filter assay.

Coexpression Analysis. A coexpression network for *CSI1* (Cluster 86) was obtained from AraGenNet at http://aranet.mpimp-golm.mpg.de/aranet/AraGenNet (29) and trimmed to facilitate readability.

GUS Construct and Staining. A genomic DNA fragment (1.4 kb) upstream from the ATG start codon of *CSI1* was cloned into pCAMBIA1305 GUS-Plus (Table S2) using BamHI and NcoI. The construct was transformed into *Arabidopsis* using *Agrobacterium*-mediated transformation. Transgenic plants were selected on hygromycin, stained for GUS activity in 100 mM sodium phosphate (pH 7.0), 10 mM EDTA, 1 mM ferricyanide, 1 mM ferrocyanide, and 1 mM 5-bromo-4-chloro-3-indolyl β-D-glucuronic acid at 37 °C, cleared in 70% ethanol, and observed under a Leica MZ12.5 stereomicroscope (Leica DFC420 digital camera).

Construction of Transgenic Lines. A 35S promoter in pH7WGR2 and pH7RWG2 (30) was replaced with a 3-kb promoter of CSI1 using Spe I and SacI to create construct pYG104 and pYG105, respectively. The full-length coding sequence of CSI1 (accession # NM_12781.4) synthesized by DNA 2.0 was introduced into pYG104 and pYG105 using Gateway LR Clonase II (Invitrogen). The verified constructs (pYG106 and pYG107) then were introduced into *csi1-6* by *Agrobacterium*-mediated transformation. Complemented lines were selected for further analysis.

Cellulose Measurement. Cellulose was measured from 4-d-old etiolated seedlings using the Updegraff method (31). Data were collected from five technical replicates for each tissue sample.

Microscopy. Anthers from 5-wk-old plants or hypocotyls of 4-d-old dark-grown seedlings were mounted on stubs under a pressure of 50 Pa in an Hitachi TM-1000 scanning electron microscope. Roots of 8-d-old light-grown seedlings were wet-mounted on slides and viewed and photographed with a Leica DM5000B epifluorescence microscope (JH Technology). ImageJ software (W. Rasband, National Institute of Health, Bethesda, MD) was used for measurement of hypocotyls and root length. Whole 5-d-old seedlings were viewed on MS plates using a Leica MZ12.5 stereomicroscope (Leica DFC420 digital camera).

Polarized Light Analysis. Roots were prepared for polarized light analysis as described previously (27). Briefly, root tips were cryofixed in liquid propane, freeze-substituted in ethanol, embedded in butyl-methyl-methacrylate, and sectioned at 2-μm thickness. Sections were imaged on an Interphako polarized-light microscope (Zeiss) equipped with an LC Polscope quantification system (Cambridge Research Instruments) implementing the universal compensator (26). This instrument operates in circularly polarized light and generates two images. The intensity of each pixel is proportional to birefringent retardance in the first image and to the azimuth of the optical axis of the crystalline elements in the second image. For display (Fig. 5) the two images are superimposed with pixel intensity giving retardance and color giving azimuth. Measurements were taken from subcellular areas of cell wall in cortex and epidermis, as viewed in longitudinal sections. Approximately 20 sections per root and three roots per genotype were measured. For analysis, the root was divided into meristem, elongation, and mature zone based on cell length. Azimuth was defined with respect to the local midline (longitudinal axis) of the root.

To assess the statistical significance of the polarized light observations, circular statistical techniques were used (32). Specifically, microfibril orientation was expressed as a unit vector corresponding to the doubled azimuth angle; to obtain the mean orientation, this unit vector was averaged over

each observation zone, and the result was halved. The angular deviation was calculated as half the (nonnegative) angular distance between the unit vectors for an individual patch, *a*, and the mean, *b*: arccos [cos (*a* − *b*)]. Zone-wise mean angular deviations of microfibrils were compared between genotypes using a Mann–Whitney U test, similar to the approach used to compare sample angular deviations reported by Wallraff (32). The distribution of zone mean angular deviations was skewed right, but the distribution became approximately normal after log transformation. Therefore, logarithms of mean angular deviations also were compared using an independent sample *t* test. The results of the *t* test on log-transformed data and the *u* test were the same.

Isolation of T-DNA Insertion Line. The identification of *csi1* knockout lines from the SIGnAL (Salk Institute Genomic Analysis Laboratory; http://signal.salk.edu/cgi-bin/tdnaexpress) collection was based on a combination of database searches and PCR amplification of T-DNA flanking regions. For T-DNA lines identified from the SIGnAL collection, seeds were obtained from the Arabidopsis Biological Resource Center (Ohio State University; http://www.biosci.ohio-state.edu/~plantbio/Facilities/abrc/abrchome.htm). PCR reactions were carried out to identify single plants for the T-DNA insertion. Primers used for T-DNA genotyping of *csi1* alleles are listed in Table S2.

Confocal Microscopy and Image Analysis. For analyses of microtubule dynamics, seeds were germinated on MS agar plates and grown vertically in darkness for 3 d at 22 °C. Seedlings were mounted between two coverslips in water. Imaging was performed on a Yokogawa CSUX1spinning disk system featuring the DMI6000 Leica motorized microscope (13) and a Leica 100×/1.4 NA oil objective. YFP was excited at 488 nm, and a band-pass filter (520/50 nm) was used for emission filtering. Image analysis was performed using Metamorph (Molecular Devices) and Imaris (Bitplane) software.

For Imaris analysis, the contrast was enhanced and normalized for each slice within a movie using ImageJ. The enhanced movie was processed in Imaris 6.2.1 from Bitplane. Automated particle detection was performed to find particles with a diameter of ∼230 nm, and tracks were generated over the lifetime of the particle. To filter noise in particle detection, only particles detected for 14 s (seven frames) were analyzed. The data for the total displacement and duration for each track in a movie were exported. Directional bias was analyzed by summing the vectors of all particles to determine the direction of greatest particle flux. The dot product of each particle's trajectory against this direction was calculated, and the velocity of each particle was plotted against its dot product. Greater differences between particle velocities going with and against the major axis result in a larger slope in a linear regression of this plot.

Database Search and Sequence Alignment. The predicted amino acid sequence of CSI1 (At2g22125) was retrieved from the Arabidopsis Information Resource (TAIR) database (www.arabidopsis.org). This protein sequence was used to identify full-length CSI1-like proteins in the National Center for Biotechnology Information GenBank protein database using BLASTP (www.ncbi.nlm.nih.gov/BLAST). CSI1-like proteins (Table S3) were aligned using ClustalW implemented in MegAlign (DNASTAR); protein alignments then were used to generate the phylogenetic tree of CSI1-like proteins (MegAlign; DNASTAR).

ACKNOWLEDGMENTS. We thank H. Höfte (INRA, Versailles, France) for providing GFPCESA3 line and S. Li and K. Hematy for helpful discussions. This work was supported in part by an award from The Balzan Foundation, Grants DE-FG02-03ER15421 (to T.I.B.) and DOE-FG02-03ER20133 (to C.R.S.) from the US Department of Energy, and the Energy Biosciences Institute. M.B., A.S., and S.P. were funded through the Max-Planck Gesellschaft.

1. Brown RM, Jr, Willison JH, Richardson CL (1976) Cellulose biosynthesis in *Acetobacter xylinum*: Visualization of the site of synthesis and direct measurement of the in vivo process. *Proc Natl Acad Sci USA* 73:4565–4569.
2. Mueller SC, Brown RM, Jr, Scott TK (1976) Cellulosic microfibrils: Nascent stages of synthesis in a higher plant cell. *Science* 194:949–951.
3. Giddings TH, Jr, Brower DL, Staehelin LA (1980) Visualization of particle complexes in the plasma membrane of *Micrasterias denticulata* associated with the formation of cellulose fibrils in primary and secondary cell walls. *J Cell Biol* 84:327–339.
4. Mueller SC, Brown RM, Jr (1980) Evidence for an intramembrane component associated with a cellulose microfibril-synthesizing complex in higher plants. *J Cell Biol* 84:315–326.
5. Somerville C (2006) Cellulose synthesis in higher plants. *Annu Rev Cell Dev Biol* 22: 53–78.
6. Persson S, et al. (2007) Genetic evidence for three unique components in primary cell-wall cellulose synthase complexes in Arabidopsis. *Proc Natl Acad Sci USA* 104: 15566–15571.
7. Desprez T, et al. (2007) Organization of cellulose synthase complexes involved in primary cell wall synthesis in *Arabidopsis thaliana*. *Proc Natl Acad Sci USA* 104: 15572–15577.
8. Fagard M, et al. (2000) PROCUSTE1 encodes a cellulose synthase required for normal cell elongation specifically in roots and dark-grown hypocotyls of Arabidopsis. *Plant Cell* 12:2409–2424.
9. Ellis C, Karafyllidis I, Wasternack C, Turner JG (2002) The Arabidopsis mutant *cev1* links cell wall signaling to jasmonate and ethylene responses. *Plant Cell* 14:1557–1566.
10. Arioli T, et al. (1998) Molecular analysis of cellulose biosynthesis in Arabidopsis. *Science* 279:717–720.
11. Taylor NG, Laurie S, Turner SR (2000) Multiple cellulose synthase catalytic subunits are required for cellulose synthesis in Arabidopsis. *Plant Cell* 12:2529–2540.
12. Scheible WR, Eshed R, Richmond T, Delmer D, Somerville C (2001) Modifications of cellulose synthase confer resistance to isoxaben and thiazolidinone herbicides in Arabidopsis *Ixr1* mutants. *Proc Natl Acad Sci USA* 98:10079–10084.
13. Paredez AR, Somerville CR, Ehrhardt DW (2006) Visualization of cellulose synthase demonstrates functional association with microtubules. *Science* 312:1491–1495.
14. Nicol F, et al. (1998) A plasma membrane-bound putative endo-1,4-β-D-glucanase is required for normal wall assembly and cell elongation in Arabidopsis. *EMBO J* 17: 5563–5576.
15. Persson S, Wei H, Milne J, Page GP, Somerville CR (2005) Identification of genes required for cellulose synthesis by regression analysis of public microarray data sets. *Proc Natl Acad Sci USA* 102:8633–8638.
16. Nüsslein-Volhard C, Wieschaus E (1980) Mutations affecting segment number and polarity in Drosophila. *Nature* 287:795–801.
17. Huber AH, Nelson WJ, Weis WI (1997) Three-dimensional structure of the armadillo repeat region of β-catenin. *Cell* 90:871–882.
18. Conti E, Uy M, Leighton L, Blobel G, Kuriyan J (1998) Crystallographic analysis of the recognition of a nuclear localization signal by the nuclear import factor karyopherin alpha. *Cell* 94:193–204.
19. Hatzfeld M (1999) The armadillo family of structural proteins. *Int Rev Cytol* 186: 179–224.
20. Davletov BA, Südhof TC (1993) A single C2 domain from synaptotagmin I is sufficient for high affinity Ca^{2+}/phospholipid binding. *J Biol Chem* 268:26386–26390.
21. Ochoa WF, et al. (2001) Structure of the C2 domain from novel protein kinase Cepsilon. A membrane binding model for $Ca^{(2+)}$-independent C2 domains. *J Mol Biol* 311:837–849.
22. Benes CH, et al. (2005) The C2 domain of PKCdelta is a phosphotyrosine binding domain. *Cell* 121:271–280.
23. Alonso JM, et al. (2003) Genome-wide insertional mutagenesis of *Arabidopsis thaliana*. *Science* 301:653–657.
24. Schindelman G, et al. (2001) COBRA encodes a putative GPI-anchored protein, which is polarly localized and necessary for oriented cell expansion in Arabidopsis. *Genes Dev* 15:1115–1127.
25. Zhong R, Kays SJ, Schroeder BP, Ye ZH (2002) Mutation of a chitinase-like gene causes ectopic deposition of lignin, aberrant cell shapes, and overproduction of ethylene. *Plant Cell* 14:165–179.
26. Oldenbourg R, Mei G (1995) New polarized light microscope with precision universal compensator. *J Microsc* 180:140–147.
27. Baskin TI, Beemster GT, Judy-March JE, Marga F (2004) Disorganization of cortical microtubules stimulates tangential expansion and reduces the uniformity of cellulose microfibril alignment among cells in the root of Arabidopsis. *Plant Physiol* 135: 2279–2290.
28. Kim J, Harter K, Theologis A (1997) Protein-protein interactions among the Aux/IAA proteins. *Proc Natl Acad Sci USA* 94:11786–11791.
29. Mutwil M, et al. (2010) Assembly of an interactive correlation network for the Arabidopsis genome using a novel heuristic clustering algorithm. *Plant Physiol* 152: 29–43.
30. Karimi M, Inzé D, Depicker A (2002) GATEWAY vectors for Agrobacterium-mediated plant transformation. *Trends Plant Sci* 7:193–195.
31. Updegraff DM (1969) Semimicro determination of cellulose in biological materials. *Anal Biochem* 32:420–424.
32. Batschelet E (1981) *Circular Statistics in Biology* (Academic, London), p 371.

Supporting Information

Gu et al. 10.1073/pnas.1007092107

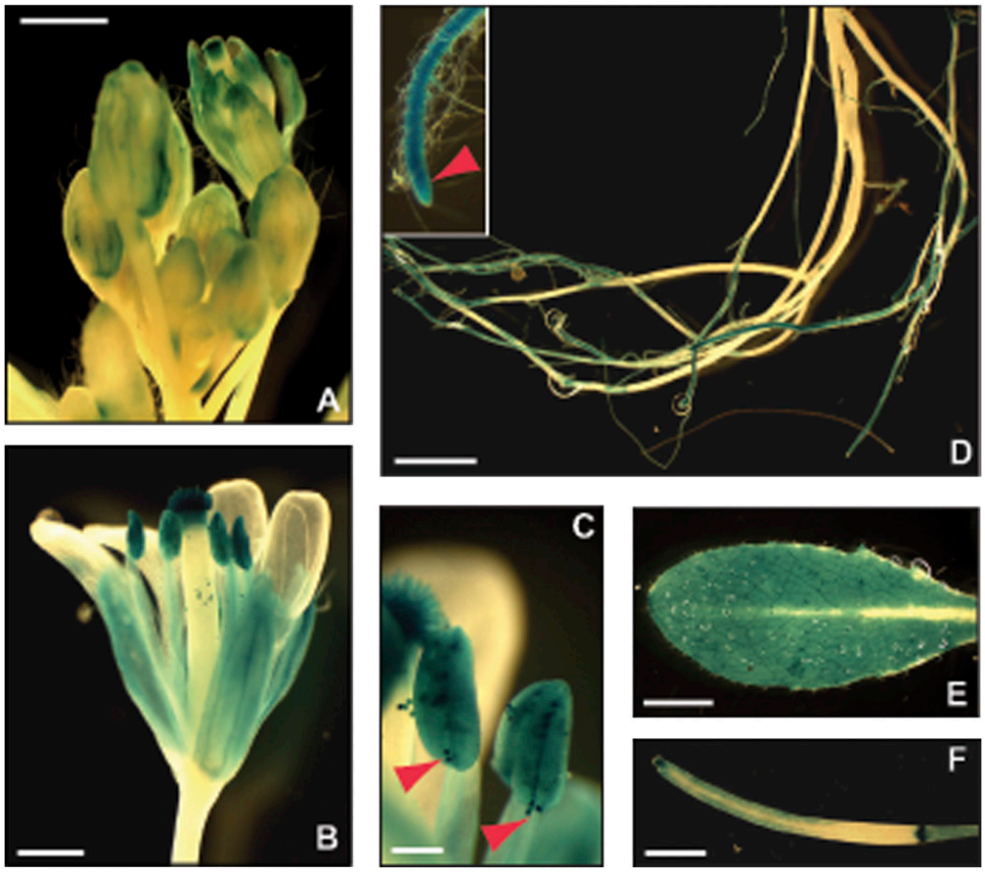

Fig. S1. *Cellulose synthase-interactive protein 1::β-glucuronidase (CSI1::GUS)* activity. Expression pattern of the *CSI1* genes assessed through *CSI1::GUS* construct lines. The GUS expression is indicated by blue. (*A* and *B*). *CSI1::GUS* activity during different developmental stages of flowers. (Scale bars: 1 mm in *A* and 400 μm in *B*.) (*C*) The *CSI1* promoter is active in pollen grains (red arrowheads). (Scale bar: 100 μm.) (*D*) Soil-grown roots from 6-wk-old plants expressing the GUS-construct for *CSI1*. *Inset* indicates GUS expression in the root tip and elongating cells (red arrowhead). (Scale bar: 2 mm.) GUS activity also was observed in rosette leaves (*E*) and in siliques (*F*). (Scale bars, 2 mm.)

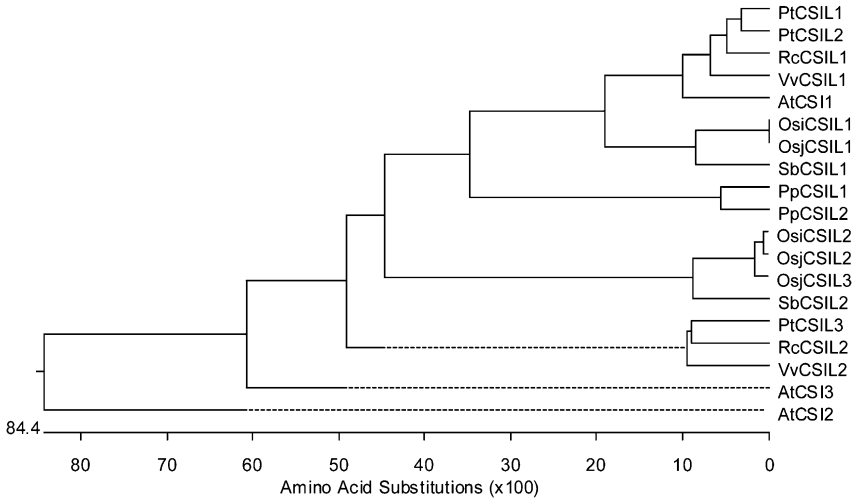

Fig. S2. Phylogeny of CSI protein in land plants. Full-length CSI-like sequences were identified in GenBank using BLASTP and aligned using ClustalW. Accessions used in this phylogeny tree are listed in Table S3.

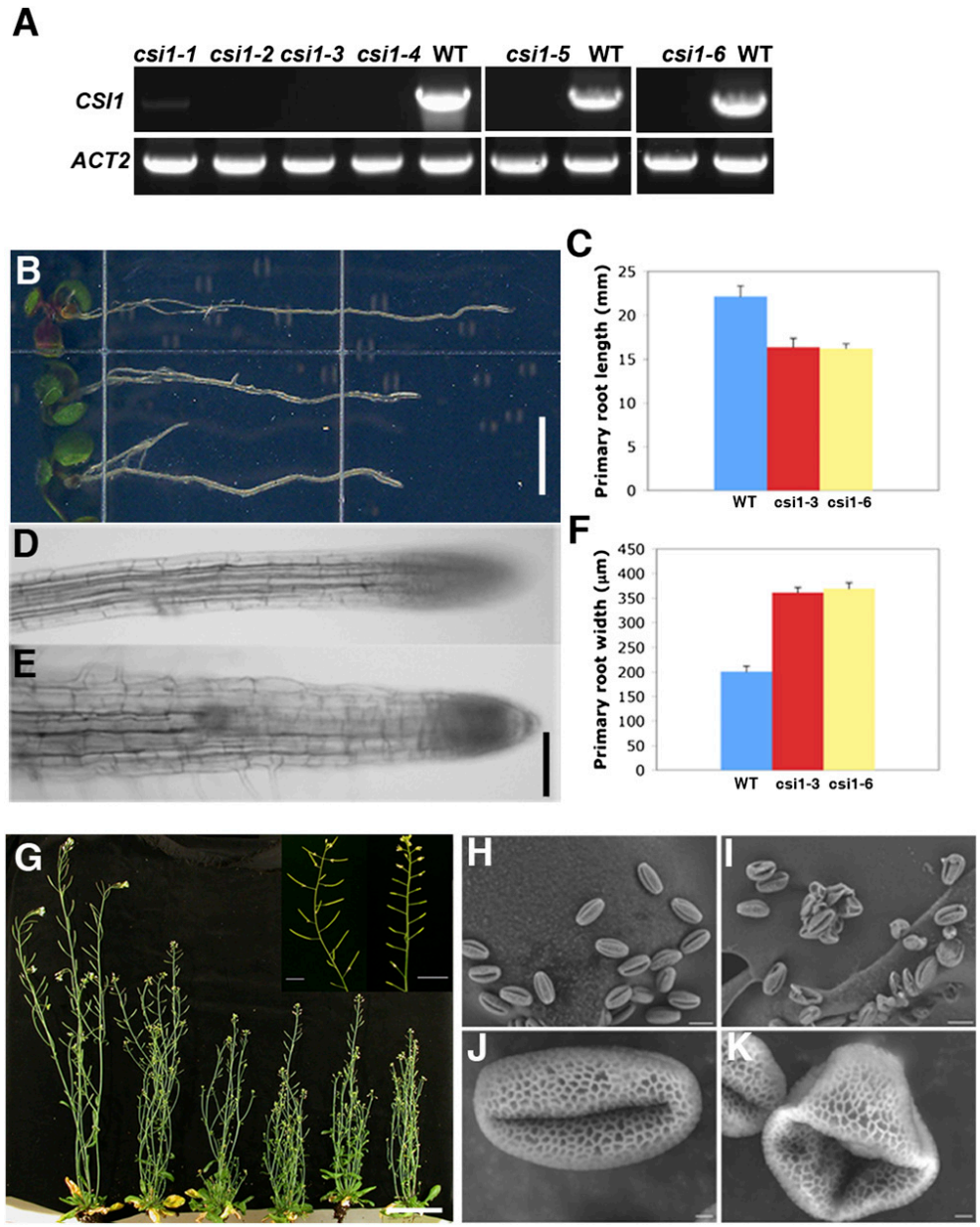

Fig. S3. Morphology of *csi1* mutants. (*A*) RT-PCR analysis of *CSI1* mRNA expression in various transfer DNA (T-DNA) insertion lines in 1-wk-old seedlings. ACTIN2 was used as control. WT, Columbia-0. (*B*) Eight-day-old Col-0 (*Top*), *csi1-3*–mutant (*Middle*), and *csi1-6*–mutant (*Bottom*) seedlings were grown on 1/2 MS supplemented with 1% sucrose. (Scale bar: 5 mm.) (*C*) Quantification of primary root length in Col-0, *csi1-3*–mutant, and *csi1-6*–mutant seedlings. Measurement data were collected from about 50 seedlings in each genotype. (*D* and *E*) High magnification of primary root morphology in Col-0 (*D*) and *csi1-3*–mutant plants (*E*). (Scale bar: 200 μm.) (*F*) Quantification of primary root width in Col-0, *csi1-3*–mutant, and *csi1-6*–mutant seedlings. Measurement data were collected from about 50 seedlings in each genotype. (*G*) Adult plant morphology in *csi1* mutants: (*Left* to *Right*) Col-0 (wild-type) and *csi1-1*, *csi1-2*, *csi1-3*, *csi1-4*, and *csi1-6* mutants. (Scale bar: 5 cm.) *Insets* show enlarged image of siliques from wild-type (Col-0) and *csi1-3*–mutant plants. (Scale bar: 1 cm.) (*H*–*K*) Morphology of mature pollen grains in wild-type (*H*) and *csi1-3*–mutant (*I*) plants examined by SEM. (Scale bar: 200 μm.) Magnified SEM images of single pollen grains from wild-type (*J*) and *csi1-3*–mutant (*K*) plants. (Scale bar: 2 μm.)

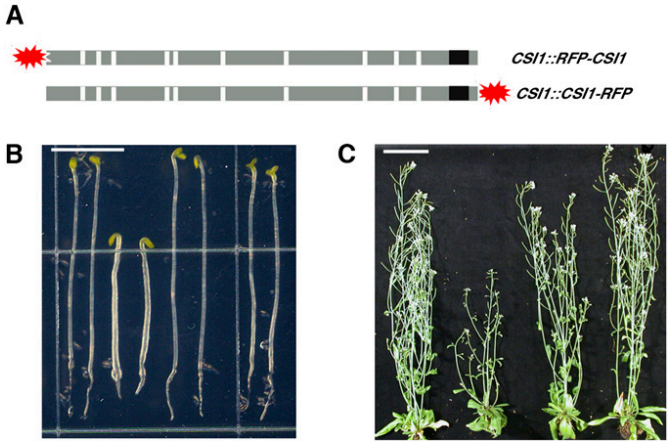

Fig. S4. Both N- and C-terminal fusion constructs complement *csi1*-mutant phenotypes. (*A*) Schematic representation of N- and C-terminal fusion constructs. (*B*) Red fluorescent protein (RFP)-fusion constructs complemented *csi1*-mutant phenotype in dark-grown hypocotyls. (Scale bar: 5 mm.) (*C*) RFP-fusion constructs complemented *csi1*-mutant phenotype in adult plants: (*Left* to *Right* in *B* and *C*) wild-type (Col-0), *csi1-6* mutant, *CSI1::CSI1-RFP* in *csi1-6* mutant, and *CSI1::RFP-CSI1* in *csi1-6* mutant. (Scale bar: 5 cm.)

Table S1. Reciprocal crosses indicate that *csi1* has pollen-specific transmission defect

Allele	Pollen donor: +/− pollen recipient: +/+			Pollen donor: +/+ pollen recipient: +/−		
	n	+/+	+/−	*n*	+/+	+/−
Expected		50%	50%		50%	50%
csi1-3	86	82%	18%	62	51%	49%

Table S2. DNA primers used in this study

Transfer DNA line	Transfer DNA genotyping	RT-PCR analysis
csi1-1 (SALK_136239)	F: CTAACAAAAGAGCAGTTGCCG R: CATCACCACCCTATCGATTTG	F: CTGAAAGTGGTGCCATAGAAGCTC R: CTTGTTAGACCACTGGAATTCT
csi1-2 (SALK_122304)	F: TAGGCACACCAAAAGATGAAC R: GAGCTACAGAGCCTGCAACAC	F: CTGAAAGTGGTGCCATAGAAGCTC R: CTTGTTAGACCACTGGAATTCT
csi1-3 (SALK_138584)	F: TAGGCACACCAAAAGATGAAC R: GAGCTACAGAGCCTGCAACAC	F: CTGAAAGTGGTGCCATAGAAGCTC R: CTTGTTAGACCACTGGAATTCT
csi1-4 (SALK_047252)	F: GCTCCGAATTTTACCTGGAAG R: AGGAATTCAGCTTTCTCCTGG	F: CTGAAAGTGGTGCCATAGAAGCTC R: CTTGTTAGACCACTGGAATTCT
csi1-5 (SALK_051146)	F: CAATTTAGCCATCTGGTTGCTCTCGG R: CAACTAGTAAGGGAA-TCGCCTTTCGAG	F: GACTTTGCCGAGATCAGCCTATTG R: GTTCCGCGACTACCGTTACAGACA
csi1-6 (SALK_115451)	F: CCGTCTTGGGTTCACTCTGCAAGGAGAA R: GGAAGCACTGCC-TTCACGTAGCATGTC	F: ATGACAAGTGCTCTTGGATG R: CAATAGCATCATTGGAAGCACTGCC
Y2H constructs	Forward primer	Reverse primer
CESA1	GGGATCCGTCAGTTTCCCAAATGGTAC	GTCGACTCAGACGATGGTGTTGATATA
CESA3	CCATGGGAGATCAGTTTCCCAAGTGG	GTCGACTCAGATGGTGGTGTTCACATA
CESA6	CCATGGGACAGTTCCCTAAATGGTAC	GTCGACTCAAACCACAGAGTTAATGTA
GUS construct	Forward primer	Reverse primer
CSI1	TTTAGGATCCCCATTGTTATGGGC (BamHI)	AATCTCCATGGAAGAGCACTTGTCAAATC (NcoI)

Table S3. Accessions used in phylogenetic tree

Name	Organism	Locus number	Accession number
AtCSI1	*Arabidopsis*	At2g22125	GI:79559926
AtCSI2	*Arabidopsis*	At1g44120	GI:15219352
AtCSI3	*Arabidopsis*	At1g77460	GI:186496022
PtCSIL1	*Populus trichocarpa*		GI:224083759
PtCSIL3	*Populus trichocarpa*		GI:224084912
PtCSIL2	*Populus trichocarpa*		GI:224096231
RcCSIL1	*Ricinus communis*		GI:255576178
RcCSIL2	*Ricinus communis*		GI:255558634
VvCSIL1	*Vitis vinifera*		GI:225438627
VvCSIL2	*Vitis vinifera*		GI:225459601
OsiCSIL1	*Oryza sativa Indica*		GI:218197824
OsiCSIL2	*Oryza sativa Indica*		GI:218185379
OsjCSIL1	*Oryza sativa Japonica*		GI:222635228
OsjCSIL2	*Oryza sativa Japonica*		GI:108864075
OsjCSIL3	*Oryza sativa Japonica*		GI:115484501
SbCSIL1	*Sorghum bicolor*		GI:242095194
SbCSIL2	*Sorghum bicolor*		GI:242067687
PpCSIL1	*Physcomitrella patens*		GI:168006338
PpCSIL2	*Physcomitrella patens*		GI:168024763

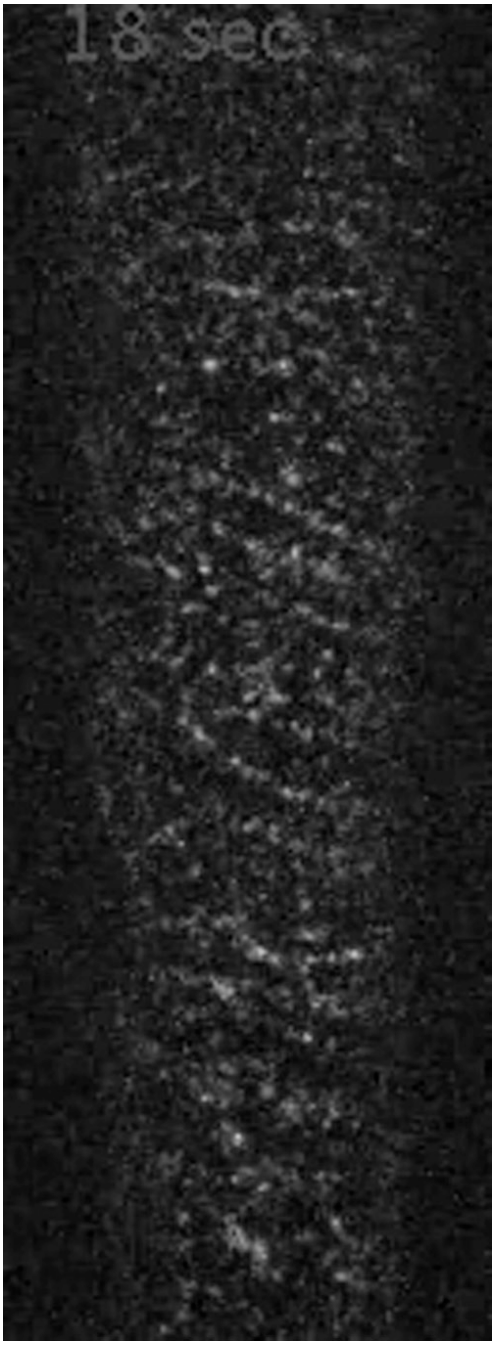

Movie S1. Time-lapse images of RFP-CSI1 at cell membrane in epidermal cells of dark-grown hypocotyls (quantified by velocity measurements in Fig. 3). Time series are 2 min long with images at 2-s intervals.

Movie S1

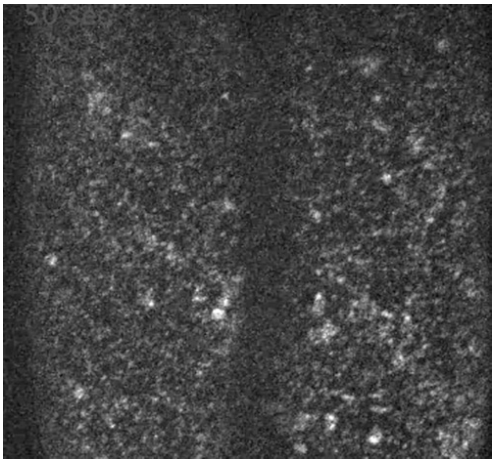

Movie S2. Time-lapse images of YFP-CESA6 at cell membrane in epidermal cells of dark grown *csi1-3* mutants (quantified by velocity measurements in Fig. 4). Time series are 2 min long with images at 2-s intervals.

Movie S2

This article is a *Plant Cell* Advance Online Publication. The date of its first appearance online is the official date of publication. The article has been edited and the authors have corrected proofs, but minor changes could be made before the final version is published. Posting this version online reduces the time to publication by several weeks.

POM-POM2/CELLULOSE SYNTHASE INTERACTING1 Is Essential for the Functional Association of Cellulose Synthase and Microtubules in *Arabidopsis* [W] [OA]

Martin Bringmann,[a] Eryang Li,[b,1] Arun Sampathkumar,[a,2] Tomas Kocabek,[b,3] Marie-Theres Hauser,[b,4] and Staffan Persson[a,4,5]

[a] Max-Planck-Institute for Molecular Plant Physiology, 14476 Potsdam, Germany
[b] Department of Applied Genetics and Cell Biology, BOKU, University of Natural Resources and Life Sciences, A-1190 Vienna, Austria

In plants, regulation of cellulose synthesis is fundamental for morphogenesis and plant growth. Cellulose is synthesized at the plasma membrane, and the orientation of synthesis is guided by cortical microtubules; however, the guiding mechanism is currently unknown. We show that the conditional root elongation *pom2* mutants are impaired in cell elongation, fertility, and microtubule-related functions. Map-based cloning of the *POM-POM2* locus revealed that it is allelic to *CELLULOSE SYNTHASE INTERACTING1* (*CSI1*). Fluorescently tagged POM2/CSI1s associated with both plasma membrane–located cellulose synthases (CESAs) and post-Golgi CESA-containing compartments. Interestingly, while CESA insertions coincided with cortical microtubules in the *pom2/csi1* mutants, the microtubule-defined movement of the CESAs was significantly reduced in the mutant. We propose that POM2/CSI1 provides a scaffold between the CESAs and cortical microtubules that guide cellulose synthesis.

INTRODUCTION

Cell expansion in plants is fundamental for cell morphogenesis and growth. The expansion is driven by vacuolar turgor pressure and is restricted by a strong, yet flexible, cell wall that permits directional cell growth. The cell wall is mainly constituted of polysaccharides, such as cellulose, hemicelluloses, and pectins, and highly glycosylated proteins (Somerville et al., 2004). Cellulose is made of β-1,4-linked glucan chains that form microfibrils by intermolecular hydrogen bonds (Somerville, 2006; Carpita, 2011; Endler and Persson, 2011). These microfibrils provide the main tensile strength to the cell walls and are hence of great importance for directed cell growth (Baskin, 2001; Cosgrove, 2005). Cellulose is believed to be synthesized at the plasma membrane by cellulose synthases (CESAs), which in higher plants have been observed to form hexameric rosette complexes (Kimura et al., 1999; reviewed in Guerriero et al., 2010). The cellulose microfibrils have been observed to align with underlying cortical microtubules (Green, 1962; Ledbetter and Porter, 1963). Consistent with these observations, in vivo studies using fluorescently labeled CESAs and microtubules revealed that the CESAs track along cortical microtubules (Paredez et al., 2006). Furthermore, perturbation of microtubule organization affects the mechanical properties of the cell wall (Baskin, 2001; Bichet et al., 2001; Sugimoto et al., 2003; Baskin et al., 2004; Wasteneys and Fujita, 2006). However, no mechanism for how the guidance of the CESAs by the microtubules occurs has been presented.

Mutant analyses and coimmunoprecipitation studies have shown that three distinct CESA subunits are necessary to form a functional complex (Somerville et al., 2004). Consequently, the primary wall CESA complex requires a CESA1, a CESA3, and a CESA6-related activity to be functional (Desprez et al., 2007; Persson et al., 2007). The CESA complexes are assumed to be assembled in the Golgi and transported to the cell surface where they are inserted into the plasma membrane adjacent to cortical microtubules (Crowell et al., 2009; Gutierrez et al., 2009). Apart from Golgi and plasma membrane localization, the CESAs are found in small post-Golgi compartments referred to as small CESA compartments (smaCCs; Gutierrez et al., 2009) or microtubule-associated CESA compartments (MASCs; Crowell et al., 2009). It has been proposed that the smaCCs/MASCs may be involved in either exo- or endocytosis of the CESAs.

Several components that are important for cell expansion have been identified through genetic screens. Subsequent cloning of the corresponding genes revealed many genes that are associated with cellulose synthesis, such as *POM-POM1/CHITINASE-LIKE1* (*POM1/CTL1*), *KORRIGAN/LION'S TAIL1/*

[1] Current address: Department of Botany, University of British Columbia, Vancouver, Canada.
[2] Current address: Sainsbury laboratory, University of Cambridge, Bateman Street, Cambridge, United Kingdom.
[3] Current address: Biology Center, Academy of Sciences of the Czech Republic, Institute of Plant Molecular Biology, 370 05 Ceske Budejovice, Czech Republic.
[4] These authors contributed equally to this work.
[5] Address correspondence to persson@mpimp-golm.mpg.de.
The authors responsible for distribution of materials integral to the findings presented in this article in accordance with the policy described in the Instructions for Authors (www.plantcell.org) are: Marie-Theres Hauser (marie-theres.hauser@boku.ac.at) and Staffan Persson (persson@mpimp-golm.mpg.de).
[W] Online version contains Web-only data.
[OA] Open Access articles can be viewed online without a subscription.
www.plantcell.org/cgi/doi/10.1105/tpc.111.093575

RADIALLY SWOLLEN2 (*KOR/LIT/RSW2*), *COBRA*, *KOBITO/ELONGATION DEFECTIVE1*, *RSW1/CESA1*, *CONSTITUTIVE EXPRESSION OF VSP1/ECTOPIC LIGNIFICATION1/RSW5/CESA3*, and *QUILL/PROCUSTE/CESA6* (Hauser et al., 1995; Arioli et al., 1998; Nicol et al., 1998; Fagard et al., 2000; Lane et al., 2001; Schindelman et al., 2001; Pagant et al., 2002; Wang et al., 2006). Mutations in any of these genes result in epidermal cell swelling, restricted root and hypocotyl elongation, and reduced cellulose content. While it is unlikely that all of these proteins partake in the CESA complex, their functions appear crucial for production of the microfibrils. However, only CELLULOSE SYNTHASE INTERACTING1 (CSI1) has so far been identified to interact directly with the primary wall CESAs (Gu et al., 2010). The interaction was identified through a yeast two-hybrid screen using the catalytic domain of CESA6 as bait and was confirmed by dual labeling of the CSI1 and CESAs (Gu et al., 2010). CSI1 is a 2150–amino acid protein that holds between 10 and 20 predicted Armadillo repeats and a C-terminal C2 domain (Gu et al., 2010). Mutations in CSI1 caused reduced movement of CESA particles in the plasma membrane, lower cellulose content, and defective cell elongation.

To gain more knowledge about components that may affect cell morphogenesis and cellulose production, we characterized and cloned the gene responsible for *pom2* (Hauser et al., 1995), which displays microtubule and cell elongation related defects. *POM2* is allelic to *CSI1*, and fluorescently labeled POM2/CSI1s are associated with both plasma membrane–located CESAs and smaCCs/MASCs. Intriguingly, while the POM2/CSI1 does not affect insertion of CESAs adjacent to cortical microtubules, the protein is essential for sustained CESA movement along the microtubules. Hence, the POM2/CSI1 protein facilitates a connection between the CESAs and cortical microtubules, either directly or in association with other proteins.

RESULTS

pom2 Has Defects in Cell Elongation and Fertility

pom2-1 and *pom2-2* were identified in a genetic screen for root morphogenesis mutants (Hauser et al., 1995). We identified two alleles, designated *pom2-3* and *pom2-4*. All alleles were recessive and developed a conditional expansion phenotype with thick short roots on media supplemented with Suc (see Supplemental Figures 1A and 1B online; Table 1). Whereas wild-type roots grew roughly 3.5 mm/d, *pom2* roots typically elongated only 0.5 to 0.7 mm/d under these conditions. On medium without Suc, the *pom2* roots also showed reduced growth and cell elongation (see Supplemental Figure 2A online; Table 1). Similar to the root phenotypes on conditions stimulating growth, skotomorphogenic hypocotyls of *pom2* seedlings were significantly shorter compared with the wild type (see Supplemental Figure 2B online). However, with the exception of *pom2-3*, full-grown *pom2* mutants were only slightly dwarfed (see Supplemental Figure 2C online). By contrast, floral organs, such as petals, sepals, stamens, and carpels, were also reduced in size (see Supplemental Figure 2D online). The extent of the size reduction of stamens was allele specific and lead to heterostyly in *pom2-1* and *pom2-2* but not in *pom2-3* and *pom2-4*. These cell expansion phenotypes indicate that POM2 is required for proper cell elongation in distinct organs.

The heterostyly correlated with fertility defects in the different *pom2* alleles. All *pom2* alleles developed significantly fewer ovules (Table 1). Whereas the wild type held around 40 ovules per gynoecium, only 20 to 30 were visible in the *pom2* alleles. *pom2-1* and *pom2-2* had severely reduced fertility and occasionally displayed one to three seeds in terminal siliques (Table 1). However, if fertilized with wild-type pollen, *pom2-1* and *pom2-2* set up to 20 seeds/silique ($n = 5$ for *pom2-1*; $n = 22$ for *pom2-2*). By contrast, all ovules of *pom2-3* and *pom2-4* were fertilized by their own pollen (Table 1). As self-fertilization of the *pom2-1* and *pom2-2* was rare, we analyzed the number of pollen released per flower. Whereas wild-type anthers release 326 pollen for Columbia (Col) and 234 for Landsberg *erecta* (L*er*), only 1.6, 5.4, 95, and 113 pollen per flower were harvested from *pom2-1*, *pom2-2*, *pom2-3*, and *pom2-4*, respectively. In addition, the majority of pollen grains were deformed (see Supplemental Figure 2E online), and pollen tube development was impaired in the *pom2* alleles (see Supplemental Figure 2F online; Table 1). Hence, the reduced fertility of the *pom2* mutants appears to be a combination of development of smaller gynoecia with fewer ovules, heterostyly, the inability of anthers to release pollen, collapsed pollen grains, and poor pollen germination rate.

pom2/csi1 Mutants Display Microtubule-Related Phenotypes and Mitotic Defects

The *pom2* mutants also displayed organ and cell twisting (Figures 1A and 1B). This was readily observed in roots and etiolated hypocotyls (left-handed) of seedlings grown on medium with or without added Suc. In addition, twisting was also observed in soil-grown rosette leaves (left-handed; Figures 1A and 1B). Twisting or spiraling of organs occurs in mutants affecting cytoskeleton organization, for example, in the microtubule-associated *clasp*, *lefty1* and *2*, and *sku6/spr1* (Thitamadee et al., 2002; Sedbrook et al., 2004; Ambrose et al., 2007; Kirik et al., 2007). To investigate whether the microtubule organization was disturbed in *pom2*, we crossed *pom2-4* to the microtubule marker lines Microtubule-Associated Protein4 (MAP4):green fluorescent protein (GFP) or mCherry:Tubulin alpha-5 (TUA5) (Marc et al., 1998; Gutierrez et al., 2009). Rapidly elongating cells in wild-type roots and etiolated hypocotyls typically hold transversely or obliquely orientated cortical microtubule arrays (Sugimoto et al., 2000; Figure 1C). However, the cortical microtubules were less well transversally arranged in rapidly elongating hypocotyl cells (between 2 and 12 mm below the apical hook) in the *pom2-4* mutant (Figures 1C and 1D). In addition, microtubule defects were also observed in the other *pom2* alleles, for example, in *pom2-1* (see Supplemental Figure 3A online). These results suggest that the organization of the microtubule array is impaired in the *pom2* mutants. We also investigated whether the microtubule dynamics were altered in *pom2/csi1* by selecting instances along kymographs in which contrast changes were unambiguously connected to a single microtubule end. Using this criterion, we found no significant differences in microtubule plus end growth (5.5 ± 2.1 μm/min in *pom2/csi1*; 4.8 ± 1.3 μm/min in the wild type), plus end

Table 1. Summary of Quantified Phenotypes of Wild-Type and *pom2* Alleles

		Length (mm)				Etiolated Hypocotyls 4.5% (μm)					
		Roots		Etiolated Hypocotyls						No. per Silique[a]	
Allele	Accession	0%	4.5%	0%	4.5%	Length of Epidermis	Diameter	Diameter of Palisade Tissue	Pollen Germination (%)	Ovules	Seeds
pom2-1	Col	**4.8 ± 2.6**	**2.7 ± 1.0**	**9.2 ± 1.9**	**5.6 ± 2.1**	n.d.	n.d.	44.3 ± 4.7	1.6	**20.9 ± 3.2**	**0 ± 0[b]**
pom2-2	Col	**3.5 ± 1.7**	**2.3 ± 0.9**	**7.1 ± 1.5**	**4.7 ± 1.8**	**201 ± 47**	**735 ± 120**	39.8 ± 5.0	21.3	**25.0 ± 6.0**	**0 ± 0[b]**
pom2-3	L*er*	**3.4 ± 1.1**	**2.2 ± 0.6**	**5.3 ± 0.9**	**3.4 ± 1.5**	n.d.	n.d.	36.8 ± 6.1	12.0	**25.5 ± 7.0**	**22.7 ± 5.9**
pom2-4	Col, Nossen	**5.1 ± 2.0**	**3.8 ± 1.1**	**7.3 ± 1.3**	**6.7 ± 1.9**	n.d.	n.d.	36.5 ± 4.1	20.3	**22.6 ± 3.9**	**18.3 ± 4.9**
Wild type	Col	10.8 ± 2.9	16.2 ± 3.3	11.9 ± 2.8	13.0 ± 3.3	389 ± 80	302.5 ± 96	32.9 ± 4.5	83.1	36.1 ± 5.0	40.0 ± 3.9
Wild type	L*er*	11.0 ± 4.1	10.6 ± 2.7	11.5 ± 2.3	10.6 ± 2.5	n.d.	n.d.	39.8 ± 5.0	45.4	44.0 ± 5.6	45.2 ± 6.1

Significant differences to the wild type are in bold; 4.5% refers to Suc supplement in MS media. n.d., not determined.
[a]Self-fertilization.
[b]Upon cross-fertilization, up to 20 seeds/siliques developed.

shrinkage (15.3 ± 9.2 μm/min in *pom2/csi1*; 11.5 ± 5.0 μm/min in the wild type), or in minus end shrinkage (2.4 ± 1.4 μm/min in *pom2/csi1*; 2.2 ± 1.7 μm/min in the wild type) when comparing *pom2/csi1* mutant cells and wild-type cells (60 microtubule ends from six cells from six seedlings). These growth and shrinkage rates are in good agreement with previously published results (Shaw and Lucas, 2011).

Apart from altered microtubule organization, mutations in several microtubule-associated genes also lead to reduced mitotic activity (Ambrose et al., 2007; Kirik et al., 2007; Sunohara et al., 2009). To test whether the *pom2* mutants also hold fewer cells that actively divide, we crossed lines expressing the mitotic marker cycB1;1:Cyclin Destruction Box (CDB):β-glucuronidase (GUS) (Hauser and Bauer, 2000) with several *pom2* mutant alleles. The activity of the meristem was quantified by histochemical GUS staining. Similar to other microtubule-associated mutants, significantly fewer cells were actively dividing in the *pom2* mutants (see Supplemental Figure 3B online). Thus, *pom2* mutants are affected both in cell elongation, microtubule organization, and meristematic activity.

POM2 Is Allelic to *CSI1* and Contributes the Main CSI Activity

POM2 was isolated by a map-based cloning strategy and was initially mapped in the middle of chromosome II between the cleaved amplified polymorphic sequence markers GPA1 and m429 (Hauser et al., 1995). By analyzing 1022 meiotic events with diverse molecular markers (see Supplemental Table 1 online), *POM2* was narrowed down to a 110-kb interval containing 36 candidate genes. This region was covered by two overlapping BACs (see Supplemental Figure 4A online). Allele-specific *Nco*I and *Eco*RV restriction fragment length polymorphisms were identified between the Col alleles *pom2-1* and *pom2-2* using the labeled BAC T16B14 as probe (see Supplemental Figure 4A online), with only a region around At2g22125 with the expected genomic fragment lengths and the detected polymorphism pattern (see Supplemental Figure 4B online). A 14.5-kb binary cosmid clone, containing the full At2g22125 gene, was identified using the (F6/R6) probe and complemented the *pom2-3* phenotypes. Mutations in all four alleles were identified through sequencing (outlined in Figure 1E), and all of the lines contained reduced levels of *POM2* mRNA (see Supplemental Figure 4C online). Furthermore, T-DNA insertion lines that correspond to At2g22125 (SALK_047252, *pom2-5*; SALK_051146, *pom2-6*; SALK_115451, *pom2-7*; and SALK_136239, *pom2-8*; all of which are mRNA nulls; Gu et al., 2010) phenocopied the *pom2* mutants; hence, *POM2* is At2g22125.

At2g22125 was recently identified as CSI1 (Gu et al., 2010) and is part of a three-member family, which contains POM2/CSI1, CSI2, and CSI3. To assess whether the other members of this family are also of importance for plant development, we obtained homozygous T-DNA insertion mutants for *CSI2* (SALK_022491 and SALK_024648) and *CSI3* (SALK_009141 and SALK_009157). These mutants were mRNA nulls or contained minute mRNA levels, as assessed via quantitative RT-PCR (qRT-PCR) (see Supplemental Figure 4D online). However, we did not observe any phenotypes in the *csi2* and *csi3* single mutants or in the double *csi2 csi3* (SALK_022491 and SALK_009141) mutants. These data suggest that POM2/CSI1 contributes the main POM2/CSI-related activity in *Arabidopsis thaliana*. However, *pom2-7/csi1-5 csi2 csi3* triple mutants did display some mild synergistic phenotypes (Figure 2), such as dwarfed plant growth, a more dramatic collapsed pollen phenotype, and increased organ twisting, suggesting that some functional redundancy may be contributed by CSI2 and CSI3.

POM2/CSI1 Colocalizes with CESAs and CESA-Containing Vesicles

To gain further insight into the function of POM2/CSI1, we made a C-terminal fusion of the protein to cyan fluorescent protein (CFP) under a 35S constitutive promoter. This construct complemented the *pom2/csi1* phenotype (*pom2-8/csi1-1*) and mimicked the published CSI1p:CSI1:red fluorescent protein behavior (Gu et al., 2010). Hence, as previously described, the POM2/CSI1 fluorescent protein was present as distinct punctae at the cell cortex in rapidly elongating hypocotyl cells and displayed bidirectional motility of ~200 to 300 nm/min when imaged with a

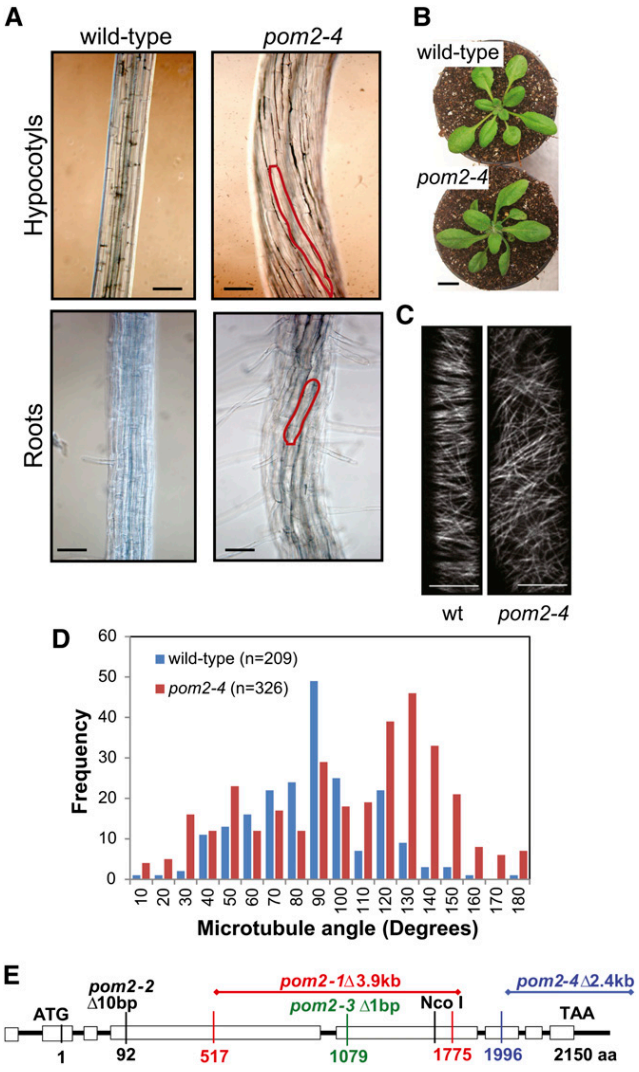

Figure 1. Positional Cloning of *POM2* and Microtubule-Related Defects in the Mutant.

(A) Six-day-old etiolated *pom2-4* hypocotyl displaying twisting of cell files (red outline).
(B) Rosette leaves of 3-week-old *pom2-4* plants that spiral.
(C) Microtubule organization in 3-d-old elongating hypocotyl cells of the wild type (wt; left) and *pom2-4* (right). Microtubules are labeled by mCherry:TUA5.
(D) Microtubule angle distribution in elongating hypocotyl cells in the wild type and *pom2-4*. Angles were measured against the growth axis. Seven cells from seven seedlings were used for the analysis.
(E) Mapped *pom2* mutations in *POM2* (At2g22125). Black line indicates introns and boxed areas exons. aa, amino acids.
Bars = 100 μm in **(A)**, 2 cm in **(B)**, and 10 μm in **(C)**.

spinning-disc confocal microscope (see Supplemental Figures 5A and 5B online; Gu et al., 2010). In addition, several of the *pom2* alleles could hold truncated proteins based on the location of the insertion and on the qRT-PCR results (Figure 1E; see Supplemental Figure 4C online). We therefore also generated a truncated POM2, in which the C2 domain was removed, and fused it to CFP. This construct did not rescue the *pom2* mutants, and the fluorescent pattern was diffuse and distinct from the cortical foci seen using the full-length POM/CSI1:CFP construct (see Supplemental Figure 5C online), suggesting that truncations of the POM2/CSI1 protein render it nonfunctional and that the C-terminal C2 domain contributes to POM2/CSI1 cellular localization.

To ensure that the POM2/CSI1:CFP punctae corresponded to plasma membrane–based CESA particles, we crossed the POM2/CSI1:CFP with a tdTomato:CESA6 line. The fluorescent signals from these two markers showed marked coincidence (see Supplemental Figure 5D online). Statistical analysis revealed that the overlap was highly significant compared with randomized signals (see Supplemental Figure 5E online). Furthermore, the CESA and POM2/CSI1 signals co-occurred throughout different cells in etiolated hypocotyls (see Supplemental Figure 5F online). Curiously, we also observed a population of cortical POM2/CSI1s that moved with velocities of well over 1000 nm/min (see Supplemental Figures 5A and 5B online). Such high velocities have not been reported for plasma membrane–bound CESAs, but rather for CESA containing vesicles (i.e., smaCCs/MASCs) at the cell cortex (Gutierrez et al., 2009).

To explore whether the rapidly moving POM2/CSI1s were associated with smaCCs/MASCs, we treated seedlings with the cellulose synthesis inhibitor isoxaben. This drug causes rapid disappearance of the plasma membrane–located CESA complexes and a concomitant accumulation of smaCCs/MASCs tethered at the cell cortex (Gutierrez et al., 2009). After isoxaben treatment, we observed a gradual increase in the number of tethered smaCCs/MASCs, as estimated from their erratic motilities (Gutierrez et al., 2009; Figure 3A). In addition, these vesicles were accompanied by POM2/CSI1 signal, indicating that the POM2/CSI1 can associate with the smaCCs/MASCs (Figure 3A). The smaCCs/MASCs may also bifurcate into smaller compartments or merge into bigger ones (Figure 3; Gutierrez et al., 2009). In agreement with this observation, we also detected merging and bifurcating fluorescent signals of the POM2/CSI1-decorated compartments (Figure 3). These events were corroborated by three-dimensional heat map analyses (i.e., we observed that the sum of the migrating smaCCs/MASCs and POM2/CSI1 branches roughly equaled the trunk of the signal) (Figures 3C and 3D).

POM2/CSI1 Co-Occurs with Microtubules and Remains at the Cell Cortex after Microtubule Depolymerization

Plasma membrane–located CESA particles track along cortical microtubules (Paredez et al., 2006). To put the POM2/CSI1 in context to the microtubules, we crossed the POM2/CSI1:CFP-expressing line with a plant expressing mCherry:TUA5. Similar to what has been shown for the CESAs, POM2/CSI1 migration occurred along cortical microtubules under control conditions (see Supplemental Figure 6A online). We quantified the coincidence of the two signals using van Steensel's cross-correlation function algorithm (Bolte and Cordelières, 2006), which confirmed colocalization of the two signals (see Supplemental Figure 6B online). To assess whether the motility and location of POM2/CSI1 depends on microtubules, we treated POM2/CSI1:CFP-expressing seedlings with oryzalin overnight. This treatment completely abolished the microtubule array, and the signal was

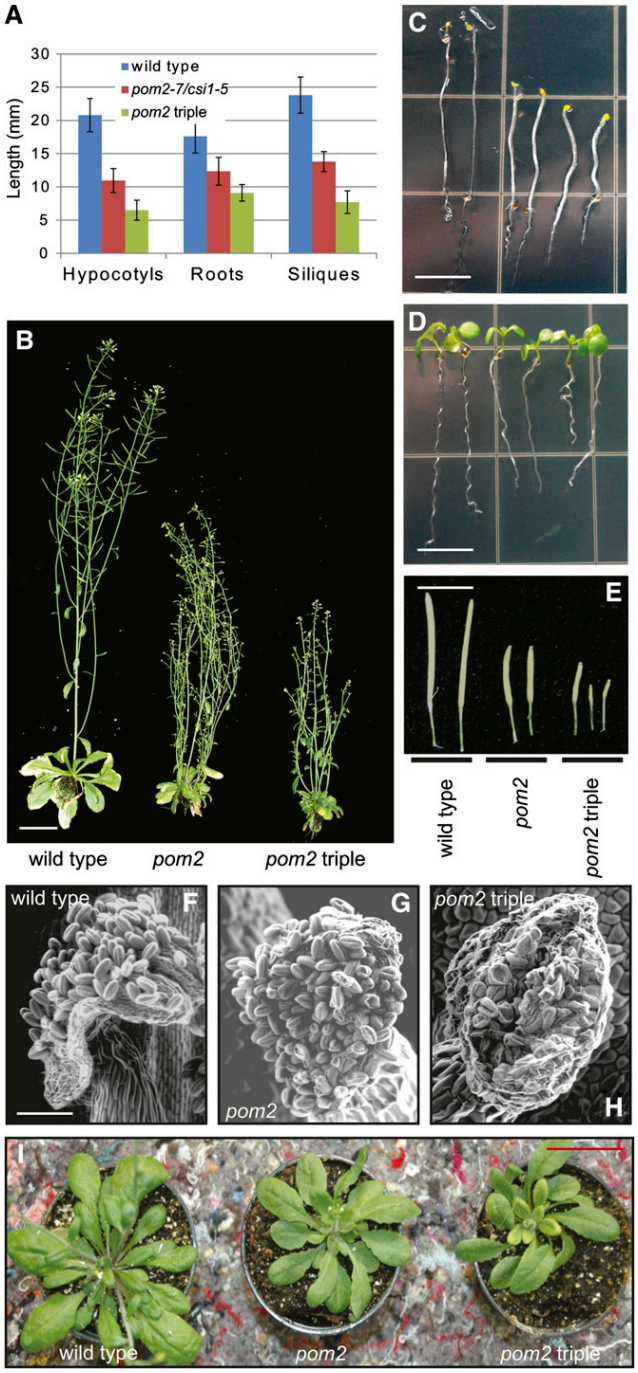

Figure 2. Triple *pom2/csi1 csi2 csi3* Mutant Phenotypes.

(A) Graph displaying length of 5-d-old etiolated hypocotyls, 5-d-old light-grown seedling roots, and mature siliques from 7-week-old soil-grown plants of wild-type, *pom2-7/csi1-5*, and *pom2-7/csi1-5 csi2 csi3* genotypes.
(B) Seven-week-old wild-type, *pom2-7/csi1-5*, and *pom2-7/csi1-5 csi2 csi3* triple mutants. Bar = 5 cm.
(C) Five-day-old etiolated wild-type, *pom2-7/csi1-5*, and *pom2-7/csi1-5 csi2 csi3* triple mutant seedlings. Bar = 5 mm.
(D) Five-day-old light-grown wild-type, *pom2-7/csi1-5*, and *pom2-7/csi1-5 csi2 csi3* triple mutant seedlings. Bar = 5 mm.
(E) Mature siliques from 7-week-old wild-type, *pom2-7/csi1-5*, and *pom2-7/csi1-5 csi2 csi3* triple mutant plants. Bar = 1 cm.
(F) to **(H)** Environmental scanning electron microscopy images of pollen grains on anthers from wild-type, *pom2-7/csi1-5*, and *pom2-7/csi1-5 csi2 csi3* triple mutant plants. Bar = 70 μm.
(I) Twisting rosette leaves in 4-week-old *pom2-7/csi1-5* and *pom2-7/csi1-5 csi2 csi3* triple mutant plants. Bar = 5 cm.

instead seen as a diffuse cytoplasmic smear (see Supplemental Figure 6E online). However, the POM2/CSI1 signal remained at the cell cortex and followed similar trajectories as the CESAs (see Supplemental Figures 6C and 6D online). The CESA and POM2/CSI1 trajectories were, however, less well defined than in the control-treated cells (Paredez et al., 2006). These results suggest that the interaction between CESAs and POM2/CSI1 is sustained in the absence of microtubules.

POM2/CSI1 Co-Occurs with Microtubule Depolymerizing Ends and smaCCs/MASCs upon Isoxaben Treatment

Exposure of cells to isoxaben causes, in addition to the accumulation of smaCCs/MASCs, tethering of the vesicles to cortical microtubules and co-occurrence of the smaCCs/MASCs with microtubule depolymerizing ends (Gutierrez et al., 2009). Similar isoxaben treatments also resulted in the co-occurrence of POM2/CSI1 foci with microtubule depolymerizing ends (Figure 4A; see Supplemental Movie 1 online). We observed POM2/CSI1 on 33 out of 67 microtubule depolymerizing plus and minus ends (three cells from three seedlings) under these conditions. These POM2/CSI1s displayed rapid movement interspersed with infrequent stops, which followed the dynamics of the microtubule ends (Figure 4A). Furthermore, multiple POM2/CSI1s that populated the same microtubule were collected by the depolymerizing end–associated POM2/CSI1s (Figures 4B to 4D; see Supplemental Movie 2 online). Hence, aggregation of the POM2/CSI1s occurred in a stepwise fashion, each step adding an additional POM2/CSI1 (Figures 4C and 4D). This behavior is similar to what has been described for smaCCs/MASCs (Gutierrez et al., 2009). The POM2/CSI1 particles also exclusively co-occurred with microtubule depolymerizing ends and not with growing ends (see Supplemental Figure 7A and Supplemental Movie 3 online), which also was reported for smaCCs/MASCs (Gutierrez et al., 2009). Interestingly, the association of POM2/CSI1 with microtubule depolymerizing ends may be connected with a bifurcation mechanism. Bifurcation of microtubule end–associated POM2/CSI1 signals occurred when depolymerization progressed across another adjacent microtubule (Figure 4D). Hence, the retracting microtubule ends may aid the bifurcation, perhaps facilitating redistribution of POM2/CSI1 and, therefore, possibly also smaCCs/MASCs, to other cellular locations.

POM2/CSI1 Does Not Affect Insertion Rates or the Spatial Distribution of CESA Deliveries

To assess how the POM2/CSI1 punctae are established at the cell cortex, we bleached the existing POM2/CSI1:CFP signal and

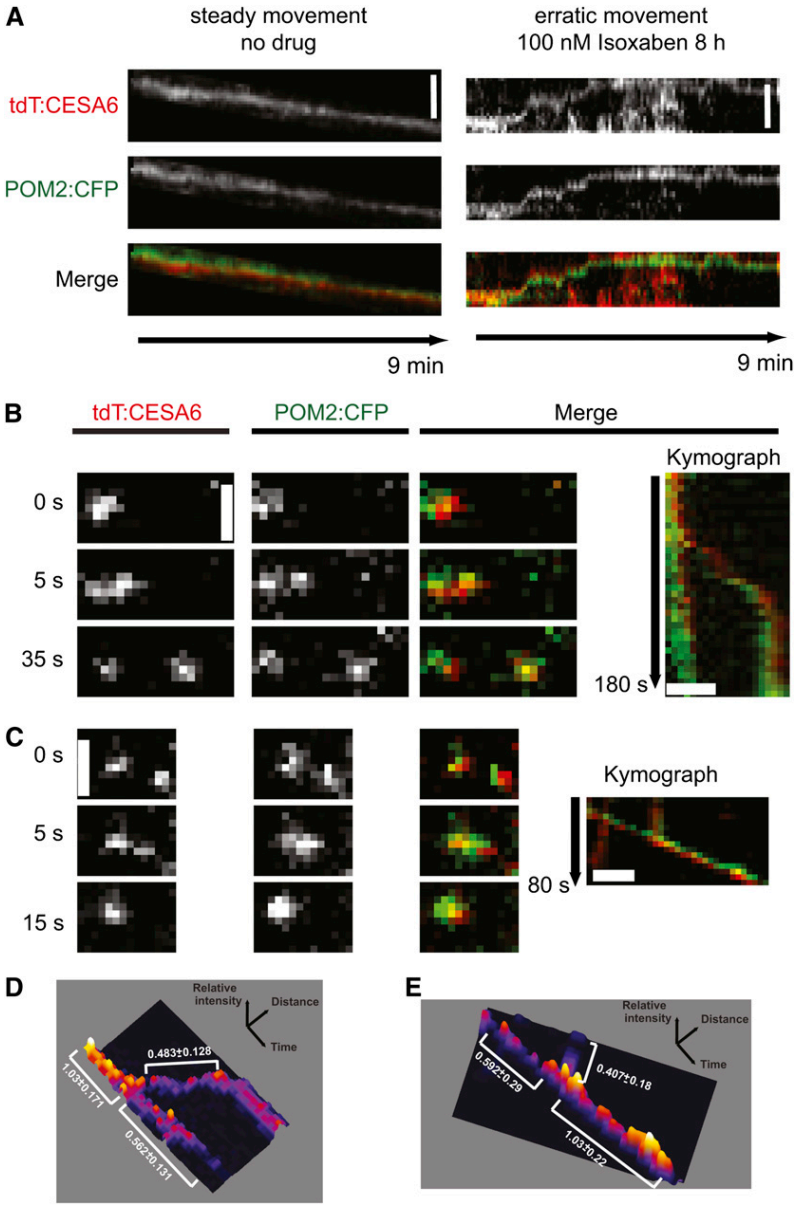

Figure 3. POM2/CSI1-Containing Compartments Can Merge and Bifurcate at the Cell Cortex.

(A) Kymographs from 4-d-old etiolated seedlings expressing tdTomato:CESA6 and POM2:CFP. Kymographs display CESA and POM2/CSI movement at the plasma membrane in nontreated cells (left) and CESA and POM/CSI1 movement at the cell cortex in isoxaben-treated (100 nm for 8 h) cells (right). **(B)** and **(C)** Images from two different time series in 4-d-old etiolated seedlings expressing tdTomato:CESA6 and POM2:CFP. The images show a split of one compartment into two (for both the CESA and POM2/CSI1 fluorescent signal) at 5 s **(B)**, and a merge of the signals at 5 s in another time series **(C)**. Right panel shows kymographs depicting the split of the signal into two (top) and the merge of two compartments into one (bottom). Bars = 2 μm. **(D)** and **(E)** Surface plots displayed as heat maps. The mean intensity of the signals above background was measured for **(B)** and **(C)** and is displayed as relative values ± SD for all pixels along the indicated trace.

observed its repopulation. The POM2/CFP fluorescence first dimly reemerged evenly across the bleached area (see Supplemental Figure 7B online), as expected from a cytosolic protein due to rapid cytoplasmic streaming. After ~60 s, distinct punctae appeared at the cell cortex that moved with constant velocities of ~200 to 300 nm/min (see Supplemental Figure 7B online). The POM2/CSI1 punctae continued to appear during the time of recovery, and after ~120 s, the bleached area was repopulated by the fluorescent foci. The establishment of distinct POM2/CSI1-related punctae at the plasma membrane could occur either through codelivery together with CESA particles or through the gradual association of cytosolic POM2/CSI1 with

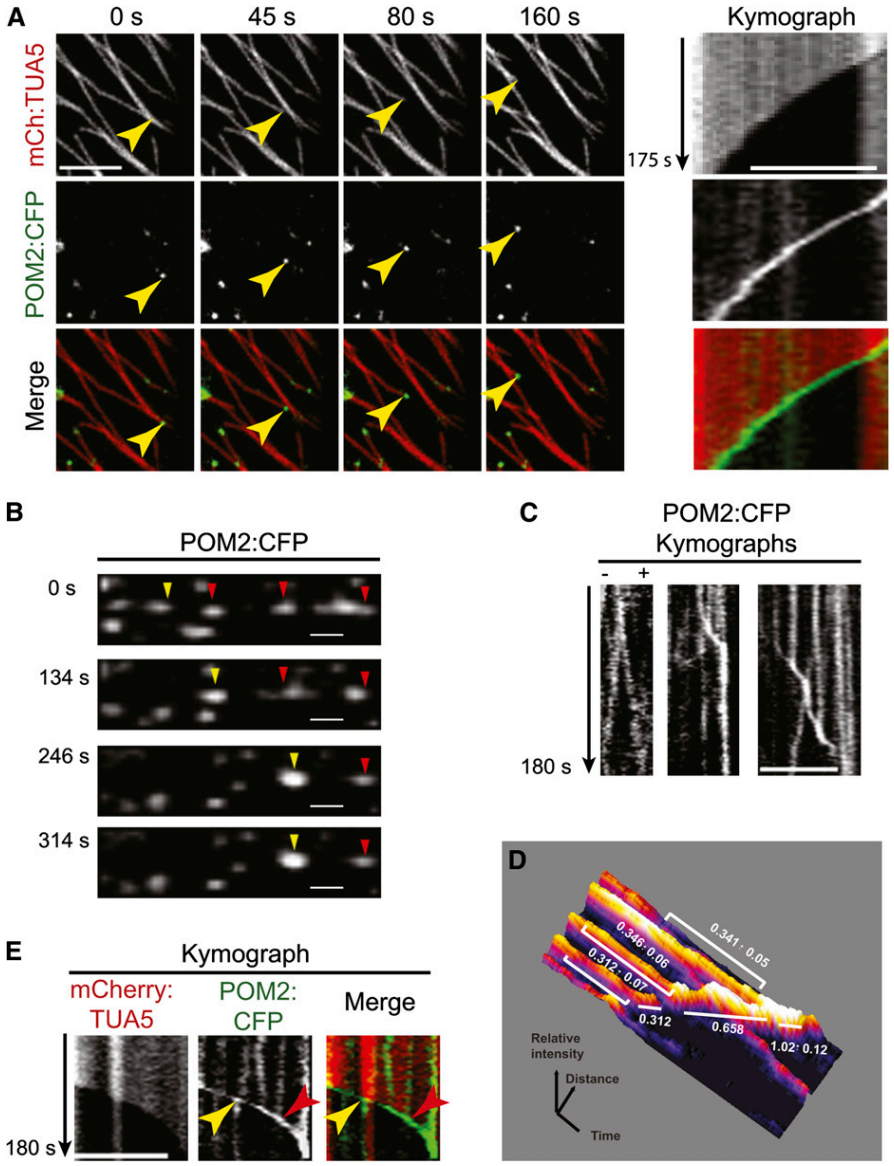

Figure 4. POM2/CSI1 Fluorescent Signals Associate with Microtubule Depolymerizing Ends.

(A) Images from time series (see Supplemental Movie 1 online) of cells in 4-d-old hypocotyls expressing mCherry:TUA5 and POM2:CFP treated with 100 nM isoxaben for 2 h. Yellow arrowheads indicate POM2/CSI1 fluorescent signal associated with a depolymerizing microtubule end. Right panel displays kymographs, which show that the POM2/CSI1 signal follows the microtubule retracting end.
(B) Time series (see Supplemental Movie 2 online) of POM2/CSI1 collecting other POM2/CSI1s. Yellow arrowheads indicate collecting POM2/CSI1 and red arrowheads collected POM2/CSI1s.
(C) Kymograph displaying POM2/CSI1 bidirectional migration (left), accelerating and stopping POM2/CSI1 (middle), and collecting POM2/CSI1 (right).
(D) Surface plot displayed as a heat map. The mean intensity of the signals above background was measured for the right kymograph in **(C)** and is displayed as relative values ± SD.
(E) Kymograph showing bifurcation and merge of POM2/CSI1 signal that is associated with a retracting microtubule end. When the end crosses another microtubule, the POM2/CSI1 signal bifurcates (yellow arrowheads). Merging events of two POM2/CSI1 signals happen along retracting microtubules that contain laterally associated POM2/CSI1 (red arrowheads).
Bars = 5 μm **(A)**, **(C)**, and **(E)** and 1 μM in **(B)**.

newly delivered CESAs that subsequently amass to a brighter puncta. To investigate this, we bleached both fluorescent signals in the dual-labeled POM2/CSI1:CFP and tdTomato:CESA6 line. We observed that the appearance of a CESA particle at the plasma membrane was accompanied by the appearance of a POM2/CSI1 fluorescent puncta at the cell cortex in 16 out of 69 (or 23%) observed delivery events (three cells from three seedlings; see Supplemental Figure 7C online). The appearance of the remaining CESA punctae occurred independently from any clear POM2/CSI1 signal at the plasma membrane (see Supplemental Figure 7C online). Bleaching of smaller areas did not appear to change the estimate of codelivery events. The co-occurrence of the two fluorescent signals observed in some of the delivery events suggests that POM2/CSI1 can accumulate with CESAs prior to plasma membrane delivery (e.g., with the smaCCs/MASCs, as discussed above). Consequently, POM2/CSI1 could have a role in the delivery of CESAs to the plasma membrane. To assess this, we generated GFP:CESA3 and mCherry:TUA5 dual-labeled lines in the *pom2* mutant background. To quantify the rate, as well as the spatial distribution, of CESA insertions, we bleached the GFP channel and measured the appearance of new CESAs at the plasma membrane. The criteria used to identify delivery events were identical to what was described by Gutierrez et al. (2009) (i.e., a CESA particle appeared in the focal plane and showed a brief period of wobbling motility, which after a short period of time reverted to a steady movement of ~200 to 400 nm/min along a linear track). We subsequently mapped these events on images of mCherry:TUA5. In the wild type, we observed an insertion rate of ~0.06 CESAs μm^{-2} min^{-1}, which corresponds to 3.1 ($\pm$0.6) insertion events μm^{-2} h^{-1} (three cells from three seedlings). This observation is in close agreement with previously reported insertion rates (4.8 insertion events μm^{-2} h^{-1}; Gutierrez et al., 2009). However, we observed similar insertion rates in the *pom2* mutants (4.2 $\pm$ 1.4 in *pom2-4*; 3.1 $\pm$ 1.4 in *pom2-5*; three cells from three seedlings); therefore, the overall rate of CESA insertion does not appear to be affected in the *pom2* mutants. Furthermore, 283 out of 324 CESA insertions, or 87%, occurred at sites occupied by microtubules in the *pom2* mutants (three cells from three seedlings for *pom2-4* and *pom2-5*, respectively; Figures 5A and 5B). This was considerably more than expected by chance (54% based on microtubule image coverage); hence, CESA insertion coincides with microtubules also in the *pom2* mutants.

POM2/CSI1 Is Essential for Coalignment of Microtubules and CESAs

After insertion, the CESAs begin to move with a steady rate along trajectories defined by the underlying microtubules (Gutierrez et al., 2009). To assess whether POM2/CSI1 has a role in this process, we analyzed the tracking behavior of the CESAs and compared the coincidence of CESA molecules and microtubules over time using Pearson correlation coefficients (Figure 5C). To do the latter, we compared the coincidence of fluorescent signals in time averages from 100 single images (500-s total imaging time) of wild-type and *pom2* cells expressing both GFP:CESA3 and mCherry:TUA5. While we observed a high correlation between CESA and microtubule fluorescence in the wild-type background, the correlation between the two channels was significantly lower in the *pom2* mutants (Figure 5C). We further measured the amount of CESAs that maintained trajectories associated with cortical microtubules in the wild type and *pom2* mutants. Only ~10% of the CESAs were associated with microtubules in the *pom2* mutants; however, 94% of the CESAs maintained trajectories along microtubules in the wild-type background (284 particles from three cells from three seedlings in the wild type, *pom2-4*, and *pom2-7*, respectively). These analyses were corroborated by visual inspection of consecutive and averaged time frame images, which revealed that the CESA trajectories moved independently of the direction of the underlying cortical microtubules in the *pom2* mutants (cf. Figures 5D to 5F; see Supplemental Movie 4 online). Thus, POM2/CSI1 is important for the microtubule-based guidance of the CESAs.

Loss of the microtubule array does not affect the velocity of CESA particles localized to the plasma membrane (Paredez et al., 2006; Chen et al., 2010; Bischoff et al., 2011). However, plasma membrane–located CESAs in the *pom2/csi1* mutants showed a two- to threefold reduction in speed compared with the wild-type background (Gu et al., 2010). One possible explanation for this is that POM2/CSI1, in addition to its role in coaligning the CESAs and microtubules, also influences the activity of the CESAs as determined by the decreased motility. Another possibility is that POM2/CSI1 contributes to a currently not recognized guiding mechanism for the CESAs independently of the microtubule array. To test the latter, we tracked individual plasma membrane located CESA particles over 100 single images (500-s total imaging time) and assessed the degree of linearity of migrating CESAs over time. We subsequently estimated the deviations from linear trajectories in the *pom2-4* mutant and the wild type by plotting the displacement in the x and y direction over time and calculating the linear regression coefficients (Figure 5G). The CESAs deviated significantly more from linear tracks in the *pom2-4* compared with the wild type (Figure 5G). However, similar deviations were also observed in oryzalin-treated wild-type cells (Figure 5G). It is therefore likely that the reduced CESA velocities observed in the *pom2* mutants correspond to an alteration in CESA activity and not an alternative guiding mechanism by POM2/CSI1. Hence, it is evident that the POM2/CSI1 not only provides for an association between the cortical microtubules and the CESAs but also is important for the maintenance of an active CESA complex. These results further show that the linear movement of the plasma membrane located CESAs is stabilized by the cortical microtubules.

DISCUSSION

Turgor-driven expansion, coupled with cell wall reorganization, is essential for anisotropic cell development and plant growth. Several genetic screens have revealed mutants with defects in cell elongation, some of which affect cellulose production. We show that the conditional root expansion mutant *pom2* affects *CSI1* (Gu et al., 2010) and that the function of the protein is essential for the guidance of the CESA complexes along the cortical microtubules.

Already in the early 1960s, Paul Green and others observed that cellulose microfibrils were disrupted by the antispindle fiber drug colchicine and proposed that the spindle fibers, later

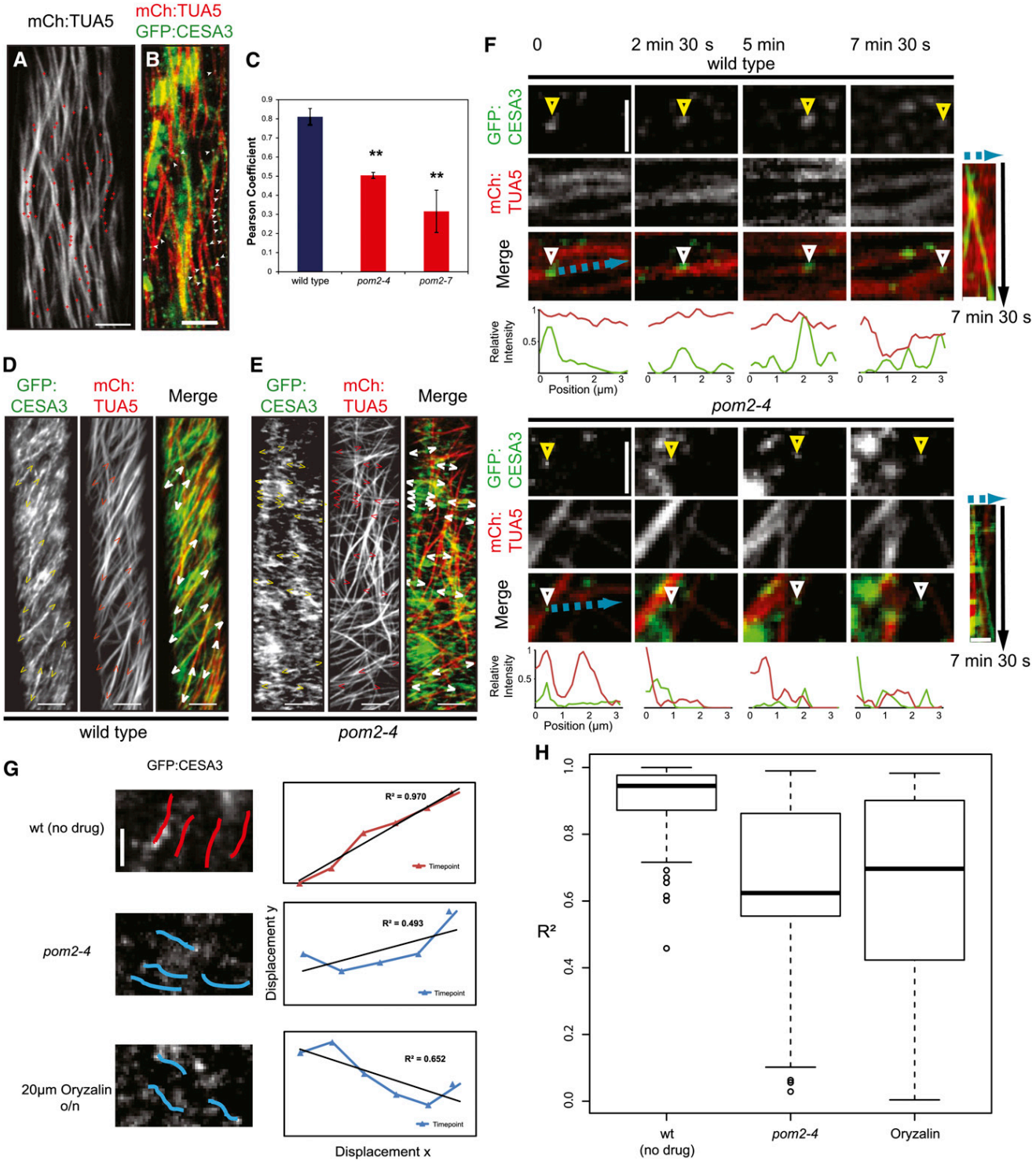

Figure 5. POM2/CSI1 Is Necessary for Coalignment of CESAs and Microtubules at the Cell Cortex.

(A) Map of CESA complex delivery sites in an elongating *pom2-4* mutant cell from a 4-d-old etiolated hypocotyl. The sites were mapped on a 10-min average projection of microtubule signal. Red plus symbols indicate CESA insertion sites.
(B) Single image frame showing CESA insertions (green channel; white arrowheads) on microtubules (red channel) in a *pom2-4* mutant cell from a 4-d-old etiolated hypocotyl. Bars = 5 µm in **(A)** and **(B)**.

termed microtubules (Ledbetter and Porter, 1963), may have a role in the orientation of microfibril deposition. This hypothesis was corroborated by live-cell imaging (Paredez et al., 2006), which showed that cortical microtubules define the trajectories of plasma membrane–based CESAs. The tight spatial and temporal link between the CESA trajectories and microtubules indicated an intimate contact between the two arrays (Baskin, 2001; Paredez et al., 2006). We show that mutations in POM2/CSI1 substantially reduce coalignment of the CESAs and cortical microtubules, suggesting that POM2/CSI1 facilitates a link between the CESAs and the microtubules during cellulose synthesis. POM2/CSI1 contains many Armadillo repeats, which are present in several microtubule binding proteins (reviewed in Tewari et al., 2010). One possible scenario could therefore be that POM2/CSI1 contributes a direct link between the CESAs and microtubules. Another scenario may involve additional components (e.g., proteins that could promote motility along the microtubules). For instance, mutations in a kinesin-like protein caused altered deposition of secondary wall cellulose microfibrils in *Arabidopsis* (Zhong et al., 2002). Similarly, mutations in the rice (*Oryza sativa*) kinesin-4 also led to deficiencies in secondary wall cellulose production (Zhang et al., 2010). While these mutants affect secondary wall cellulose synthesis, it is possible that kinesin-related activity also could play a role in primary wall cellulose production, perhaps by supporting the means of motility for POM2/CSI1 and, hence, the CESAs, along the microtubules. Interestingly, an Armadillo repeat protein, KAP3, associates with kinesins and is important for cargo movement along microtubules in neuronal axons (reviewed in Manning and Snyder, 2010).

While it is possible that active microtubule-associated machinery could be involved in promoting migration of the CESA complex along the microtubule, it is perhaps more likely that polymerization of the cellulose microfibril drives CESA motility. For example, both CESA and POM2/CSI1 motility can be observed in the absence of a microtubule array (see Supplemental Figure 6C online; Paredez et al., 2006). Providing that this hypothesis is correct, and also that the main POM2/CSI1 activity is related to guidance of the CESAs along cortical microtubules, we would expect the CESA complexes to migrate with a similar speed in *pom2/csi1* mutant cells as in wild-type cells. However, this is not the case. The rate of CESA migration is reduced two- to threefold in the *pom2/csi1* background (Gu et al., 2010). This raises some interesting questions regarding the function of POM2/CSI1 and regarding the role of microtubules in the maintenance of CESA migration. Two recent reports show that disruption of the microtubule array can promote CESA migration (Chen et al., 2010; Bischoff et al., 2011), which further corroborates that the CESA activity supports CESA motility. For example, one of these studies showed that the migration of CESA5 was reduced in etiolated *prc1-1* seedlings compared with the wild type (Bischoff et al., 2011). However, removal of the microtubules using oryzalin restored CESA5 migration to speeds observed in wild-type seedlings. These data suggest that the removal of microtubules should result in CESA migratory rates comparable to control seedlings. Yet, the abolished coalignment of the CESAs and cortical microtubules in the *pom2/csi1* mutants still result in reduced CESA velocities. Several scenarios may explain this observation. For example, it is possible that POM2/CSI1 may provide an additional layer of guidance to the CESA migration, perhaps via the putative C2 domain that is present in the C terminus of POM2/CSI1 that may interact with plasma membrane lipids. Such interactions could provide directionality of the CESA complex based on the lipid environment. If this hypothesis is true, one would expect a different CESA complex directionality in wild-type cells without microtubules and cells from *pom2/csi1* mutants. However, we observed similar deviations in linear tracking behavior of CESAs in oryzalin-treated wild-type cells and in *pom2/csi1* cells (Figure 5G). These results support an important function of POM2/CSI1 in microtubule-based tracking of the CESAs. The reduced CESA motility in the *pom2/csi1* mutants could instead be due to an important function of POM2/CSI1 for CESA activity, perhaps by modulating the CESA active sites with which POM2/CSI1 appears to interact (Gu et al., 2010). In support of this, mutations in several components that affect cellulose synthesis, such as KOR and CESA6, lead to reduced CESA motility (Paredez et al., 2008; Bischoff et al., 2011). It is also possible that POM2/CSI1 facilitates a docking site for other proteins necessary for CESA activity (e.g., for Suc synthase) that may provide substrate for cellulose synthesis.

While mutations in POM2/CSI1 result in phenotypes that typically are observed in cellulose-deficient mutants, such as cell elongation deficiency, collapsed pollen grains, and reduced cellulose levels (Gu et al., 2010), the *pom2/csi1* mutants also displayed defects in microtubule organization, cell file spiraling, and organ twisting. Spiraling, or twisting, phenotypes have been

Figure 5. (continued).

(C) Quantification of colocalization between GFP:CESA3 and mCherry:TUA5 trajectories in 500-s time averages using Pearson correlation (n = 9 cells from 9 seedlings). Error bars indicate SD. Asterisks indicate significance (**P value < 0.01).

(D) and **(E)** Average projections of 53 frames in elongating control **(D)** and *pom2-4* **(E)** cells in 4-d-old etiolated hypocotyls expressing mCherry:TUA5 and GFP:CESA3. Brackets indicate CESA migration trajectories. Bars = 5 μm.

(F) Time frames of individual plasma membrane–located CESAs in the wild type (top) and *pom2-4* (bottom) in relation to cortical microtubules. CESAs (arrowheads) track along microtubules in the wild type (top), but the tracking of CESAs in *pom2-4* is independent of the microtubule orientation (bottom). Kymographs of the observations are supplied to the right of the respective time frames. The intensity of both channels was plotted along the cyan trace.

(G) and **(H)** Degree of linearity of moving CESAs over time. The displacement of individual CESA particles (145 particles from nine seedlings; between 45 and 50 particles per treatment and line) was traced over 8 min (100 frames). The left panel shows examples of individual traces. x and y coordinates at different time points were plotted (**[G]**, right panel) and fitted against a linear curve. Deviations from linearity result in a low R^2 value; ideal linear traces are represented with an R^2 of 1. The distribution of R^2 values (right panel) shows a significant reduction in linear CESA movement in *pom2/csi1* mutants and in oryzalin-treated cells (*t* test: the wild type (wt) versus *pom2-4* and/or oryzalin treatment; P < 0.01, *pom2* versus oryzalin treatment; P > 0.5).

reported for mutations in several microtubule-associated proteins, such as SKU6/SPIRAL1, LEFTY1 and 2, and CLASP (Thitamadee et al., 2002; Sedbrook et al., 2004; Kirik et al., 2007), and perturbation of these proteins also lead to microtubule defects. Although cellulose-deficient mutants (i.e., mutants that have reduced CESA velocities and cellulose content) typically display defects in microtubule organization (Paredez et al., 2008), no spiraling phenotypes have been reported. Moreover, *clasp* and other microtubule-related mutants also affect mitotic activity, presumably by disturbances in the mitotic spindle formation (Ambrose et al., 2007; Kirik et al., 2007; Sunohara et al., 2009). Interestingly, *pom2*/*csi1* mutants also held a reduced number of cells that actively divided in the root meristem. Considering that no alterations in mitotic activity were observed in the cellulose-deficient mutant *ctl1*/*pom1* (Hermans et al., 2011), it is apparently not the reduction in cellulose per se that caused the impaired mitotic activity. Rather, certain defects in the microtubule stability or arrangement affect the mitotic activity. Although POM2/CSI1 appears to be more strongly connected to the CESAs than the microtubules, it is clear that the protein also executes important microtubule related functions. Hence, the microtubule-related phenotypes displayed by the *pom2*/*csi1* mutants corroborate the role of POM2/CSI1 in microtubule-related processes, which support that the protein facilitates a direct or indirect connection between the CESAs and microtubules.

Delivery of CESA particles to the plasma membrane may be facilitated either via the Golgi or via the post-Golgi compartments, which are referred to as smaCCs/MASCs (Crowell et al., 2009; Gutierrez et al., 2009). The latter compartments are induced by treating cells with isoxaben or osmotic stress (Crowell et al., 2009; Gutierrez et al., 2009). Interestingly, in addition to the close colocalization of CESA and POM2/CSI1 at the plasma membrane, we also observed pronounced colocalization of POM2/CSI1 signal with smaCCs/MASCs. Hence, POM2/CSI1 can associate with CESAs, or CESA-containing compartments, also at other locations than the plasma membrane. While the function of the smaCCs/MASCs is unclear, it has been proposed that the vesicles may hold CESA complexes that are in transit to the plasma membrane (Gutierrez et al., 2009). Considering that POM2/CSI1s can associate with the smaCCs/MASCs, one possible scenario would be that CESAs and POM2/CSI1s are codelivered to the plasma membrane. However, we only observed codelivery of a minor part of the observed delivery events. One reason for this observation may be that POM2/CSI1s are codelivered with CESAs from the smaCCs/MASCs only and not with CESAs that are inserted directly from Golgi-derived compartments. For example, it is possible that either the cortical microtubules or the plasma membrane composition could provide an advantageous environment for POM2/CSI1s to interact with CESAs at the cell cortex. Consistent with this, we did not observe any convincing colocalization of POM2/CSI1 and CESAs associated with rapidly moving Golgi. We therefore favor the occurrence of two types of delivery events: one in which POM2/CSI1 molecules already are associated with CESAs prior to insertion (possibly defined by the smaCCs/MASCs) and another in which POM2/CSI1 molecules continuously associate with the already delivered CESAs (presumably delivered directly from the Golgi). While some POM2/CSI1s were codelivered with the CESAs, we did not observe an alteration in CESA delivery rate in the *pom2*/*csi1* mutants compared with the wild type. CESA insertions preferentially coincide with cortical microtubules (Gutierrez et al., 2009). Considering the importance of POM2/CSI1 for coalignment of the microtubules and CESAs, it appeared plausible that POM2/CSI1 could establish an initial contact point between the CESAs and microtubules prior to insertion (e.g., via the smaCCs/MASCs association). Nevertheless, we observed that the CESA insertion coincided with microtubules also in the absence of POM2/CSI1. In addition, the absence of POM2/CSI1 also did not affect the behavior of the microtubule-tethered smaCCs/MASCs (see Supplemental Figure 8 online). We therefore propose that the mechanisms governing the insertion of the CESAs and of the motility patterns of the smaCCS/MASCs are different from the mechanism of microtubule-based guidance of the plasma membrane–located CESAs.

In summary, our results show that POM2/CSI1 can associate with CESA molecules that are actively synthesizing cellulose and CESA-containing compartments at the cell cortex. This association does not contribute to the rate of CESA insertions or to the localized insertions of CESAs adjacent to cortical microtubules. Rather, POM2/CSI1 is required for the guidance of CESAs along microtubules during cellulose synthesis.

METHODS

Plant Material

pom2-1 and *pom2-2* were previously isolated in a screen for root morphogenesis mutants (Hauser et al., 1995). *pom2-3* was a donation of T. Wada and was isolated from an ethyl methanesulfonate–mutagenized population in L*er*. *pom2-4* was isolated from a T-DNA–mutagenized progeny of a cross between Col and Nossen kindly provided by Christian Luschnig. *pom2-5* (SALK_047252), *pom2-6* (SALK_051146), *pom2-7* (SALK_115451), *pom2-8* (SALK_136239), *csi2* (SALK_022491 and SALK_024648), and *csi3* (SALK_009141 and SALK_009157) are T-DNA insertion lines from the Arabidopsis Stock Center (http://www.Arabidopsis.org/; Alonso et al., 2003). The marker line expressing cycB1;1:CDB:GUS was a gift from John Celenza. Col-0 seeds containing the constructs mCherry:TUA5 and GFP:CESA3 as well as tdTomato:CESA6 and MAP4:GFP (Desprez et al., 2007; Gutierrez et al., 2009) were kindly donated by Ryan Gutierrez, David Ehrhardt, and Herman Höfte.

Growth Conditions and Phenotypic Characterization

Seedlings were cultivated after stratification for at least 2 d at 4°C vertically on sterile nutrient plates according to Hauser et al. (1995). Plants were propagated on soil with a 16-h-light/8-h-dark cycle according to Hauser et al. (1995). Homozygous plants of *pom2-1*, *pom2-2*, and *pom2-4* were used as female parents for crosses. Reciprocal crosses were only successful with *pom2-3*. For hypocotyl measurements under skotomorphogenic conditions, nutrient agar plates with sterile seeds were wrapped in aluminum foil. After 4 d at 4°C of stratification, the covered plates were transferred to 22°C and incubated for another 7 d. Cell walls were visualized with propidium iodine (10 μg/mL). Cell and organ sizes were measured using differential interference contrast microscopy on chloral hydrate–cleared preparations as described by Müller et al. (2002) on whole seedling or plant organ levels. Alternatively, seeds were sterilized and germinated on nutrient plates after stratification for at least 2 d at 4°C and measured after 5 d of growth at 22°C. For confocal microscopy of hypocotyls expressing diverse marker lines, seedlings were cultivated on Murashige and Skoog (MS) media in light (16-h

photoperiod) or dark conditions at 21°C for 3 or 4 d as described by Sampathkumar et al. (2011).

Drug Treatments

Drug treatments were performed essentially as described by Sampathkumar et al. (2011). Seedlings were immersed in 2 mL of solution with drugs or a control solution in 12-well cell culture plates in the dark and were subsequently imaged. A stock solution of oryzalin was dissolved in DMSO, and working stocks were made fresh by further dilution in water (stock solutions; 20 mM oryzalin in DMSO and 20 μM isoxaben in water).

Meristem Activity and Pollen Germination

Meristem activity was quantified in the GUS-stained seedlings of crosses between different *pom2* mutants and the cycB1;1:CDB:GUS according to Hauser and Bauer (2000). Histochemical GUS staining was done as described by Hauser and Bauer (2000). For pollen germination assays (Azarov et al., 1990), anthers of soil-grown plants were harvested at different developmental stages. Pollen was applied to a microscope slide covered with a thin layer of pollen germination medium (3% [w/v] agar, 25% [w/v] Suc, 0.7 mM $CaCl_2$, 1 mM $MgSO_4$, 2 mM $Ca[NO_3]_2$, 0.25 mM K_2HPO_4, 1 mM K_2SO_4, and 8 mM H_3BO_3 adjusted to pH 7.4). After incubation in a humid chamber at 24°C for ~17 h, pollen grains were considered as germinated if the pollen tube length exceeded one grain diameter.

Mounting of Seedlings for Confocal Microscopy

Seedlings were mounted in half-strength MS medium supplemented with 1% (w/v) Suc and buffered with 10 mM MES, pH 5.7, or between a cover glass and a 1-mm thick 1% agar pad affixed on a circular cover slip (Roth), thus stabilizing the sample and preventing it from compression and mechanical damage.

Genetic Mapping and Chromosomal Walking toward the *pom2* Locus

Mapping was performed with the F2 progeny of a cross between *pom2-3* and Wassilewskija (Ws). The phenotypes of >2000 F2 seedlings were scored on nutrient agar plates. A total of 511 *pom2* seedlings were used for fine mapping with the microsatellite marker F14M13 and the duplex analysis markers F7D8_91, T16B14_20, T26C19_19, and T26C19_43 (Hauser et al., 1998; see Supplemental Table 1 online). Genomic DNA isolation and PCR analyses were performed as described by Hauser et al. (1998). Allele-specific polymorphisms were detected with DNA gel blot analysis of *Nco*I- and *Eco*RV-digested genomic DNA and probed with the digoxigenin-labeled BAC clone T16B14 as described by Adhami et al. (1999). Overlapping PCR fragments of the genomic region around the polymorphic *Nco*I site from wild-type Col, L*er*, *pom2-1*, *pom2-2*, *pom2-3*, and *pom2-4* and of the cDNA clones RZL02E12, APZL03F11, and RZL15D2 were sequenced on the ABI-Prism 310 genetic analyzer using the BigDye terminator cycle sequencing chemistry (Perkin-Elmer, Applied Biosystems, and Amersham). Ambiguous exon/intron borders were confirmed by RT-PCR (for primers, see Supplemental Table 2 online) and sequencing. *pom2-1* has a 3.9-kb deletion from amino acid 517 in exon IV to amino acid 1755 in exon V, causing a predicted protein of 912 amino acids; *pom2-2* has a short AATGCGTGAG deletion in exon IV that causes a frame shift and leads to a stop codon at amino acid 119; *pom2-3* has a single base pair deletion at the beginning of exon V leading to a frame shift and a premature stop codon at amino acid 1108; *pom2-4* has a 2446-bp deletion starting in exon IV and ending in the adjacent gene (see Figure 1E for schematic view).

Cosmid Library Screen, Transformations, and Constructs

A cosmid carrying a 14.5-kb genomic region of the *POM2* locus was isolated from a genomic L*er* library constructed in pBIC20 (Meyer et al., 1996) and used to transform the *pom2-3* allele and wild-type controls by the floral dipping method of Clough and Bent (1998). T1 transformants were selected on MS plates containing 100 μg mL^{-1} kanamycin. The segregation of the resistance and the phenotype was scored in 13 independent T2 lines. *POM2/CSI1*cDNA was amplified from the full-length cDNA containing clone RZL02e12 (obtained from the Kazusa DNA Research Institute, Japan; see Supplemental Table 3 online) and transferred to the vector pENTRY/SD/D Topo (Invitrogen), followed by homologous recombination to the destination vector pGBPGWC using Gateway technology (Invitrogen). Col-0 plants expressing POM2:CFP were generated by *Agrobacterium tumefaciens*–mediated transformation (Clough and Bent, 1998). T1 transgenic plants were selected on kanamycin and resistant progeny was used for spinning disc confocal microscopy as described by Sampathkumar et al. (2011).

Microscopy

Light microscopy was performed using Leica stereomicroscopes (MZ12.5 or MZFLIII and the digital camera DFC420 or DC500). Microtubules were visualized in the F2 progeny of crosses between *pom2-1*, *pom2-3*, *pom2-4*, and the MAP4:GFP marker line with a confocal laser scanning microscope (Leica TCS-SP2). Seedlings expressing mCherry:TUA5, POM2:CFP, and dual-labeled lines of GFP:CESA3 and mCherry:TUA5, POM2:CFP, and mCherry:TUA5 as well as tdTomato:CESA6 and POM2:CFP were imaged on a confocal microscope equipped with a CSU-X1 Yokogawa spinning disc head fitted to a Nikon Ti-E inverted microscope, a CFI APO TIRF 3100 oil immersion objective (numerical aperture of 1.49), an Evolve charge-coupled device camera (Photometrics Technology), and a 31.2 lens between the spinning disc and camera. GFP was excited at 491 nm, mCherry at 561 nm, and CFP at 405 nm using a multichannel dichroic and an ET455/50M, ET525/50M, or ET595/50M band-pass emission filter (Chroma Technology) for CFP, GFP, and mCherry/tdTomato, respectively. Image acquisitions were performed using Metamorph online premier, version 7.5. Typical exposure times were 600 ms for GFP and 300 ms for mCherry. Environmental scanning electron microscopy was performed as described by Persson et al. (2007).

General Image Processing and Analysis

All images were processed using ImageJ software (W.S. Rasband; National Institutes of Health). Background correction was performed using the "subtract background" tool (rolling ball radius 30 to 40 pixels), and StackReg was used to correct focus drift. Linear adjustments in pixel values were made when measuring signal intensities. Microtubule angles were measured with regard to the growth axis and always in a clockwise direction using the angle tool in ImageJ.

Colocalization Analysis

All colocalization analyses were done with the Jacop plugin for ImageJ (Bolte and Cordelières, 2006). Pearson coefficients were calculated for the time-averaged signals of GFP:CESA3 and TUA5:mCherry as well as POM2:CFP and GFP:CESA3 and compared with randomized images using Costes randomization and automatic threshold (Costes et al., 2004). Colocalization analysis of POM2:CFP and mCherry:TUA5, as well as POM2:CFP and tdTomato:CESA6, was performed using the van Steensel's cross-correlation function mechanism, which determined the degree of co-occurrence of the fluorescent signals of two channels by shifting the corresponding channels in relation to each other in the x

direction (shift = 20 pixels; van Steensel et al., 1996). Correlation maxima at a shift of 0 pixels indicate that colocalization of both channels is apparent for most fluorescent foci.

Analysis of Fluorescent Particle and Microtubule Dynamics Using Kymographs and Three-Dimensional Heat Maps

Kymographs were made using the multiple Kymograph plugin for ImageJ (http://www.embl.de/eamnet/html/body_kymograph.html), applying a line width of three pixels. Slopes of the kymographs were measured with the angle tool in ImageJ. POM2 and CESA particle velocities as well as microtubule growth and shrink velocities were calculated from the slopes of the kymographs as follows:

$$v = \frac{\sin(a) \times d}{n \times r}$$

where v = velocity (μm/min), a = angle between fluorescent trace and orthogonal axis (time axis) of kymograph (rad), d = distance of movement (μm), n = number of frames, and r = frame rate (min). Three-dimensional heat maps of kymographs were generated using the Interactive 3D Surface Plots plugin (http://rsbweb.nih.gov/ij/plugins/surface-plot-3d.html). CESA tracks were defined as trajectories of CESAs during steady movement (seen as lines in time average images). CESA particles were considered to be associated with microtubules if they tracked (with steady motion) along microtubule fluorescent signal over a time frame of 120 frames (5-s intervals) = 10 min. Microtubule angles were measured as described by Sampathkumar et al. (2011). The ImageJ angle tool was used to determine the angle between the microtubule and the longitudinal axis of the cell.

Analysis of CESA Delivery Sites at Cortical Microtubules

Delivery events of CESAs were analyzed as described by Gutierrez et al. (2009). Wild-type plants and mutant plants for *pom2-4* and *-5* expressing GFP:CESA3 and mCherry:TUA5 were bleached with a 2-s, 405-nm laser pulse, followed by image acquisition in 5-s time intervals over 300 frames. Photobleaching was performed by a fluorescence recovery after photobleaching/photo ablation system (Roper Scientific) integrated into the setup above.

GFP:CESA3 and POM2:CFP Density Measurements and Delivery Rates

Particle numbers of tdTomato:CESA6 and POM2:CFP were determined using the particle tracker plugin for ImageJ (Sbalzarini and Koumoutsakos, 2005) combined with counting by eye. In the case of CESA density quantification, areas covered with background fluorescence caused by Golgi vesicles were not taken into consideration. CESA insertion rates were determined by calculating the slope of CESA density (particles/μm^2) plotted against bleach recovery time (min) for at least three biological replicates through regression of the linear phase of recovery.

qRT-PCR Analysis of T-DNA Insertion Lines

The qRT-PCR reaction was performed using the primers presented in Supplemental Tables 2 and 3 online. Power SYBRGreen (Agilent) was used as the detector. Reactions were run on an ABI Prism 7900 HT fast real-time PCR system (Applied Biosystems). mRNA from *Arabidopsis thaliana* leaves was extracted using the RNAeasy extraction kit (Qiagen) following the supplier's instructions. cDNA synthesis was performed using the Superscript III reverse transcription kit (Invitrogen). Cycle threshold values were normalized to the housekeeping gene *UBI10* (Czechowski et al., 2005). Alternatively, total RNA of seedlings and organs was isolated according to the manufacturers' protocols using TRI reagent (Molecular Research Center). After DNase I (Roche) treatment, 2.5 to 5 μg total RNA was reverse transcribed with Superscript I (Invitrogen) and 2 μM oligo(dT)$_{18}$ primers (Karsai et al., 2002). Absolute and relative copy numbers of individual mRNA species were calculated with standard curves of known molar concentrations for each of the genes. The expression was normalized to the housekeeping gene *TUB9*. At least three different RNA isolations and cDNA synthesis were used for quantification, and each cDNA was measured in triplicate. Primers, gene name, and the size of genomic and cDNA amplicons are listed in Supplemental Tables 1 and 2 online. In silico expression analysis was done using the Web-based program Spot History with two clones on the AFGC chip (ID132C7T7 and ID192M4T7) and one clone on the Affimetrix chip (SpotID 418556 as At2g22125).

Accession Numbers

Sequence data from this article can be found in the Arabidopsis Genome Initiative under the following accession numbers: POM2/CSI1 (At2g22125), CSI2 (At1g44120), CSI3 (At1G77460), CESA6 (At5g64740), CESA3 (At5g05170), TUA5 (At5g19780), T26C19 (AF076243), and T16B14 (AC007232).

Supplemental Data

The following materials are available in the online version of this article.

Supplemental Figure 1. Phenotypes of *pom2* and Wild-Type Seedlings after Germination on Medium Supplemented with 4.5% Suc.

Supplemental Figure 2. *pom2* Mutant Phenotypes.

Supplemental Figure 3. *pom2* Mutants Are Impaired in Meristematic Activity and Microtubule Organization.

Supplemental Figure 4. Schematic Representation of the Positional Cloning Strategy of *POM2* and qPCR Analyses.

Supplemental Figure 5. POM2/CSI1:CFP Behavior and Colocalization with CESA Complexes.

Supplemental Figure 6. Co-Occurrence of POM2/CSI1 and Microtubules at the Cell Cortex in Etiolated Hypocotyls.

Supplemental Figure 7. POM2/CSI1 Only Moves Together with Depolymerizing Microtubule Ends, and Delivery of CESAs and POM2/CSI1 to the Plasma Membrane.

Supplemental Figure 8. Mutations in POM2/CSI1 Have No Visible Effect on the Attachment of smaCCs/MASCs to Microtubules.

Supplemental Table 1. Summary of the Molecular Markers Used for Fine Mapping the *POM2* Locus.

Supplemental Table 2. Primers Used for Sequencing and Real-Time PCR Analyses.

Supplemental Table 3. Primers for *POM2* Cloning, Genotyping, and qRT-PCR Analysis.

Supplemental Movie 1. POM2/CSI1 Can Track along Depolymerizing Microtubule Ends.

Supplemental Movie 2. POM2/CSI1 Collecting Other POM2/CSI1s.

Supplemental Movie 3. POM2/CSI1 Is Only Associated with Depolymerizing Microtubule Ends.

Supplemental Movie 4. Coalignment of CESAs and Cortical Microtubules Is Lost in *pom2/csi1* Mutants.

ACKNOWLEDGMENTS

We thank Takuji Wada for the *pom2-3* allele, Christian Luschnig for the *pom2-4* allele, Ryan Gutierrez and Dave Ehrhardt for tdTomato:CESA6,

and John Celenza for the cycB1;1:CDB:GUS marker line. We also thank Nicole Schlager, Gernot Resch, Norma Funke, and Anja Froehlich for technical assistance, Thomas Nedoma for the initial mapping, Albert Karsai for T-DNA segregation analysis, and the other members of the lab for advice and patience. The cosmid library was a kind gift of Erwin Grill and Andreas Bachmair. We thank Thomas Herter and Yi Zhang for experimental support. We thank the Kazusa DNA Research Institute (RIKEN) for providing the cDNA clones of *POM2*. E.L. was supported by the Asia-Europe Forestry Exchange Program and Austria Science Foundation (FWF) Project P13353. T.K. was financed through the AKTION Österreich-Tschechische Republik Project 21p8. This project was further supported by the FWF Project P14477 to M.-T.H. M.B., A.S., and S.P. were funded through the Max-Planck Gesellschaft and through Deutsche Forschungsgemeinshaft Grant PE1642/5-1. This project was further supported by FWF Projects P14477 and F03707 to M.-T.H.

AUTHOR CONTRIBUTIONS

M.B., M.-T.H., and S.P. designed the research. M.B., E.L., A.S., T.K., M.-T.H., and S.P. performed the research. M.B., E.L., A.S., M.-T.H., and S.P. analyzed data. M.B., A.S., M.-T.H., and S.P. wrote the article.

Received November 7, 2011; revised December 29, 2011; accepted January 12, 2012; published January 31, 2012.

REFERENCES

Adhami, F., Müller, S., and Hauser, M.-T. (1999). Nonradioactive labeling of large DNA fragments for genome walking, RFLP and northern blot analysis. Biotechniques **27:** 314–320.

Alonso, J.M., et al. (2003). Genome-wide insertional mutagenesis of *Arabidopsis thaliana*. Science **301:** 653–657.

Ambrose, J.C., Shoji, T., Kotzer, A.M., Pighin, J.A., and Wasteneys, G.O. (2007). The *Arabidopsis* CLASP gene encodes a microtubule-associated protein involved in cell expansion and division. Plant Cell **19:** 2763–2775.

Arioli, T., et al. (1998). Molecular analysis of cellulose biosynthesis in Arabidopsis. Science **279:** 717–720.

Azarov, A.S., Tokarev, B.I., and Netchepurenko, A.E. (1990). Effect of sodium chloride on pollen germination and pollen tube growth in vitro in *Arabidopsis thaliana* (L.) Heynh. Arabidopsis Inf. Serv. 27. http://www.arabidopsis.org/ais/1990/azaro-1990-aacdq.html.

Baskin, T.I. (2001). On the alignment of cellulose microfibrils by cortical microtubules: A review and a model. Protoplasma **215:** 150–171.

Baskin, T.I., Beemster, G.T.S., Judy-March, J.E., and Marga, F. (2004). Disorganization of cortical microtubules stimulates tangential expansion and reduces the uniformity of cellulose microfibril alignment among cells in the root of Arabidopsis. Plant Physiol. **135:** 2279–2290.

Bichet, A., Desnos, T., Turner, S., Grandjean, O., and Höfte, H. (2001). BOTERO1 is required for normal orientation of cortical microtubules and anisotropic cell expansion in Arabidopsis. Plant J. **25:** 137–148.

Bischoff, V., Desprez, T., Mouille, G., Vernhettes, S., Gonneau, M., and Höfte, H. (2011). Phytochrome regulation of cellulose synthesis in Arabidopsis. Curr. Biol. **21:** 1822–1827.

Bolte, S., and Cordelières, F.P. (2006). A guided tour into subcellular colocalization analysis in light microscopy. J. Microsc. **224:** 213–232.

Carpita, N.C. (2011). Update on mechanisms of plant cell wall biosynthesis: How plants make cellulose and other (1->4)-β-D-glycans. Plant Physiol. **155:** 171–184.

Chen, S., Ehrhardt, D.W., and Somerville, C.R. (2010). Mutations of cellulose synthase (CESA1) phosphorylation sites modulate anisotropic cell expansion and bidirectional mobility of cellulose synthase. Proc. Natl. Acad. Sci. USA **107:** 17188–17193.

Clough, S.J., and Bent, A.F. (1998). Floral dip: A simplified method for Agrobacterium-mediated transformation of *Arabidopsis thaliana*. Plant J. **16:** 735–743.

Cosgrove, D.J. (2005). Growth of the plant cell wall. Nat. Rev. Mol. Cell Biol. **6:** 850–861.

Costes, S.V., Daelemans, D., Cho, E.H., Dobbin, Z., Pavlakis, G., and Lockett, S. (2004). Automatic and quantitative measurement of protein-protein colocalization in live cells. Biophys. J. **86:** 3993–4003.

Crowell, E.F., Bischoff, V., Desprez, T., Rolland, A., Stierhof, Y.D., Schumacher, K., Gonneau, M., Höfte, H., and Vernhettes, S. (2009). Pausing of Golgi bodies on microtubules regulates secretion of cellulose synthase complexes in *Arabidopsis*. Plant Cell **21:** 1141–1154.

Czechowski, T., Stitt, M., Altmann, T., Udvardi, M.K., and Scheible, W.R. (2005). Genome-wide identification and testing of superior reference genes for transcript normalization in Arabidopsis. Plant Physiol. **139:** 5–17.

Desprez, T., Juraniec, M., Crowell, E.F., Jouy, H., Pochylova, Z., Parcy, F., Höfte, H., Gonneau, M., and Vernhettes, S. (2007). Organization of cellulose synthase complexes involved in primary cell wall synthesis in *Arabidopsis thaliana*. Proc. Natl. Acad. Sci. USA **104:** 15572–15577.

Endler, A., and Persson, S. (2011). Cellulose synthases and synthesis in Arabidopsis. Mol. Plant **4:** 199–211.

Fagard, M., Desnos, T., Desprez, T., Goubet, F., Refregier, G., Mouille, G., McCann, M., Rayon, C., Vernhettes, S., and Höfte, H. (2000). PROCUSTE1 encodes a cellulose synthase required for normal cell elongation specifically in roots and dark-grown hypocotyls of *Arabidopsis*. Plant Cell **12:** 2409–2424.

Green, P.B. (1962). Mechanism for plant cellular morphogenesis. Science **138:** 1404–1405.

Gu, Y., Kaplinsky, N., Bringmann, M., Cobb, A., Carroll, A., Sampathkumar, A., Baskin, T.I., Persson, S., and Somerville, C.R. (2010). Identification of a cellulose synthase-associated protein required for cellulose biosynthesis. Proc. Natl. Acad. Sci. USA **107:** 12866–12871.

Guerriero, G., Fugelstad, J., and Bulone, V. (2010). What do we really know about cellulose biosynthesis in higher plants? J. Integr. Plant Biol. **52:** 161–175.

Gutierrez, R., Lindeboom, J.J., Paredez, A.R., Emons, A.M., and Ehrhardt, D.W. (2009). Arabidopsis cortical microtubules position cellulose synthase delivery to the plasma membrane and interact with cellulose synthase trafficking compartments. Nat. Cell Biol. **11:** 797–806.

Hauser, M.T., Adhami, F., Dorner, M., Fuchs, E., and Glössl, J. (1998). Generation of co-dominant PCR-based markers by duplex analysis on high resolution gels. Plant J. **16:** 117–125.

Hauser, M.T., and Bauer, E. (2000). Histochemical analysis of root meristem activity in *Arabidopsis thaliana* using a cyclin:GUS (β-glucuronidase) marker line. Plant Soil **226:** 1–10.

Hauser, M.T., Morikami, A., and Benfey, P.N. (1995). Conditional root expansion mutants of Arabidopsis. Development **121:** 1237–1252.

Hermans, C., Porco, S., Vandenbussche, F., Gille, S., De Pessemier, J., Van Der Straeten, D., Verbruggen, N., and Bush, D.R. (2011). Dissecting the role of CHITINASE-LIKE1 in nitrate-dependent changes in root architecture. Plant Physiol. **157:** 1313–1326.

Karsai, A., Müller, S., Platz, S., and Hauser, M.T. (2002). Evaluation of a homemade SYBR green I reaction mixture for real-time PCR quantification of gene expression. Biotechniques **32:** 790–792, 794–796.

Kimura, S., Laosinchai, W., Itoh, T., Cui, X., Linder, C.R., and Brown,

R.M., Jr. (1999). Immunogold labeling of rosette terminal cellulose-synthesizing complexes in the vascular plant *Vigna angularis*. Plant Cell **11:** 2075–2086.

Kirik, V., Herrmann, U., Parupalli, C., Sedbrook, J.C., Ehrhardt, D.W., and Hülskamp, M. (2007). CLASP localizes in two discrete patterns on cortical microtubules and is required for cell morphogenesis and cell division in Arabidopsis. J. Cell Sci. **120:** 4416–4425.

Lane, D.R., et al. (2001). Temperature-sensitive alleles of RSW2 link the KORRIGAN endo-1,4-beta-glucanase to cellulose synthesis and cytokinesis in Arabidopsis. Plant Physiol. **126:** 278–288.

Ledbetter, M.C., and Porter, K.R. (1963). A "microtubule" in plant cell fine structure. J. Cell Biol. **19:** 239–250.

Manning, B.D., and Snyder, M. (2010). Drivers and passengers wanted! The role of kinesin-associated proteins. Trends Cell Biol. **10:** 281–289.

Marc, J., Granger, C.L., Brincat, J., Fisher, D.D., Kao, Th., McCubbin, A.G., and Cyr, R.J. (1998). A GFP-MAP4 reporter gene for visualizing cortical microtubule rearrangements in living epidermal cells. Plant Cell **10:** 1927–1940.

Meyer, K., Benning, G., and Grill, E. (1996). Cloning of plant genes based on the genetic map position. In Genome Mapping in Plants, A.H. Patterns, ed (New York: Academic Press), pp. 137–154.

Müller, S., Fuchs, E., Ovecka, M., Wysocka-Diller, J., Benfey, P.N., and Hauser, M.T. (2002). Two new loci, *PLEIADE* and *HYADE*, implicate organ-specific regulation of cytokinesis in Arabidopsis. Plant Physiol. **130:** 312–324.

Nicol, F., His, I., Jauneau, A., Vernhettes, S., Canut, H., and Höfte, H. (1998). A plasma membrane-bound putative endo-1,4-beta-D-glucanase is required for normal wall assembly and cell elongation in Arabidopsis. EMBO J. **17:** 5563–5576.

Pagant, S., Bichet, A., Sugimoto, K., Lerouxel, O., Desprez, T., McCann, M., Lerouge, P., Vernhettes, S., and Höfte, H. (2002). KOBITO1 encodes a novel plasma membrane protein necessary for normal synthesis of cellulose during cell expansion in *Arabidopsis*. Plant Cell **14:** 2001–2013.

Paredez, A.R., Persson, S., Ehrhardt, D.W., and Somerville, C.R. (2008). Genetic evidence that cellulose synthase activity influences microtubule cortical array organization. Plant Physiol. **147:** 1723–1734.

Paredez, A.R., Somerville, C.R., and Ehrhardt, D.W. (2006). Visualization of cellulose synthase demonstrates functional association with microtubules. Science **312:** 1491–1495.

Persson, S., Paredez, A., Carroll, A., Palsdottir, H., Doblin, M., Poindexter, P., Khitrov, N., Auer, M., and Somerville, C.R. (2007). Genetic evidence for three unique components in primary cell-wall cellulose synthase complexes in Arabidopsis. Proc. Natl. Acad. Sci. USA **104:** 15566–15571.

Sampathkumar, A., Lindeboom, J.J., Debolt, S., Gutierrez, R., Ehrhardt, D.W., Ketelaar, T., and Persson, S. (2011). Live cell imaging reveals structural associations between the actin and microtubule cytoskeleton in *Arabidopsis*. Plant Cell **23:** 2302–2313.

Sbalzarini, I.F., and Koumoutsakos, P. (2005). Feature point tracking and trajectory analysis for video imaging in cell biology. J. Struct. Biol. **151:** 182–195.

Schindelman, G., Morikami, A., Jung, J., Baskin, T.I., Carpita, N.C., Derbyshire, P., McCann, M.C., and Benfey, P.N. (2001). COBRA encodes a putative GPI-anchored protein, which is polarly localized and necessary for oriented cell expansion in Arabidopsis. Genes Dev. **15:** 1115–1127.

Sedbrook, J.C., Ehrhardt, D.W., Fisher, S.E., Scheible, W.R., and Somerville, C.R. (2004). The *Arabidopsis* sku6/spiral1 gene encodes a plus end-localized microtubule-interacting protein involved in directional cell expansion. Plant Cell **16:** 1506–1520.

Shaw, S.L., and Lucas, J. (2011). Intrabundle microtubule dynamics in the Arabidopsis cortical array. Cytoskeleton (Hoboken) **68:** 56–67.

Somerville, C. (2006). Cellulose synthesis in higher plants. Annu. Rev. Cell Dev. Biol. **22:** 53–78.

Somerville, C., Bauer, S., Brininstool, G., Facette, M., Hamann, T., Milne, J., Osborne, E., Paredez, A., Persson, S., Raab, T., Vorwerk, S., and Youngs, H. (2004). Toward a systems approach to understanding plant cell walls. Science **306:** 2206–2211.

Sugimoto, K., Himmelspach, R., Williamson, R.E., and Wasteneys, G.O. (2003). Mutation or drug-dependent microtubule disruption causes radial swelling without altering parallel cellulose microfibril deposition in *Arabidopsis* root cells. Plant Cell **15:** 1414–1429.

Sugimoto, K., Williamson, R.E., and Wasteneys, G.O. (2000). New techniques enable comparative analysis of microtubule orientation, wall texture, and growth rate in intact roots of Arabidopsis. Plant Physiol. **124:** 1493–1506.

Sunohara, H., Kawai, T., Shimizu-Sato, S., Sato, Y., Sato, K., and Kitano, H. (2009). A dominant mutation of TWISTED DWARF 1 encoding an alpha-tubulin protein causes severe dwarfism and right helical growth in rice. Genes Genet. Syst. **84:** 209–218.

Tewari, R., Bailes, E., Bunting, K.A., and Coates, J.C. (2010). Armadillo-repeat protein functions: Questions for little creatures. Trends Cell Biol. **20:** 470–481.

Thitamadee, S., Tuchihara, K., and Hashimoto, T. (2002). Microtubule basis for left-handed helical growth in Arabidopsis. Nature **417:** 193–196.

van Steensel, B., van Binnendijk, E.P., Hornsby, C.D., van der Voort, H.T., Krozowski, Z.S., de Kloet, E.R., and van Driel, R. (1996). Partial colocalization of glucocorticoid and mineralocorticoid receptors in discrete compartments in nuclei of rat hippocampus neurons. J. Cell Sci. **109:** 787–792.

Wang, J., Howles, P.A., Cork, A.H., Birch, R.J., and Williamson, R.E. (2006). Chimeric proteins suggest that the catalytic and/or C-terminal domains give CesA1 and CesA3 access to their specific sites in the cellulose synthase of primary walls. Plant Physiol. **142:** 685–695.

Wasteneys, G.O., and Fujita, M. (2006). Establishing and maintaining axial growth: wall mechanical properties and the cytoskeleton. J. Plant Res. **119:** 5–10.

Zhang, M., Zhang, B., Qian, Q., Yu, Y., Li, R., Zhang, J., Liu, X., Zeng, D., Li, J., and Zhou, Y. (2010). Brittle Culm 12, a dual-targeting kinesin-4 protein, controls cell-cycle progression and wall properties in rice. Plant J. **63:** 312–328.

Zhong, R., Burk, D.H., Morrison III, W.H., and Ye, Z.H. (2002). A kinesin-like protein is essential for oriented deposition of cellulose microfibrils and cell wall strength. Plant Cell **14:** 3101–3117.

POM-POM2/CELLULOSE SYNTHASE INTERACTING1 Is Essential for the Functional Association of Cellulose Synthase and Microtubules in *Arabidopsis*

Martin Bringmann, Eryang Li, Arun Sampathkumar, Tomas Kocabek, Marie-Theres Hauser and Staffan Persson

Plant Cell; originally published online January 31, 2012;
DOI 10.1105/tpc.111.093575

Figure 1

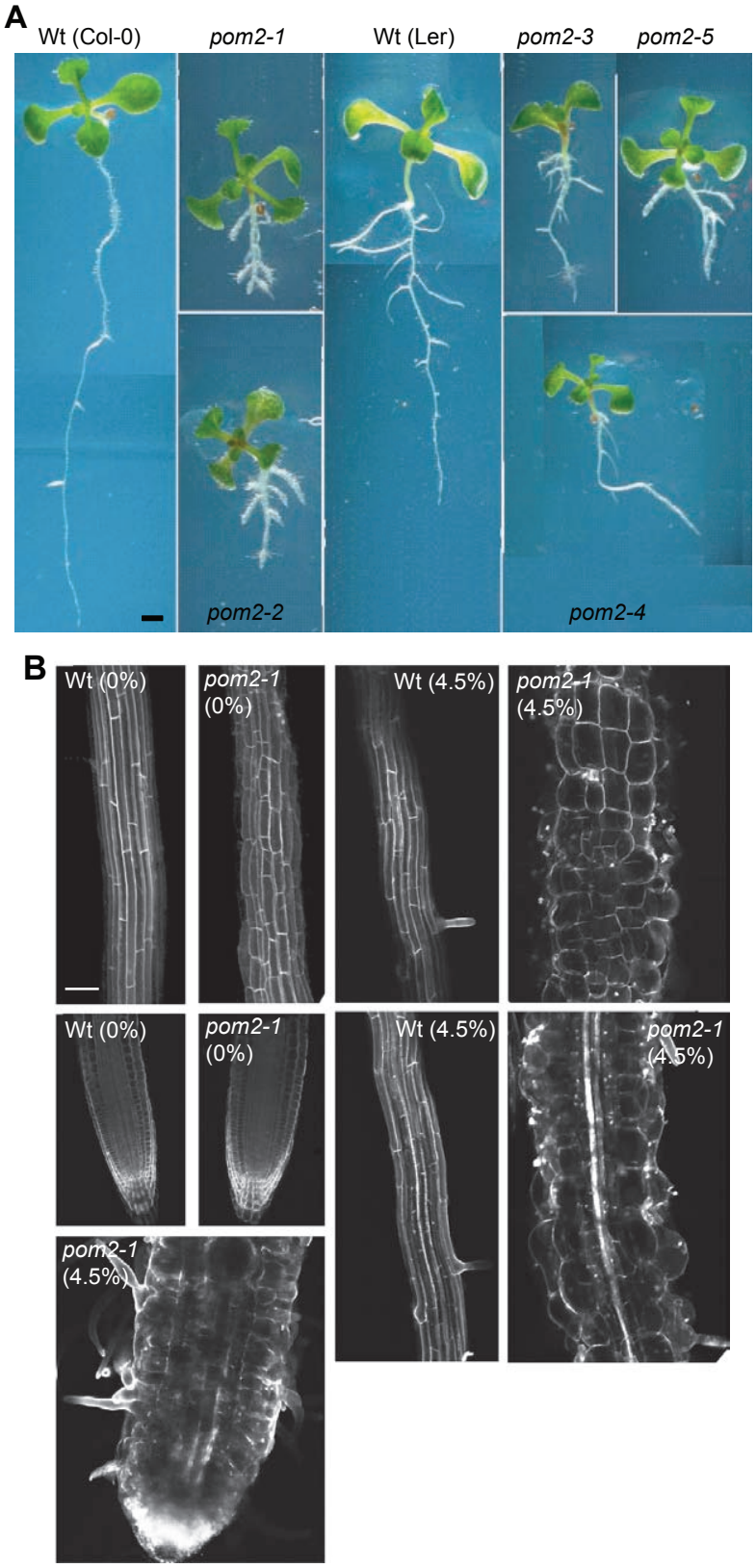

Figure 1. Phenotypes of *pom2* and wild type (Wt) seedlings after germination on medium supplemented with 4.5% sucrose. A. Eleven-day-old light-grown seedlings germinated on medium with 4.5% sucrose. Scale bar=1 mm. **B.** Conditional cell expansion phenotype of meristems and mature parts of roots cultivated on MS medium supplemented with 4.5% and 0% sucrose. Cells were visualized with propidium iodine. Scale bar=100 µm.

Figure 2

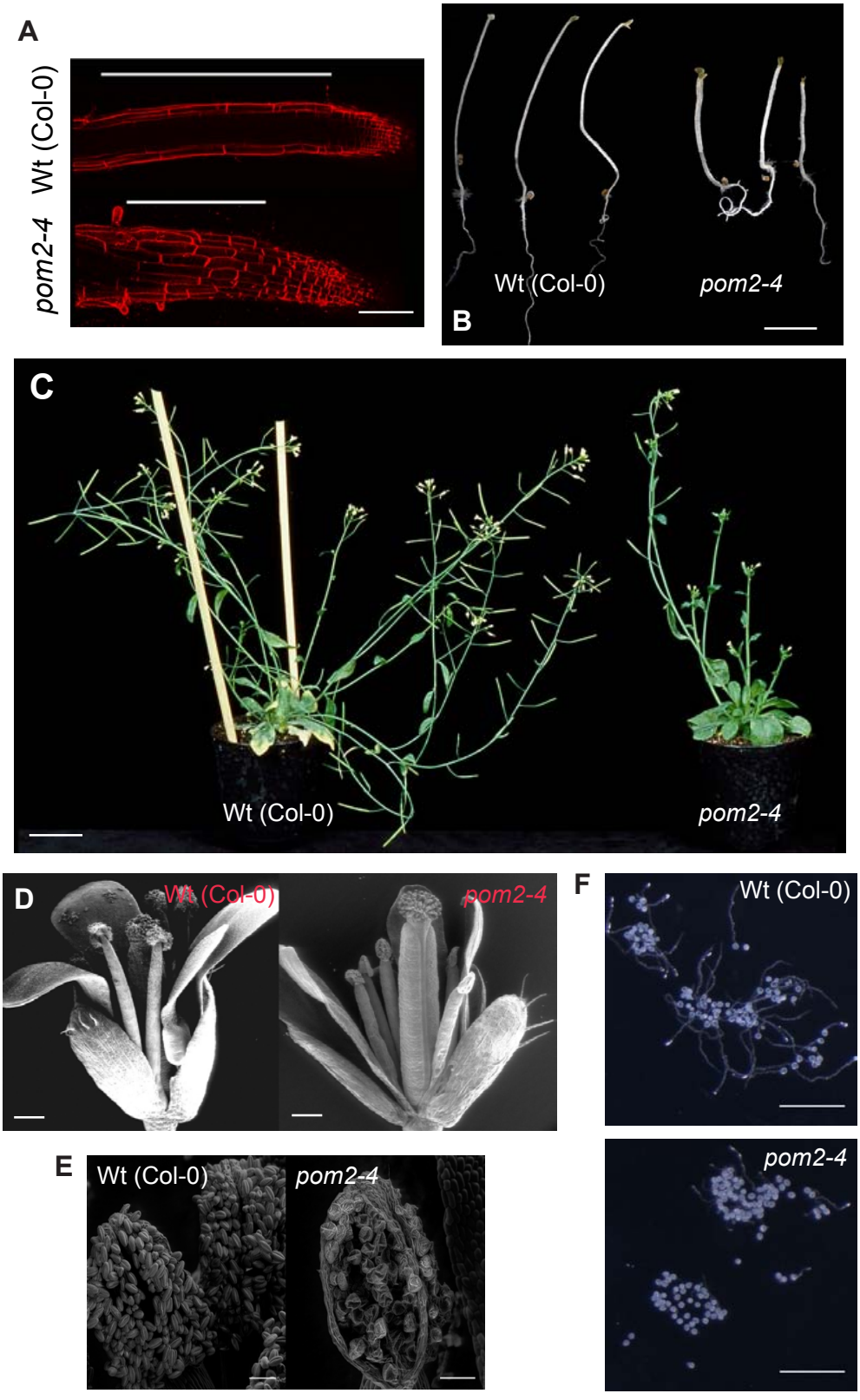

Figure 2. *pom2* mutant phenotypes. A. Root elongation zone of six-day-old light-grown wild type (upper; Wt (Col-0)) and *pom2-4* (lower) seedlings visualized with FM4-64. White bars indicate approximate elongation zone. Scale bar= 100 µm. **B.** Six-day-old etiolated seedlings grown on media supplemented with 1% sucrose. Scale bar=5 mm. **C.** Seven-week-old wild type and *pom2-4* plants. Scale bar=5 cm. **D.** Environmental Scanning Electron Microscopy (ESEM) images of open flowers of wild type and *pom2-4*. Scale bars=70 µm. **E.** ESEM images of pollen grains on anthers in wild type and *pom2-4* flowers. Scale bars=20 µm. **F.** Pollen germination assay of wild type and *pom2-4* pollen. Scale bars=200 µm.

Figure 3

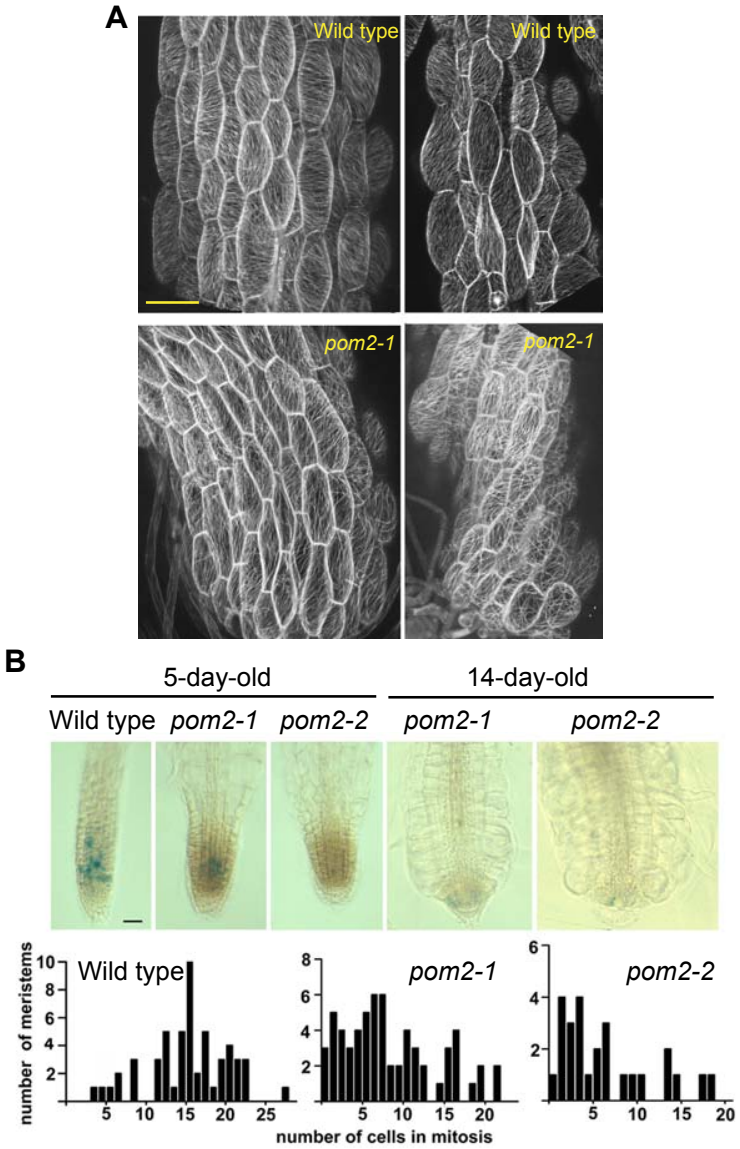

Figure 3. *pom2* mutants are impaired in meristematic activity and microtubule organization. A. Microtubule organization visualized with the MAP4-GFP marker in hypocotyls of light-grown seedlings on medium without sucrose. Upper panel, wild type; lower panel, *pom2-1*. Scale bar=100 µm. **B.** Upper panel. Typical histochemical staining of the cycB1;1:CDB:GUS reporter in five-day-old wild type and *pom2* mutant seedlings (left) and 14-day-old *pom2* mutant seedlings (right). Lower panel. Quantitative analysis of meristematic activity. Most of the wild type meristems hold more than 15 cells undergoing mitosis. In contrast, 70% of *pom2-1*, and 80% of *pom2-2* meristems have less than 10 cells in mitosis. Scale bar=50 µm.

Figure 4

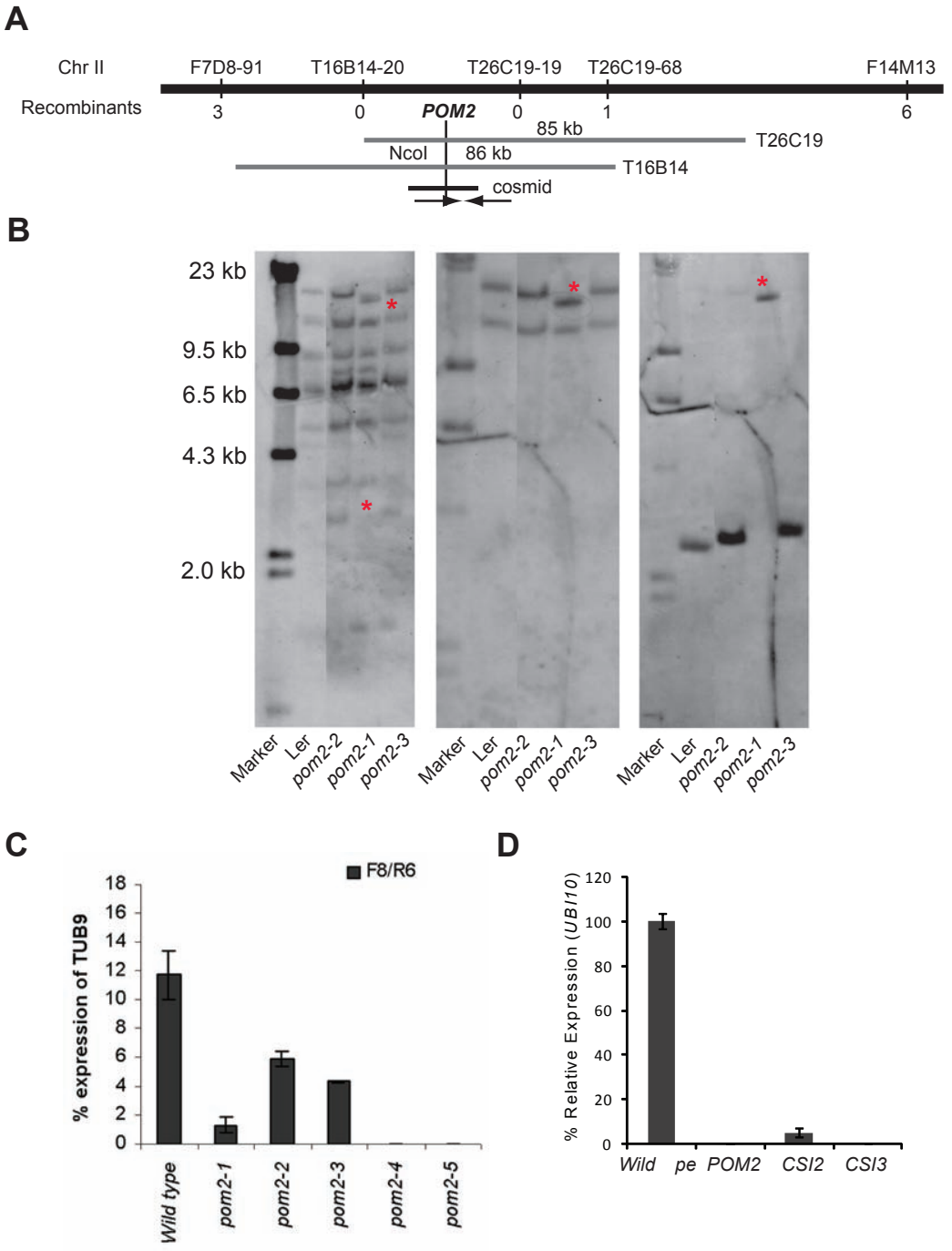

Figure 4. Schematic representation of the positional cloning strategy of *POM2* and qPCR analyses. A. Genomic region of the *POM2* locus with the molecular markers and the number of recombinants. The two BAC clones covering the *POM2* locus and the NcoI site, which is polymorphic in the different *pom2* alleles are indicated. Chr II, Chromosome II. **B.** Southern blots of NcoI- and EcoRV-digested DNA from wild-type and *pom2* alleles using a digoxigenic-labeled BAC T16B14 as probe. Asterisks indicate polymorphism. **C.** qPCR of 11-day-old seedlings of the *pom2* alleles with the primers F8 and R6. Relative expression was normalized using TUB9. At least three different RNA isolations were analyzed, and each cDNA was measured in triplicate. **D.** qPCR of the *pom2/c i1 c i2 c i3* triple mutant. The relative expression levels were normalized against UBI10 (Czechowski et al., 2005). The qPCR was performed on the triple mutant line generated from SALK_115451 (*pom2-7*), SALK_022491 (*c i2*) and SALK_009141 (*c i3*). Error bars in (**C**) and (**D**) indicate standard deviation from three independent experiments.

Figure 5

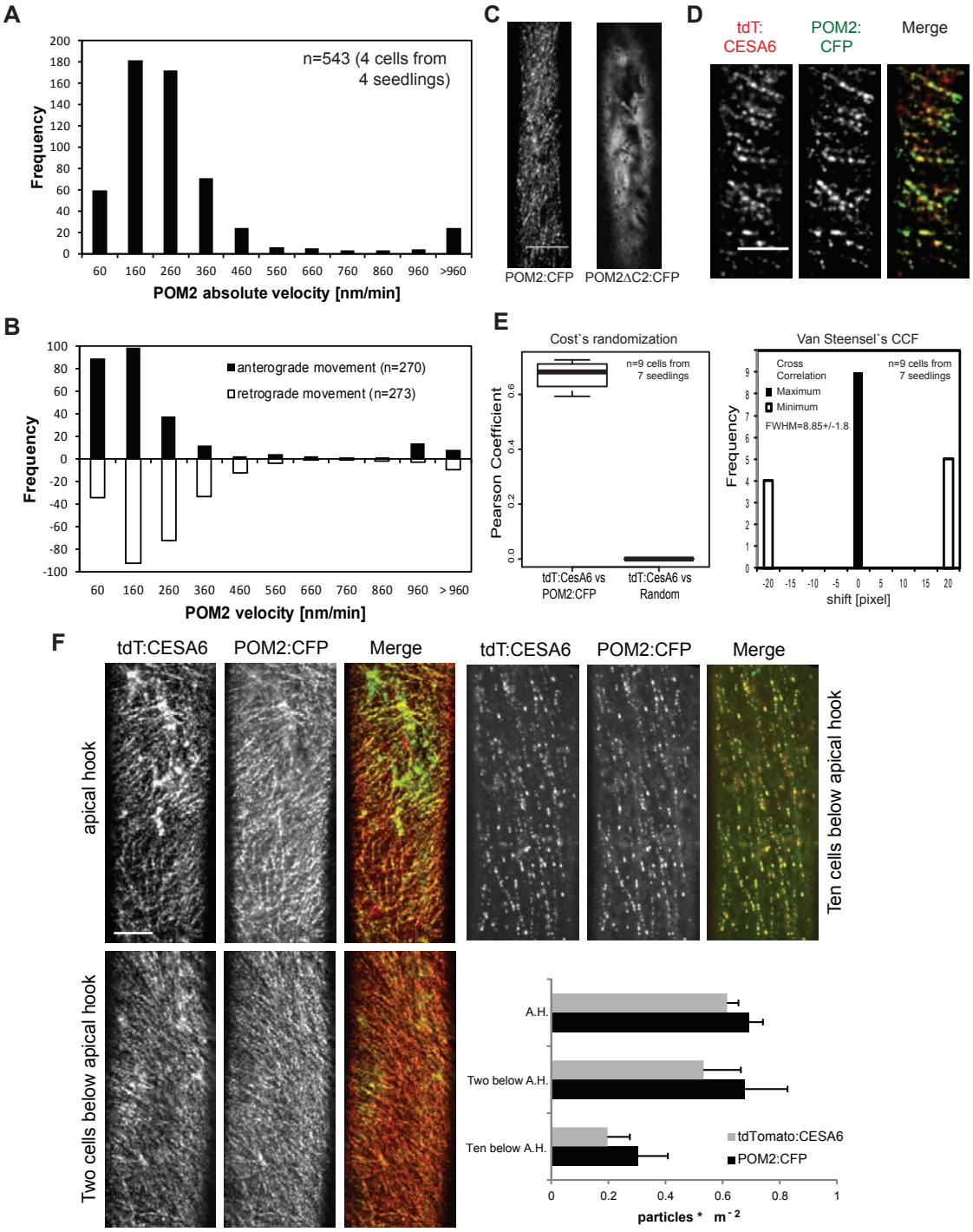

Figure 5. POM2/CSI1:CFP behavior and co-localization with CESA complexes. A. POM2/CSI1:CFP velocities at the cell cortex in elongating cells of four-day-old etiolated seedlings. Data were obtained from four cells in four different seedlings. **B.** Bi-directional movement of the POM2/CSI1 as analyzed by the direction of tracks in kymographs from time average images from the cell cortex in elongating cells of four-day-old etiolated seedlings expressing POM2/CSI1:CFP. **C.** Fluorescent pattern of full-length POM2/CSI1 fused to CFP and a truncated version of POM2/CSI1, in which the C2 domain was removed, fused to CFP. Images represent Z-stacks of 20 images (total distance 2 µm). Scale bars= 10 µm. **D.** Representative image of elongating cells of four-day-old etiolated seedlings expressing both POM2/CSI1:CFP and tdTomato:CESA6. Image was taken at the interface of the cell cortex and plasma membrane. Scale bars= 5 µm. **E.** Quantification of POM2/CSI1 and CESA co-localization from images as in (**D**). The co-occurrence of fluorescent signals was quantified by Pearson correlation, and was compared against randomized fluorescent images with similar pixel sizes and densities. **F.** The fluorescent signals of POM2/CSI1 and CESAs co-occur and display a similar distribution in different cells (six cells from three seedlings) throughout four-day-old etiolated hypocotyls. Graph shows particle densities for the two molecules in the different cells. A.H. stands for apical hook. Error bars represent standard deviations. Scale bar= 5 µm.

Figure 6

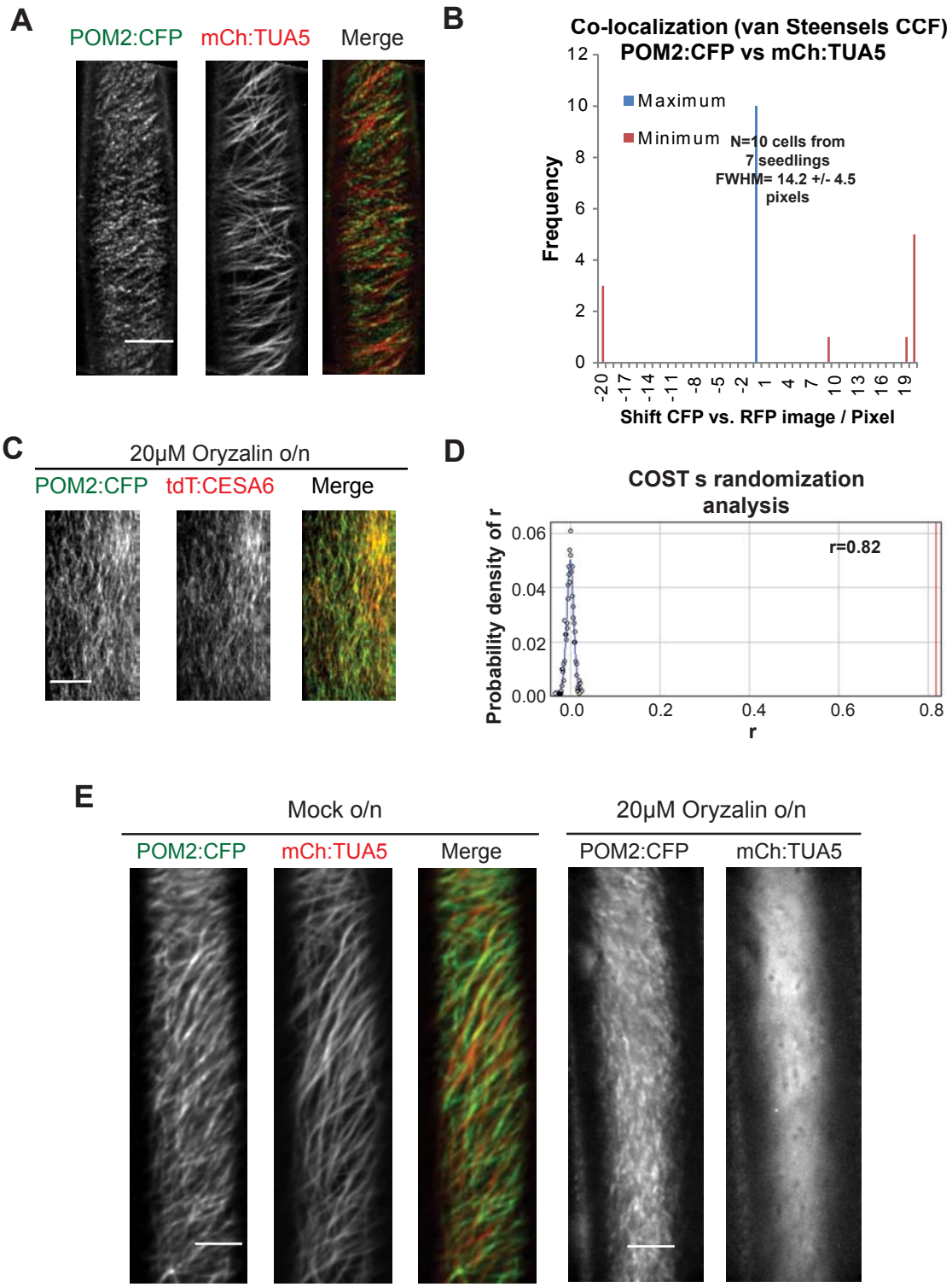

Figure 6. Co-occurence of POM2/CSI1 and microtubules at the cell cortex in etiolated hypocotyls. A. Elongating cell in a four-day-old etiolated Arabidopsis hypocotyl expressing POM2/CSI1:CFP and mCherry:TUA5. Scale bar= 5 µm. **B.** Co-localization was investigated using van Steensel's CCF logarithm, which measures coincidence between two signals when frames are shifted in relation to each other. Note the high correlation of the signals in frames with no shift. **C.** Elongating cells in a four-day-old etiolated Arabidopsis hypocotyls expressing POM2/CSI1:CFP and tdTomato:CESA6 treated with 20 µM oryzalin overnight (o/n). Note the high coincidence of signals in merge. Similar oryzalin treatment completely abolished the cortical microtubule array (**E**). Scale bar= 5 µm. **D.** Statistical analysis of co-occurence of the POM2/CSI1 and CESA signals using COST's randomization analysis. Blue curve indicates distribution of Pearson coefficients in 1000 randomizations, red line indicates Pearson coefficient for comparison of original channels. r; Pearson correlation coefficient. **E.** Four-day-old etiolated seedlings expressing POM2/CSI1:CFP and mCherry:TUA5 were treated with 20 µM oryzalin overnight and the fluorescent patterns were compared with those of mock-treated seedlings. Note that POM2/CSI1 signal is still present at the cell cortex after oryzalin treatment. Scale bars= 5 µm.

Figure 7

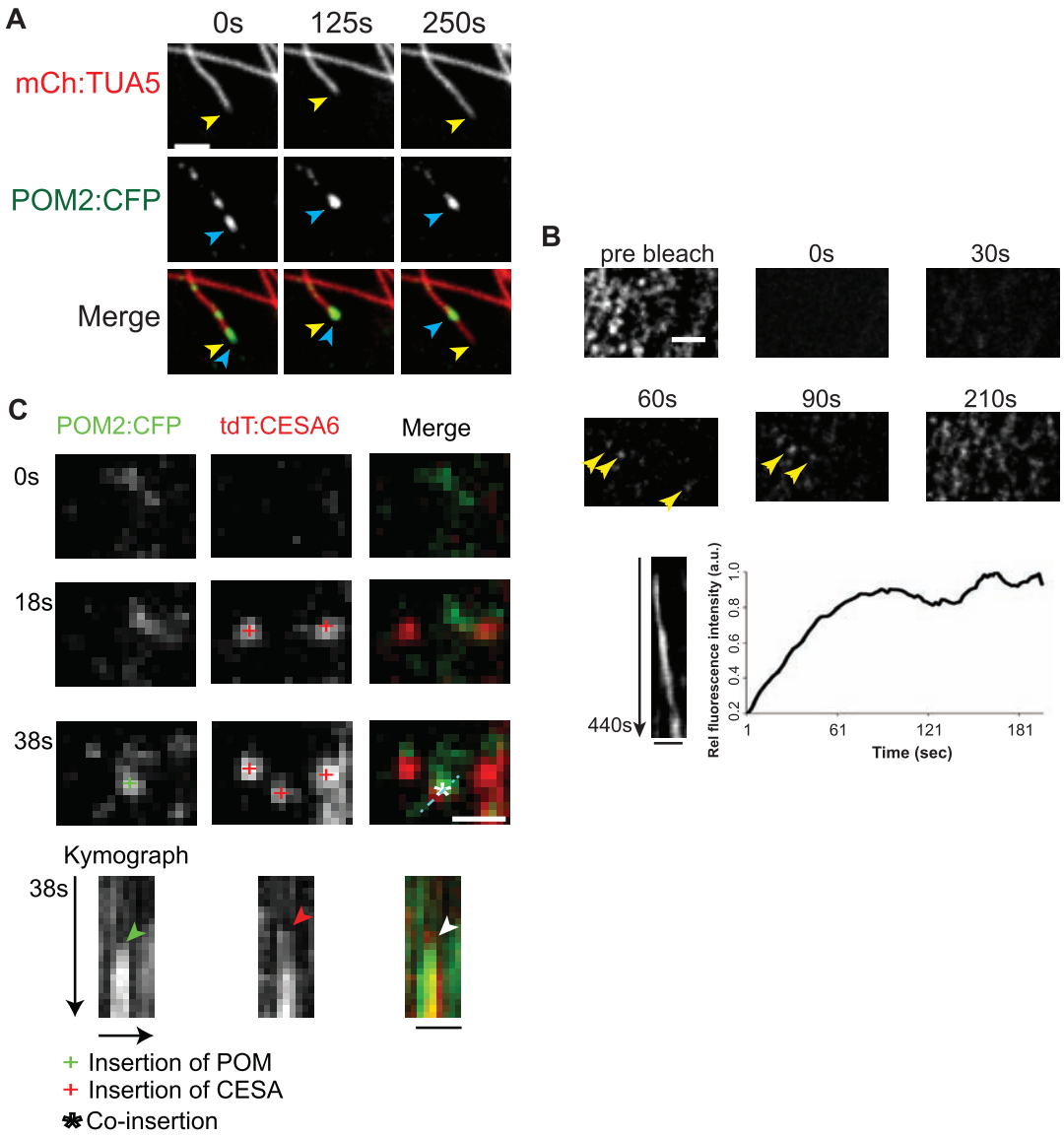

Figure 7. POM2/CSI1 only moves together with depolymerizing microtubule ends, and delivery of CESAs and POM2/CSI1 to the plasma membrane. A. Images from time series of cells in four-day-old hypocotyls expressing mCherry:TUA5 and POM2:CFP treated with 100 nM isoxaben for 2 h. Blue arrowheads indicate a POM2/CSI1 tracking together with a depolymerizing microtubule end. Yellow arrowheads indicate movement of the microtubule end. Note that depolymerization causes POM2/CSI1 movement, whereas polymerization does not. Scale bar= 5 µm. **B.** Analysis of recruitment of new POM2/CSI1 to the cell cortex by photo-bleaching regions at the cell cortex in elongating cells of four-day-old etiolated seedlings. Yellow arrowheads indicate appearance of distinct POM2/CSI1 punctae at the cell cortex. Scale bar= 5 µm. Kymograph displays migration of POM2/CSI1 puncta that appeared after photo-bleach. Scale bar= 2 µm. Graph displays relative (Rel) fluorescence intensity that re-emerges after bleach. a.u.; arbitrary units. **C.** Upper panel shows delivery events of CESAs and POM2/CSI1 that was investigated after photobleaching. Red plus signs signify delivery of CESA complexes, and green plus signs show delivery of POM2/CSI1. Co-delivery events are indicated in the merged channel with an asterisk. Lower panel shows kymographs drawn along the cyan dashed line in the upper panel. Arrowheads indicate a delivery event of a CESA complex (red) and POM2/CSI1 (green). Scale bars=1 µm.

Figure 8

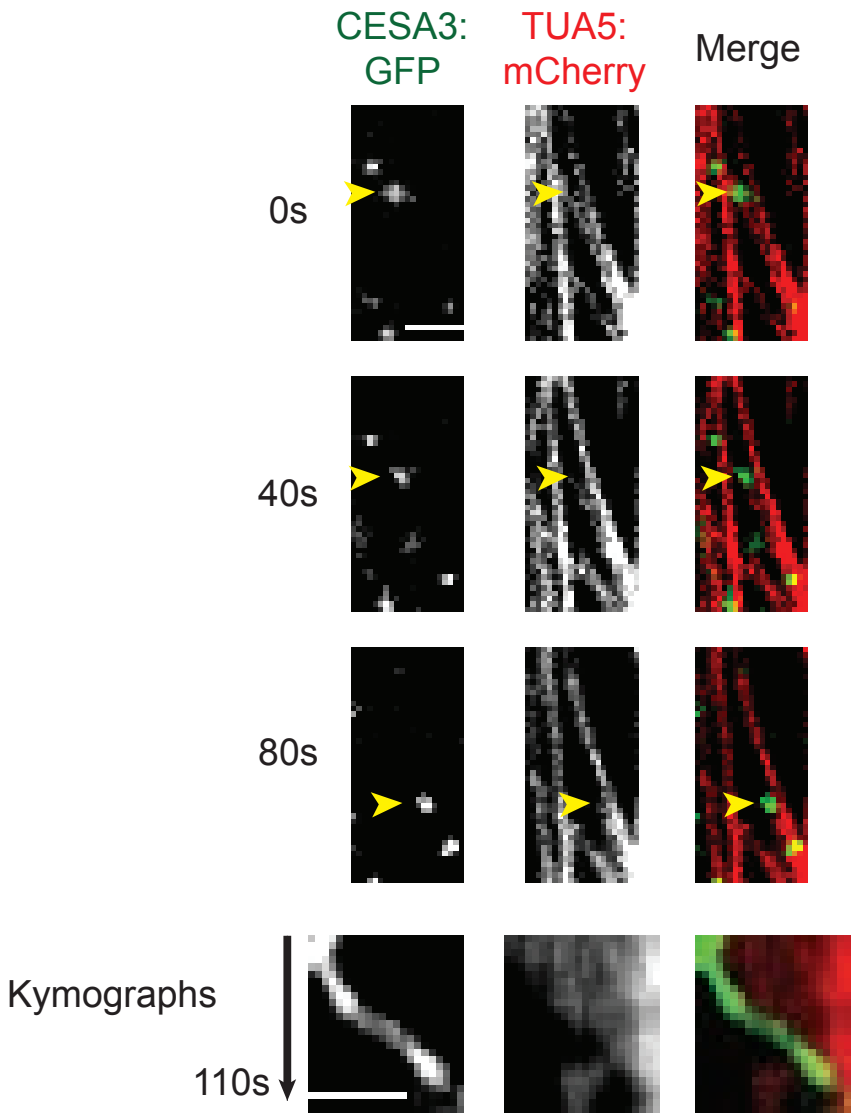

Figure 8. Mutations in POM2/CSI1 have no visible effect on the attachment of smaCCs/MASCs to microtubules. Three h treatment with 1 µM isoxaben of four-day-old *pom2-5* seedlings expressing mCherry:TUA5 and POM2/CSI1:CFP led to accumulation of CESA containing compartments (smaCC /MASC) that co-localized with cortical microtubules. As in wild type plants, smaCCs / MASCs co-occurred with microtubule depolymerizing ends (yellow arrowheads). Lower panel shows kymographs that display the migration of a POM2/CSI1 along the microtubule depolymerizing end. Scale bars = 2 µm.

Table S1. Summary of the molecular markers used for fine mapping the POM2 locus.

Indicated are the primer sequences, size of PCR amplicons and the relative migration behavior of the microsatellite and duplex analysis markers on high resolution gels of the accessions Columbia (Col), Landsberg (Ler) and Wassilewskija (Ws) (Hauser et al., 1998).

Primer Name	Genbank accession No.	Primer pairs 5' → 3'	Fragment Length	Migration behavior of Homo- and Hetero-duplexes
F14M13-R F14M13-F	AC006592	TCG GTT TCT GTA TTA CAT GGC A GCA ATG ATA ATC AGT AAA AGG GAG	130 bp	Col≠Ler=Ws Col/Ws=Col/Ler, no Ler/Ws
F7D8-91 R F7D8-91 F	AC007019	AGC CGG AAA CCA GAT TGA GC GTA GTC GTT TGT ATA GGT CAG GTC	485 bp	Col≠Ler≠Ws Col/Ws≠Col/Ler≠Ler/Ws
T16B14-20 R T16B14-20 F	AC007232	GCA TTG TTT TCT TCC CCA TAG G CGC ATC ATC GGT CAC TGT GAG	336 bp	Col=Ws≠Ler Ler/Ws=Col/Ler, no Col/Ws
T26C19-19 R T26C19-19 F	AC007168	CCT GTT TTC AGC TTT GGG TTT C CAC TTG ATT TCG AAT CAA ATC CCT C	357 bp	Col=Ws≠Ler Ler/Ws=Col/Ler, no Col/Ws
T26C19-43 R T26C19-43 F	AC007168	CCA TCG AAT TTC CAA GAG TTT C TGG TTG GGG AGT TAT TGT AGC	394 bp	Col=Ws≠Ler Ler/Ws=Col/Ler, no Col/Ws

Table S2: Primers used for sequencing and real-time PCR analyses

Primer Name	Primer Pairs 5' → 3'	Fragment Length (bp) cDNA	Genomic
F0 R0	CTCTCGTCTTATTCGCTTCTC TGCATTGGGCAACACTTGCT	370	1246
F1 R1	CAGAGACCGGACAACCAGC TTCACCGCCATCGTTATTAGAC	1255	1255
F2 R2	GCACTTGCAAGTTTGTATGGGA GTTCACAGAATCTGTCAATGCAG	1175	1175
F3 R3	CAGTGAAGTGTCAGAGAAGGTC GACTAGCTAGAGCTTGTGCTG	1061	1233
F4 R4	GCACATGCAACAATGAAGGCT CAAATGGAAAAGTGGCTCCACC	1343	1343
F5 R5	CAGAACTGCTTCGAATCCTCAC CTCTTGAACGGTGTGATTAGAG	1171	1171
F6 R6	AGGTCGTCTTGGATCTGATCAG CATGAGAAGCTCTCGTCCCA	630	811
F8* R8 R9*	CACAAGAAGCTGCCTTGGATGC GAATCCCGTTAGACCAATCAAAG CTTATACGGTGTGCTGCCTC	2140	2315
TUB9-F TUB9-R	GTACCTTGAAGCTTGCTAATCCTA GTTCTGGACGTTCATCATCTGTTC	470	360

* F8 and R6 used for Genomic, cDNA sequencing and Real-time PCR analyses, Genomic size is 452 bp, and cDNA size is 340 bp.
* F6 and R9 used for genomic sequencing, genomic size is 3193 bp, and cDNA size is 2925 bp.

Table S3. Primers for *POM2* cloning, genotyping and qRT-PCR analysis.

Primer sequence 5'->3'	Purpose
caccATGacaagtgctcttggatgg	POM2 Gateway cloning forward primer
cttgttagaccactggaattctat	POM2 Gateway cloning reverse primer
ggcaggacaggctgaccaa	POM2 Gateway cloning reverse primer □ C2 Domain
TGGTAACCCGAGTGTGTTCTGC	pom2-5 qRT PCR forward primer
AGGACCTGTCGATATCACCTTGG	pom2-5 qRT PCR reverse primer
TTGTTTGCCGGGAAGTCTCACG	CSI2 qRT PCR forward primer
AGCTTCAGCCTCTGGTTTCCTC	CSI2 qRT PCR reverse primer
TGATGTTCCCCCCAAAGGA	CSI3 qRT PCR forward primer
CCTAGAGTCGTCTTTCCAAATGTG	CSI3 qRT PCR reverse primer
TGAGGGCTAGAGCACTCTCAC	pom2-5 left border genotyping primer
TCAGAGCCTTGAATCTTGCTC	pom2-5 right border genotyping primer
GCGTGGACCGCTTGCTGCAACT	lbB1 SALK insertion specific genotyping primer
ccttttgtatcaatacgatctgc	pom2-5 genotyping of complementation lines fow
gcagaaagaaagaggcgaaa	pom2-5 genotyping of complementation lines rev

3 Discussion

3.1 Fifty years of alignment hypothesis – new players reveal mechanism

As introduced in section 1.4, experiments by Paul Green (1962), Ledbetter and Porter (1963) and Mueller and Brown (1980) provided the basis for a general hypothesis to account for the various aspects of oriented cellulose synthesis. This was initially put forward by Heath (1974). He suggested that freely moving CESAs in the plasma membrane are guided by cortical microtubules.

Tobias Baskin (2001) carried Heath's hypothesis a bit further and coined the term "alignment hypothesis". Baskin also pointed out that there had to be an additional mechanism for cellulose microfibril alignment, since cellulose microfibrils tended to form parallel arrays also in the absence of microtubules. Baskin therefore suggested an alternative mechanism of microfibril alignment, where the orientation of the nascent microfibril was maintained by components of the extracellular matrix, such as scaffold proteins or polysaccharides that are oriented. This, however, raises the question about how these scaffold components become organized. Indeed, orientation of cellulose microfibrils in non-elongating cells seemed to be microtubule independent. This gave rise to geometrical models of microfibril alignment (Mulder and Emons, 2001).

After the breakthrough experiments of Paredez *et al.* (2006), Emons *et al.* (2007) suggested research directions, to be addressed with the new set of tools available. Many of them have been pursued so far, for instance regarding CESA delivery (Gutierrez *et al.*, 2009; Crowell *et al.*, 2009), CESA activation (Chen *et al.*, 2010; Bischoff *et al.*, 2011) and functional characterization of proteins involved in cellulose synthesis (e.g. Sanchez-Rodriguez *et al.*, 2012).

With the current tools in hand, it should be possible to find new candidate genes involved in fine-tuning cellulose synthesis related functions. It may even become possible to look for deviations in the behavior of individual CESA molecules, for example in mutant and chemical genetics screens.

Various fluorescent markers that are tagged to components associated with compartments important for cellulose synthesis are also readily available. These range from ER and Golgi-related markers, to different cytoskeletal and CESA markers. Discovery of new cellulose synthesis-related proteins will of course make even more marker proteins available, which in turn can be used to deepen our knowledge regarding cellulose production.

Based on this thesis, and on a complementary research paper from a competing group (Li *et al.*, 2012), POM2/CSI1 must be considered as a new important

player in cellulose synthesis, particularly for the alignment hypothesis. In brief, the work presented this thesis provided new insight into the CESA- microtubule alignment, CESA delivery and CESA activation.

3.2 Identification of candidate genes that influence cellulose synthesis

Many genetic screens make use of a forward genetics approach. In this thesis we used a combined effort of co-expression analysis, and of both forward and reverse genetics. Using these approaches, together with more detailed molecular characterizations, we found that the protein POM2/CSI1 is essential for co- alignment of the CESAs and the cortical microtubules.

3.2.1 Co-expression analysis as a tool for candidate gene prediction

While the two complementary strategies (co-expression analysis and genetic screens) turned out to be quite successful, it is important to note that the relative work-load of the two approaches is different. Currently, the use of web-based co-expression tools is easy and user-friendly, and returns genes that may be linked to a certain biological process (Usadel *et al.*, 2009), and that subsequently can be targeted through reverse genetics. We initially established a co-expression pipeline using a binning approach of genes into gene families, or rather pfams (Mutwil *et al.*, 2009). This early approach only incorporated genes that were associated with a specific pfam at that time. Nevertheless, we found, for example, that the pfam corresponding to COBRA, which contains glycosyl-phosphatidyl inositol-anchored proteins of which one member is responsible for anisotropic cell expansion and control of cellulose orientation in *Arabidopsis* (Roudier *et al.*, 2005), was consistently co-expressed to the CESA containing pfam (Glycolyl transferase 2 (GT2)) throughout different *Arabidopsis* tissues. In addition, several pfams involved in cell adhesion (pfam02469), microtubule binding (pfam03999), kinesins (pfam00225) and a pfam referred to as harpin-induced (pfam07320) co-occured with the GT2 pfam. In contrast to a simpler gene-to-gene comparison, this analysis indicated that members of the pfams continously connected to the GT2 pfam may contribute important functions during cellulose production.

Co-expressed genes tend to be functionally related (Usadel *et al.*, 2009). This has been shown to hold true also for cellulose synthesis in that many genes that are co-expressed with the primary or secondary wall *CESA* genes are of importance for the respective processes (Persson *et al.*, 2005; Brown *et al.*, 2005). Interestingly, already in these publications the *POM2/CSI1* gene was found to be transcriptionally coordinated with the primary wall *CESA* genes (Persson *et al.*,

2005). While the *POM2/CSI1* gene in this work was not among the top 10 genes co-expressed with the *CESA*s, it is important to note that the microarray data included in these early sets may not have covered all tissue and organ types in *Arabidopsis*. This may also be a reason why the *POM2/CSI1* gene showed a tighter correlation with the *CESA* genes in later publications (Mutwil *et al.*, 2008b; 2011). As anticipated, these studies also included several known components that affect primary wall cellulose synthesis, including *KORRIGAN*, *COBRA* and *CTL1/POM1* (Persson *et al.*, 2005).

3.2.2 Yeast-two-hybrid screens revealed POM2/CSI1 as interaction partner of the primary CESAs

Gu *et al.* (2010) identified proteins that bind to a 541 amino acid stretch of the presumed cytosolic part of the primary CESAs, which holds the tentative catalytic domain, in a yeast-two-hybrid screen. Among others, POM2/CSI1 was found to interact with the bait in this screen. Further experiments showed, that POM2/CSI1 also can interact with CESA1 and 3 and that it co-localizes with them *in vivo*.

3.2.3 Genetic screens identified *pom2/csi1* as root expansion defective mutant

Both forward and reverse genetics suggested that *pom2/csi1* was important for cellulose synthesis. *POM2/CSI1* T-DNA insertion lines, which showed drastically reduced or no expression of the *POM2/CSI1* gene, showed root and hypocotyl expansion defects and measurable reduction in total cellulose content (Gu *et al.*, 2010). These kind of phenotypes are often observed in cellulose deficient mutants, such as *ctl1* (Zhong *et al.*, 2002) or *procuste* (*prc;* Fagard *et al.*, 2000).

Interestingly, *pom2* was previously identified in a forward genetic screen by Hauser *et al.* (1995). Detailed map-based cloning revealed that the mutation affected the CSI1 gene (Bringmann *et al.*, 2012), which we previously had described as a primary CESA interactor, important for cellulose production and CESA motility in Arabidopsis hypocotyls (Gu *et al.*, 2010). Hence, we referred to the locus as *POM2/CSI1*.

Thus, many avenues that indicated a role for POM2/CSI1 in the process of cellulose synthesis laid the foundation for this thesis. Nevertheless, molecular characterization using molecular and cell biology, together with biochemistry, was essential to come to mechanistic insight regarding the protein's function.

3.3 POM2/CSI1 possesses a molecular structure that renders it an integrative structural protein

POM2/CSI1 protein domain annotation suggests an integrative function for processes at the plasma membrane. POM2/CSI1 contains between one and twenty armadillo repeat domains, depending on the stringency used, distributed throughout the protein, and a C-terminal C2 domain. The protein appears to be plant specific, and is conserved across land plants. Nonetheless, knowledge transfer from animal armadillo repeat proteins may be important to infer additional functionality for POM2/CSI1.

Perhaps the most well-known members of the armadillo repeat containing class of proteins in animals are β-catenin and importin-α. In Drosophila, β-catenin binds to other armadillo repeat containing proteins, such as α-catenin, to facilitate connections between cell-cell contacts (established by cadherins) and the actin cytoskeleton (Nusslein-Volhard and Wieschaus, 1980; Xu and Kimelman, 2007). Importin-α contains 10 armadillo repeats downstream of an importin-binding site and transports cargo proteins with nuclear localization signal (NLS) to the nucleus (Coates, 2003).

Armadillo repeat containing proteins are also found in the plant kingdom. Similar to their animal homologues, the combination of armadillo repeats and other protein domains is very wide, which suggest involvement in multiple cellular processes (Coates, 2003; Tewari *et al.*, 2010). Coates *et al.* (2006) for instance described the class of Arabidopsis proteins which has the highest sequence similarity to β-catenin (ARABIDILLO1 and 2). The authors showed, that ARABIDILLO1 is a nuclear localized F-box containing protein, which positively regulates lateral root formation. This is potentially mediated via protein degradation of downstream regulatory proteins.

Armadillo repeat proteins may also support microtubule-dependent cell morphogenesis. Sakai *et al.* (2008) reported that the microtubule-binding ARMADILLO REPEAT KINESIN1 (ARK1) interacts with the NEVER IN MITOSIS A (NIMA)-related kinase 6 (NEK6). This interaction influenced cell morphogenesis in *Arabidopsis* epidermal cells by promotion of microtubule depolymerization at the cortex. Similar to *pom2/csi1*, mutants of *ark2* show root twisting that could be suppressed by microtubule stabilizing drugs, such as taxol or propyzamide. Armadillo repeat proteins, such as POM2/CSI1, may therefore link the microtubule cytoskeleton to important processes that determine cell shape.

Apart from the many armadillo repeats, POM2/CSI1 also harbors a C-terminal C2 domain. C2 domains form layers of β-sheets, which can bind to phospholipids in membranes (for comparison see Figure 6). This association can be

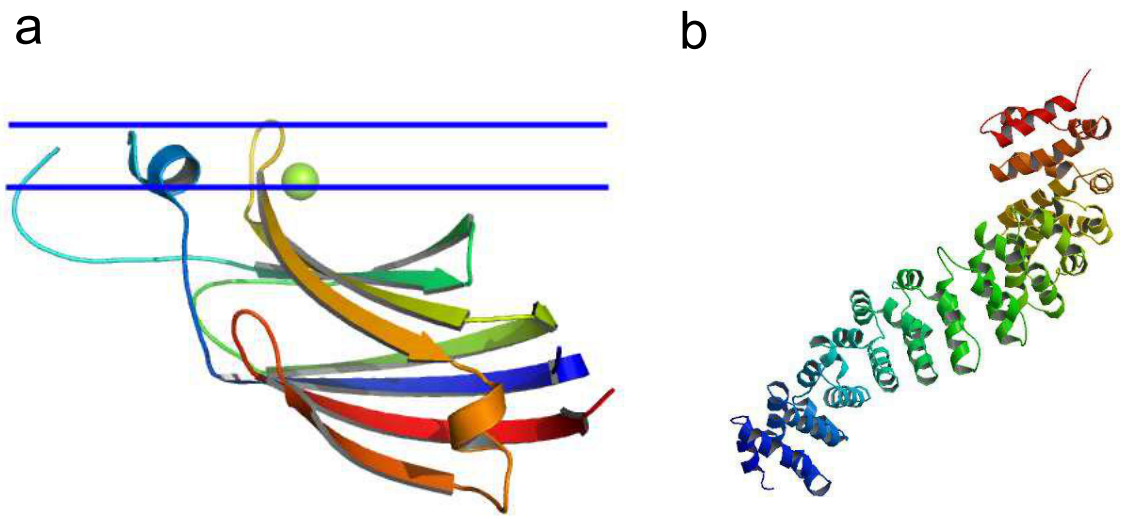

Figure 6: The POM2/CSI1 protein harbours a C- terminal C2 domain and at least 10 armadillo repeat domains. **(a)** A C2 domain consists of two layers of β– sheets (arrows) which can attach to the lipid bilayer (blue lines) laterally through electrostatic interactions. Binding of Ca^{2+} ions may enhance the interaction strength which may lead to interlace of lipophilic loops to the lipid bilayer. The green ball represents a Mg^{2+} ion. Image taken from Ochoa *et al.* (2001). **(b)** Armadillo repeat region of β– catenin. Depicted is a 12 armadillo repeat region forming a long, positively charged helix of helices wich facilitates protein- protein interaction (Huber *et al.*, 1997).

enhanced by binding of Ca^{2+}. Upon Ca^{2+} binding, the electrostatic potential of the C2 domain changes. The membrane association then becomes stronger and lipophilic loops can interlace to the membrane, leading to membrane buckling (Martens and McMahon, 2008). Therefore, C2 domains, e.g. in Synaptotagmin 1, are considered electrostatic switches with great importance for vesicle shuttling, affecting both exo- and endocytosis in animal neurons (Yao *et al.*, 2011).

The C-terminal C2 domain of POM2/CSI1 could target the POM2/CSI2 protein to the plasma membrane. In support of this, we observed a cytoplasmic smear instead of the normal punctae patterning of cyan fluorescence when we expressed a truncated POM2ΔC2:CFP in *Arabidopsis* lacking the C2 domain. Considering the importance of Ca^{2+} for the functionality, it will be interesting to determine the influence of the ion on POM2/CSI1 function. As mentioned above, POM2/CSI1 seems to have both an important function in aligning the CESAs with the microtubules, and also some as of yet unknown regulatory effect on CESA activity. Therefore it is crucial to find out if, and in which way POM2/CSI1 binds to the plasma membrane. Ca^{2+} binding could be an important mechanism to facilitate membrane association and integrate POM2 into a broader signalling network.

3.4 Molecular characterization of POM2/CSI1

3.4.1 POM2/CSI1's role in CESA delivery to the plasma membrane

One possible role for POM2/CSI1 was in the insertion of the CESAs to the plasma membrane. The POM2/CSI1 could perhaps serve as a spatial indicator for delivery of CESAs at cortical microtubules. Gutierrez *et al.* (2009) had previously shown, that CESA delivery preferentially occurred at foci close to cortical microtubules. POM2/CSI1's ability to bind CESAs, and potentially to microtubules, *in vivo* would have rendered it an ideal candidate for such a function.

We consequently designed experiments with the following assumptions: If POM2/CSI1 is important for CESA delivery and its function is lost, we would (i) assume a reduction in delivery rate of the CESAs, and/or (ii) we would assume that the loci of CESA insertions were randomly distributed throughout the plasma membrane.

We tackled question (i) with fluorescence recovery after photo-bleaching (FRAP) experiments comparing CESA delivery rates in *pom2/csi1* mutants with wild-type plants, and question (ii) with co-localization analysis of CESA insertions with and microtubules after photo-bleach (Bringmann *et al.*, 2012).

Both experiments came out negative, i.e. CESA delivery rate was unaltered in *pom2/csi1* mutants compared to wild-type, as was the location of the insertions. Consequently, we concluded that POM2/CSI1 has no, or only minor roles in the insertion of the CESAs into the plasma membrane.

3.4.2 POM2/CSI1 is required for alignment of microtubules and CESAs and enhances CESA activity

Fusions of the POM2 protein to fluorescent tags such as RFP and CFP enabled us to characterize its subcellular localization and spatiotemporal behavior. More importantly, we could put this information in context to what we already knew about the CESAs and the mictotubules. Interestingly, we found the fluorescent signal for POM2/CSI1 as distinct foci distributed evenly along the cell cortex (Gu *et al.*, 2010; Bringmann *et al.*, 2012). These data were in close agreement with the localization and behavior of the primary wall CESAs (Paredez *et al.*, 2006); however, no POM2/CSI1 signal was apparent at Golgi bodies, which is the case for the primary wall CESAs . In agreement with the former, and also with the yeast-two-hybrid analysis in which the catalytic domains of the CESAs interacted with POM2/CSI1, we found that POM2:CFP co-localized with both tdTomato:CESA6 and with the microtubule marker mCherry:TUA5 at the cell cortex with high statistical significance (Bringmann *et al.*, 2012). These results confirmed the notion

that the POM2/CSI1 protein is directly involved in cellulose synthesis by interaction with the CESAs.

Furthermore, cellulose orientation was disturbed in *pom2/csi1* mutants as shown by polarized light analysis (Gu *et al.*, 2010). Based on these results, POM2/CSI1 was suggested to be responsible for spatial orientation of cellulose microfibrils through some form of guiding principle of the CESA complexes at the plasma membrane (Gu *et al.*, 2010).

Using combinations of CESA and microtubule markers, we could subsequently unravel the mechanistic cause for these phenotypes.

3.4.2.1 POM2/CSI1 is co-localized with the CESAs in the cell cortex but not at the Golgi Given the role of POM2/CSI1 in guidance of CESAs along microtubules after delivery, we wanted to elucidate when and where the association between POM2/CSI1 and CESA happened. Interestingly, we could show that the majority of POM2/CSI1 proteins bound to the CESAs after the complexes were delivered to the plasma membrane, and also during formation of isoxaben-induced vesicular compartments (SmaCCs or MASCS; Gutierrez *et al.*, 2009; Crowell *et al.*, 2009).

It is important to remember that the cytoplasmic parts of the CESAs, i.e. including the catalytic part that POM2/CSI1 presumably interacts with, will remain cytoplasmic during all the phases of CESA secretion. Hence, the same part of the complex will be exposed to potential binding to the cytosolic POM2/CSI1 at the Golgi, at the plasma membrane, and at the smaCCs/MASCs. Nevertheless, we found that the POM2/CSI1 preferentially bound to CESAs at the plasma membrane and at the smaCCs/MASCs (Bringmann *et al.*, 2012).

How could such a selective binding occur? One possibility is that the cytoplasmic environment is different around the CESAs depending on the sub-cellular location. For example, the CESAs are clearly in close association with the microtubules at the plasma membrane, and the smaCCs/MASCs are also tracking together with microtubules and microtubule ends (Gutierrez *et al.*, 2009; Bringmann *et al.*, 2012). POM2/CSI1's affinity to microtubules and the plasma membrane (potentially facilitated through its C2 domain) might preferentially locate it to the cell cortex and thus largely prevent association to cytoplasmic Golgi bodies.

Several different reasons for this behavior are probable. For example, binding of POM2/CSI1 might enhance CESA activity. If such activation occurred before the CESAs reach the plasma membrane, cellulose could be produced already in the Golgi, which could result in cellulose aggregates in the Golgi and perhaps perturbation of Golgi function. Gutierrez *et al.* (2009) showed that CESAs stall for a short period of time after delivery to the plasma membrane, indicating that

they are ”activated” shortly after delivery. This could be seen in two different ways; (i) Either this ”activation” period means that the CESAs need to synthesize a certain amount of cellulose microfibril before movement occurs. This is consistent with the idea that the synthesis of the microfibril moves the CESAs through the plasma membrane. (ii) Or, it could also mean that certain co-factors, such as POM2/CSI1, need to bind to the CESAs in sufficient amounts to start synthesis. We observed that steady movement of CESAs (indicating cellulose synthesis) was preferentially accompanied by POM2/CSI1 interaction. Therefore, it is plausible that POM2/CSI1 takes part in some form of activation process of the CESA complex, perhaps assisted by other tentative interactors.

Along the same line, stabilization in terms of structural support of the CSC in the plasma membrane might require a specific set of proteins, which is not present at the Golgi. POM2/CSI1 could stabilize the CESA complex in a certain confirmation, at the plasma membrane, or facilitate binding for other stabilizing/activating proteins.

It is intriguing, that POM2/CSI1 binds to the putative catalytic domain of the CESAs (Gu *et al.*, 2010). It is hence possible that POM2/CSI1, apart from its role in guiding the CESAs along the microtubules, also could regulate CESA activity. Along the same line, CESAs showed drastically reduced activity in pom2/csi1 mutants (Gu *et al.*, 2010).

If the driving force for the CSCs is generated through their own activity, i.e. the propulsion of the extruded cellulose microfibril, it seems improbable that the attachment to the microtubules would have an impact on the speed. In support of this, it was shown that abolishment of the microtubule array by oryzalin treatment did not reduce CESA motility (Chen *et al.*, 2010; Bischoff *et al.*, 2011). However, changes in spatial organization, and deviations from straight linear trajectories of CESAs, were observed if microtubules or POM2/CSI1 were abolished (Paredez *et al.*, 2006; Bringmann *et al.*, 2012). Therefore, CESA guidance and activation seem to be largely independent processes. However, POM2/CSI1 is apparently important for both of them.

3.4.2.2 POM2 bridges microtubules and CESAs The bridging function of the CESAs and microtubules by POM/CSI1 seems relatively straightforward. The large POM2/CSI1 protein holds interaction sites that can directly bind to CESAs (Gu *et al.*, 2010) and to the microtubules (Li *et al.*, 2012), and can therefore directly link these structures. Still, we have no satisfying imagination of how the CESA movement works.

However, a major conundrum is how the POM2/CSI1 mediates smooth movement of the CESAs along the microtubules. Li *et al.* (2012) showed that,

POM2/CSI1 directly binds to microtubules with affinities in the range of MAP2. Still, the authors do not speculate on how movement along microtubules is facilitated by a protein that binds to microtubules with relatively high affinity. Some form of gliding/sliding mechanism could be involved, or frequent switches between a binding and a releasing state between POM2/CSI1 and the microtubules might be possible.

In my opinion, the binding mechanism must involve a balance between the two forces that control CESA movement. These would be the propulsion by the nascent microfibril on the one hand, and the binding to the microtubules through POM2/CSI1 on the other hand. As the microfibrils appear to be twisted structures (Fernandes *et al.*, 2011; Matthews *et al.*, 2011), it seems logical to assume that the CSCs could rotate around their center during cellulose synthesis. In this case they could not stay attached to the microtubules through only one focal point, as this binding would be restricted to only one site of the CSC. Alternatively, if only one focal point exists then the protein (POM2/CSI1) involved in the connection would have to allow for rotation of the CSC through some type of gliding/sliding mechanism on top of the protein (POM2/CSI1). Our FRAP analysis indicated that multiple POM2/CSI1s were associated with each CSC locus (estimated from increasing POM2:CFP fluorescence intensities at distinct CESA foci over time). This suggests that the individual CESAs in the CSC bind to POM2/CSI1, resulting in up to 36 POM2/CSI1s per CSCs (under the assumption that the CSC holds 36 CESAs).

One tentative model would then be, that POM2/CSI1 proteins form a ring-like structure, laid out laterally around the CSC catalytic domain part, that facilitates a rotational, forward directed movement of the CSC along the microtubules (see Figure 7b for a schematic view of this scenario). Thus, a movement would be accomplished through the activity of CSC (propulsion by the microfibril). This movement would force the binding of one POM2/CSI1 to release itself of the microtubules and allow for the next to engage. While this may seem like a tractive model, x-ray or NMR structures of the CESAs and the POM2/CSI1 will be necessary to confirm or revise it.

3.4.2.3 POM2/CSI1 might be involved in activation of the CESAs The reduced velocity of CESAs in the *pom2/csi1* background indicates that the POM2/CSI1 protein might support the CESAs in gaining full activity (Gu *et al.*, 2010). But how can CESA activation through POM2/CSI1 be explained? Many scenarios seem possible.

One scenario could be that binding of POM2/CSI1 affects the confirmation of the catalytic part of the CSCs. Such conformational changes could be induced

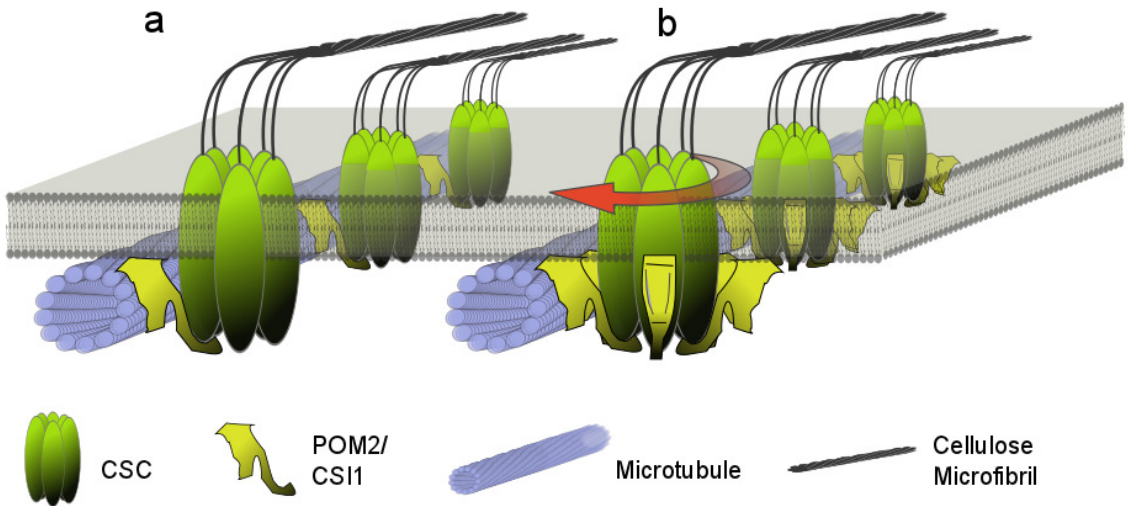

Figure 7: Dynamic bridging of microtubules and moving CSCs could be facilitated through POM2/CSI1 in two scenarios. **(a)** In a sliding mechanism, a single POM2/CSI1 is attached to the CSC. Relatively low microtubule affinity could lead to forward directed movement of the CSC through a gliding of POM2/CSI1 along the side of a microtubule. **(b)** An alternative mechanism involves rotation of the CSC during cellulose synthesis (red arrow). In this scenario, POM2/CSI1 bind to every CESA subunit and act as transient contacts which bind subsequently to the microtubule, resulting in rotation of the CSC along with forward directed migration. In both cases, the driving force is the propulsion of the nascent microfibril.

by POM2/CSI1-binding near the active site, or through the establishment of a favourable environment for substrate supply.

Perhaps one way for a regulation of the CSCs by POM2/CSI1 could be mediated through post-translational modifications of either the CESAs or the POM2/CSI1. Accordingly, it will be important to identify post-translational modifications of POM2/CSI1 and CESAs. It is already known that the CESAs can be phosphorylated, and that this affects the activity of the complex at the plasma membrane (Chen *et al.*, 2010). Furthermore, preliminary mass spectrometry analyses suggested, that POM2/CSI1 harbors several potential phosphorylation sites (Arsova, Schulze personal communication). Post translational regulations, in which phosphorylation/ dephosphorylation of POM2/CSI1 change the protein confirmation, might provide for a mechanism by which the POM2/CSI1 controls CESA activities.

As discussed above, POM2/CSI1 is a large protein with multiple potential interacting sites. Consequently, POM2/CSI1 could interact to other components also involved in cellulose synthesis. In section 1.2.1, I introduced UDP-Glucose as substrate for cellulose synthesis. UDP-Glucose can be produced by cytosolic sucrose synthase (SUS; reviewed by Joshi and Mansfield, 2007). Speculations about a direct binding of one of the SUS family members to the CSC have been put forward (Amor *et al.*, 1995; Salnikov *et al.*, 2001; Kimura *et al.*, 1999). However, such binding has never been shown. One possibility would be that POM2/CSI1 func-

tions as a bridge between SUS and the CSC. Hence, an obvious next step would be to search for further interaction partners of POM2/CSI1.

Another possibility is that the POM2/CSI1 has a weaker affinity for the microtubules *in vivo*, which could support a sliding guiding mechanism for the CESAs. It is also possible that the protein is linked to motor-proteins, which could pull the CSC along the microtubules under ATP consumption. While this is possible, the microfibril synthesis appears more probable for CSC movement. Also, as discussed above, the existence of microtubules does not seem to be crucial for the maintenance of CESA velocities, which makes it hard to believe, that motor-proteins are involved in CESA tracking.

Another hypothesis for the reduced CESA velocities in the pom2/csi1 mutant background was put forward by Li *et al.* (2012). They speculate that the reduced motility of CESAs in absence of POM2/CSI1 may be due to the loss of CESA orientation. In their opinion, CESAs which move off the microtubule tracks are more prone to bump into one another and therefore have a reduced motility. This scenario seems unlikely to me, since one in that case would expect an uneven distribution of velocities, with a fraction of CESAs moving with "normal" speed and another fraction moving with strongly reduced speed due to recent collision events. However, CESA velocities in the pom2/csi1 background were evenly distributed around 150-200 nm/min. Moreover, the number of expected collision events should depend on CESA diameter $\times$ CESA number per cell surface unit. Typically, only up to 10 % of the total cell surface is covered with CESAs in rapidly elongating hypocotyl cells (as estimated from FRAP analysis conducted for publication 3), which I doubt would be enough to observe a substantial velocity reduction due to frequent collision events.

Therefore, I hypothesize that POM2/CSI1 has a more direct effect on CESA activity, potentially by altering the CESA active site, or facilitating contact to further enhancers of CESA activity, such as SUS.

3.4.3 *pom2/csi1* mutants have twisted organs

Besides the discussed cellulose-deficiency phenotypes, *pom2/csi1* mutants displayed left-handed twisting in hypocotyls and roots (Bringmann *et al.*, 2012). Organ twisting is a known phenotype for microtubule defects (Kirik *et al.*, 2007; Ishida *et al.*, 2007; Buschmann *et al.*, 2009). Most twisting mutants comprise mutations in the tubulins. Especially mutations in the interaction region of α- and β-tubulin lead to a disturbed microtubule array and, in turn, organ twisting (Ishida *et al.*, 2007).

The reason for the apparent organ twist in *pom2/csi1* therefore seemed to be

the disturbed microtubule array. It is, however, important to note that many cellulose deficient mutans hold disorganized microtubule arrays (Paredez *et al.*, 2006; Sanchez-Rodriguez *et al.*, 2012). Yet, it is unclear why this defect led to a twisting organ and cell phenotype in *pom2/csi1* and not in other cellulose deficient mutants, such as the *CESA6* mutant *prc*.

In contrast to isotropic growth, twisted organs still hold a distinct (helical) growth orientation. In other words, the twisted cells maintain a certain anisotropic organization. We know that the orientation of cellulose fibers is the key mechanism for directed cell expansion (see introduction). Consequently, there must be a certain self-organization of CESAs when the microtubule array (or the connection to it) is absent. We have shown, that CESA trajectories are less linear but not entirely random in the pom2/csi1 mutant and in wild-type plants after microtubule depolymerization (Bringmann *et al.*, 2012). The CESAs still maintain a certain pattern, apparently leading to the observed helical growth.

The disorder of the microtubule array appears to me like a secondary effect. The reduction of CESA activity (and orientation) might lead to a feedback on the microtubule array. Possibly there are sensor proteins that measure the integrity of the cell wall. Disoriented cellulose might lead to shearing forces that might be sensed, which in turn triggers mechanisms that induce re-orientation of the microtubule array. However, such regulatory mechanisms might run out of control, if the connection between microtubules and CESAs is broken.

In addition, we could show that mutations in the POM2/CSI1 did not affect microtubule dynamics (Bringmann *et al.*, 2012). These data suggest that maybe some pleiotropic effects, e.g. changes in hormone levels, may cause the changes in the microtubule organization. Still, it is possible that POM2/CSI1 contributes to the microtubule organizing machinery by interacting with microtubule organizing proteins.

3.5 Contribution of this thesis to society and global development

This thesis was done during which shrinking resources, and CO_2 induced global warming, demand new ways of thinking in global energy policy. Carbon-neutral energy sources, such as polysaccharide-derived bio-ethanol have the potential to overcome dependency on fossil-based combustibles and thus to protect the global climate. However, starch-derived bio-ethanol production ultimately leads to competition for land used for food or feed crops. It is therefore desirable to make use of the cellulosic parts of crop plants and use biomass plants that do not compete with food crops, do not cause land-clearing and that offer advantages

in reducing greenhouse-gas emissions (Tilman *et al.*, 2009). The potential for so called second genereation biofuels from plants like *Miscanthus x giganteus*, *Agave* or Napier Grass *(Pennisetum purpureum)* has been discussed by Somerville *et al.* (2010).

Cellulose is the most abundant biopolymer in the world. It can be hydrolyzed to glucose which can be further fermented to ethanol. However, this process is still too costly to be economically attractive. Much research currently focuses on the improvement of cost efficiency of cellulose degradation to fermentable sugars from corn-stover and other ligno-cellulosic plant material (McMillan *et al.*, 2011; Soudham *et al.*, 2011; Lee *et al.*, 2011). At the same time the knowledge about the mechanisms underpinning cellulose production is still very limited. The research presented in this thesis gives new insights into the control of cellulose synthesis in the model plant *Arabidopsis thaliana*. Hopefully, this might in future lead to a better understanding of cellulose production and approaches for cellulose improvement.

3.6 Conclusion and future research

The work carried out for this thesis involved an interdisciplinary approach. The development of new bioinformatic tools provided the basis to find candidate genes that could connect CESAs and the cytoskeleton. Classic forward genetic screens and map-based cloning further contributed to the search by the identification of POM2 as being allelic to CSI1. The major piece of work, however, employed cell and molecular biology.

It will be intriguing to see what contribution the new knowledge acquired through this thesis can bring to further these models. Importantly, for the first time we observed an uncoupling between CESA and the microtubules in rapidly expanding cells. Building on this, many new questions can begin to be addressed: Do mechanical forces act primarily on the microtubules as suggested by Hamant *et al.* (2008) which in turn control CESA orientation? Or is the stress mediated more via the "outside to the inside", e.g. is stress emanating from neighboring cells relayed via the cellulose that lead to microtubule re-orientation? In the future, collaborations with biophysicists, bioinformaticians and mathematicians will elaborate on this and many more questions.

To support this kind of interdisciplinary approach, it is desirable to extend microscopy-based analysis to a systemic level. Cutting edge selective plane illumination microscopy (SPIM) has shown this potential in animal developmental biology (Weber and Huisken, 2011). Right now our analysis is limited to epidermal hypocotyl cells at distinct developmental stages. Technical progress will

hopefully enable us to investigate complete developmental programs in whole plants. First attempts to extend the biological material are already being carried out, for example in pavement leaf cells (Sampathkumar, Ivakov, Persson, personal communication).

While the research directions proposed above are provided with thicker brush strokes, there are of course also explicit experiments that can directly follow up the presented data.

Firstly, it will be necessary to identify further interaction partners for POM2/CSI1, if they exist. For this, we started pull-down experiments using anti-CFP antibodies and yeast-two-hybrid screens using different regions of the POM2 protein as bait. Potential interaction partners are currently cloned and fused to fluorescent markers in order to co-localize them with POM2:CFP.

pom2 mutants display a microtubule and a cellulose defect. However, there is still the question about cause and effect. In other words, is the influence of POM2/CSI1 on microtubule orientation direct or indirect? It will be difficult to disentangle this question, but this question may bring valuable information to get new insights into regulation of the CESA- microtubule interplay. The new interactors of POM2/CSI1 might provide insight into this question. The microtubule-induced twisting effect is not only seen for hypocotyls and roots, but also for stems in adult plants. This is due to post-meristematic alteration of phyllotaxis (Landrein, Hamant, personal communication). Currently, in depth phyllotactic analysis of *pom2/csi1* and other mutants is ongoing. Thus, the influence of POM2/CSI1 mediated CESA guidance is investigated also on a broader developmental level.

A third set of experiments relates to self organization of CSCs when the connection to the microtubules is missing. We showed that CESA trajectories were prone to deviate from linear trajectories in the absence of POM2/CSI1. However, CESAs do not track absolutely randomly after oryzalin treatments Paredez *et al.* (2006). Also, there are cell types where the close interaction between CSCs and microtubules is abolished (Emons *et al.*, 2007). Still, these cells have a parallel array of cellulose microtfibrils. Obviously, the CSC-microtubule interaction mediated by POM2/CSI1 can be abolished. But how do the CSCs find orientation without structural support from the microtubules? This question seems a rather complex task and involves analysis of CESA containing membrane domains and the identification of microfibril supporting structures in the apoplast as suggested by Baskin (2001).

The fourth set of experiments should tackle the question: How is the POM2/CSI1 binding to CESAs and microtubules regulated? As mentioned earlier, we have started phosphoproteomic analysis on immuno- purified

POM2:CFP protein. Preliminary results indicate, that there are phosphorylated peptides within the POM2/CSI1 protein. This goes well along with preliminary data from yeast two hybrid screens, which suggest interactions to kinases and phosphatases (data not shown). If we successfully detect underlying mechanisms of POM2/CSI1 regulation (potentially through phosphorylation or other post-translational modifications), we may be able to link these to CESA behaviour.

In summary, the results presented in this thesis unravelled the microtubule guiding mechanism for CESAs that has long been sought for. In addition, we now know that tracking CESAs in the plasma membrane are linked to the microtubules by POM2/CSI1, which, however, has no influence on the microtubule-dependent delivery of CESAs.

Acknowledgements

There are a lot of people who supported me during my PhD and made this time one of the greatest in my life. No matter if I needed help during the obligatory hard times, or if I wanted to share my excitement and happiness when things finally worked out. I was always surrounded by excellent people.

A major impact on the success of my work was achieved by Staffan Persson, my direct supervisor. Together, we developed project ideas, discussed results and wrote up our papers. He helped me to become an autonomous scientist with own ideas and concepts, which should be the goal of every PhD student. And I will never forget our night- outs and DJ- collaborations, that made us become friends after all.

I thank my dear colleagues that were very patient with my constant questions about my latest findings and my (partly) bad jokes. Especially I would like to mention Lutz, Anne, Clara, Dani, Colin, Anja, Norma and of course the dudes Arun and Marek. Especially conferences and lab retreats were a real blast with these people.

Special thanks have to go to Anett Döring. She became one of my dearest friends during my PhD and gave me a lot of strength.

Armin Schlereth, my first scientific mentor who supervised my diploma thesis was there, whenever I needed him. I am happy to have somebody who helps me whenever I get stuck in science, and I will appreciate his advice also in future.

I thank my family for everything. My parents who supported me morally and financially, who gave me a home whenever I needed it and my brother Andi as well as all my friends.

Finally, I thank all the collaborators that contributed to this work, most importantly Prof. Marie- Theres Hauser and Eryang Li from Vienna as well as Ina

Talke, IMPRS and POGS for support and funding.

List of Figures

1 Composition of primary cell walls 4
2 The CSC is a hexameric rosette- shaped enzyme complex 5
3 CESA trafficking to the plasma membrane 8
4 Microtubule structure and dynamics 12
5 CESAs and microtubules align at the cell cortex 17
6 C2 and armadillo domains form the POM2/CSI1 protein 74
7 POM2/CSI1 facilitates dynamic interaction between CESAs and Microtubules 79

Abbreviations

ADP	Adenosine diphosphate
ARK	ARMADILLO REPEAT KINESIN
ATP	Adenosine triphosphate
BLAST	Basic local alignment search tool
CESA	Cellulose Synthase
CEV	CONSTITUTIVE EXPRESSION OF VSP
CFP	Cyan fluorescent protein
CINV	CYTOSOLIC INVERTASE
CLASP	CLIP ASSOCIATED PROTEIN
COB	COBRA
CSC	Cellulose Synthase Complex
CSI	CELLULOSE SYNTHASE INTERACTING
CTL	CHITINASE-LIKE
EB	END BINDING
EC	Enzyme Commission (number of enzymes)
ELD	ELONGATION DEFECTIVE
ELI	ECTOPIC LIGNIFICATION
EMS	Ethyl methane sulfonate
ER	Endoplasmic Reticulum
FRAP	Fluorescence recovery after photo-bleaching
GAX	Glucoronoarabinoxylan
GDP	Guanosine diphosphate
GFP	Green fluorescent protein
GPI	Glycophosphatidylinositol
GT	Glycolsyl transferase
GTP	Guanosine triphosphate
HG	Homogalacturonan
KOB	KOBITO
KOR	KORRIGAN
LIS	LISSENCEPHALY
MAP	Microtubule associated protein
MOR	MICROTUBULE ORGANIZATION
NEK	NEVER IN MITOSIS A RELATED KINASE
NIMA	NEVER IN MITOSIS A
pfam	protein family
POM	POM-POM
PRC	PROCUSTE
RFP	Red fluorescent protein

RG Rhamnogalacturonan
RSW RADIALLY SWOLLEN
SPR SPIRAL
SUS sucrose synthase
TGN Trans Golgi Network
TIP Plus end trackers
UDP uridine diphosphate
UGP UDP-glucosepyrophosphate
XG Xyloglucan
YFP Yellow fluorescent protein

References

Ambrose C., Allard J.F., Cytrynbaum E.N. and Wasteneys G.O. A CLASP-modulated cell edge barrier mechanism drives cell-wide cortical microtubule organization in Arabidopsis. *Nat Commun*, 2:430, 2011.

Amor Y., Haigler C.H., Johnson S., Wainscott M. and Delmer D.P. A membrane-associated form of sucrose synthase and its potential role in synthesis of cellulose and callose in plants. *Proc. Natl. Acad. Sci. U.S.A.*, 92:9353–9357, 1995.

Arioli T., Peng L., Betzner A.S., Burn J., Wittke W., Herth W., Camilleri C., Hofte H., Plazinski J., Birch R., Cork A., Glover J., Redmond J. and Williamson R.E. Molecular analysis of cellulose biosynthesis in Arabidopsis. *Science*, 279:717–720, 1998.

Baroja-Fernandez E., Munoz F.J., Li J., Bahaji A., Almagro G., Montero M., Etxeberria E., Hidalgo M., Sesma M.T. and Pozueta-Romero J. Sucrose synthase activity in the sus1/sus2/sus3/sus4 Arabidopsis mutant is sufficient to support normal cellulose and starch production. *Proc. Natl. Acad. Sci. U.S.A.*, 109:321–326, 2012.

Barratt D.H., Derbyshire P., Findlay K., Pike M., Wellner N., Lunn J., Feil R., Simpson C., Maule A.J. and Smith A.M. Normal growth of Arabidopsis requires cytosolic invertase but not sucrose synthase. *Proc. Natl. Acad. Sci. U.S.A.*, 106:13124–13129, 2009.

Bartolini F. and Gundersen G.G. Generation of noncentrosomal microtubule arrays. *J. Cell. Sci.*, 119:4155–4163, 2006.

Baskin T.I. On the alignment of cellulose microfibrils by cortical microtubules: a review and a model. *Protoplasma*, 215:150–171, 2001.

Beeckman T., Przemeck G.K., Stamatiou G., Lau R., Terryn N., De Rycke R., Inze D. and Berleth T. Genetic complexity of cellulose synthase a gene function in Arabidopsis embryogenesis. *Plant Physiol.*, 130:1883–1893, 2002.

Bischoff V., Desprez T., Mouille G., Vernhettes S., Gonneau M. and Hofte H. Phytochrome regulation of cellulose synthesis in Arabidopsis. *Curr. Biol.*, 21:1822–1827, 2011.

Blanchoin L., Boujemaa-Paterski R., Henty J.L., Khurana P. and Staiger C.J. Actin dynamics in plant cells: a team effort from multiple proteins orchestrates this very fast-paced game. *Curr. Opin. Plant Biol.*, 13:714–723, 2010.

Bringmann M., Li E., Sampathkumar A., Kocabek T., Hauser M.T. and Persson S. POM-POM2/CELLULOSE SYNTHASE INTERACTING1 Is Essential for the Functional Association of Cellulose Synthase and Microtubules in Arabidopsis. *Plant Cell*, 2012.

Brown D.M., Zeef L.A., Ellis J., Goodacre R. and Turner S.R. Identification of novel genes in Arabidopsis involved in secondary cell wall formation using expression profiling and reverse genetics. *Plant Cell*, 17:2281–2295, 2005.

Buschmann H., Hauptmann M., Niessing D., Lloyd C.W. and Schaffner A.R. Helical growth of the Arabidopsis mutant tortifolia2 does not depend on cell division patterns but involves handed twisting of isolated cells. *Plant Cell*, 21:2090–2106, 2009.

Cai G. and Cresti M. Microtubule motors and pollen tube growth–still an open question. *Protoplasma*, 247:131–143, 2010.

Caplow M. and Fee L. Concerning the chemical nature of tubulin subunits that cap and stabilize microtubules. *Biochemistry*, 42:2122–2126, 2003.

Carpita N. and McCann M. The Plant Cell Wall. *Biochemistry and molecular biology of plants*, pages 52–109, 2000. (Buchanan, B. and Gruissem, W. and Jones, R. eds) American Society of Plant Biologists, Rockville MD.

Chen S., Ehrhardt D.W. and Somerville C.R. Mutations of cellulose synthase (CESA1) phosphorylation sites modulate anisotropic cell expansion and bidirectional mobility of cellulose synthase. *Proc. Natl. Acad. Sci. U.S.A.*, 107:17188–17193, 2010.

Cifuentes C., Bulone V. and Emons A.M. Biosynthesis of callose and cellulose by detergent extracts of tobacco cell membranes and quantification of the polymers synthesized in vitro. *J Integr Plant Biol*, 52:221–233, 2010.

Coates J.C. Armadillo repeat proteins: beyond the animal kingdom. *Trends Cell Biol.*, 13:463–471, 2003.

Coates J.C., Laplaze L. and Haseloff J. Armadillo-related proteins promote lateral root development in Arabidopsis. *Proc. Natl. Acad. Sci. U.S.A.*, 103:1621–1626, 2006.

Coleman H.D., Yan J. and Mansfield S.D. Sucrose synthase affects carbon partitioning to increase cellulose production and altered cell wall ultrastructure. *Proc. Natl. Acad. Sci. U.S.A.*, 106:13118–13123, 2009.

Conde C. and Caceres A. Microtubule assembly, organization and dynamics in axons and dendrites. *Nat. Rev. Neurosci.*, 10:319–332, 2009.

Cosgrove D.J. Growth of the plant cell wall. *Nat. Rev. Mol. Cell Biol.*, 6:850–861, 2005.

Crowell E.F., Bischoff V., Desprez T., Rolland A., Stierhof Y.D., Schumacher K., Gonneau M., Hofte H. and Vernhettes S. Pausing of Golgi bodies on microtubules regulates secretion of cellulose synthase complexes in Arabidopsis. *Plant Cell*, 21:1141–1154, 2009.

Crowell E.F., Gonneau M., Stierhof Y.D., Hofte H. and Vernhettes S. Regulated trafficking of cellulose synthases. *Curr. Opin. Plant Biol.*, 13:700–705, 2010.

Cyr R. and Palevitz B. Microtubule- binding proteins from carrot I. Initial characterization and microtubule bundling. *Planta*, 95(3):245–260, 1989.

Desprez T., Juraniec M., Crowell E.F., Jouy H., Pochylova Z., Parcy F., Hofte H., Gonneau M. and Vernhettes S. Organization of cellulose synthase complexes involved in primary cell wall synthesis in Arabidopsis thaliana. *Proc. Natl. Acad. Sci. U.S.A.*, 104:15572–15577, 2007.

Doblin M.S., Kurek I., Jacob-Wilk D. and Delmer D.P. Cellulose biosynthesis in plants: from genes to rosettes. *Plant Cell Physiol.*, 43:1407–1420, 2002.

Ehrhardt D.W. Straighten up and fly right: microtubule dynamics and organization of non-centrosomal arrays in higher plants. *Curr. Opin. Cell Biol.*, 20:107–116, 2008.

Emons A.M., Hofte H. and Mulder B.M. Microtubules and cellulose microfibrils: how intimate is their relationship? *Trends Plant Sci.*, 12:279–281, 2007.

Endler A. and Persson S. Cellulose synthases and synthesis in Arabidopsis. *Mol Plant*, 4:199–211, 2011.

Fache V., Gaillard J., Van Damme D., Geelen D., Neumann E., Stoppin-Mellet V. and Vantard M. Arabidopsis kinetochore fiber-associated MAP65-4 cross-links microtubules and promotes microtubule bundle elongation. *Plant Cell*, 22:3804–3815, 2010.

Fagard M., Desnos T., Desprez T., Goubet F., Refregier G., Mouille G., McCann M., Rayon C., Vernhettes S. and Hofte H. PROCUSTE1 encodes a cellulose synthase required for normal cell elongation specifically in roots and dark-grown hypocotyls of Arabidopsis. *Plant Cell*, 12:2409–2424, 2000.

Fernandes A.N., Thomas L.H., Altaner C.M., Callow P., Forsyth V.T., Apperley D.C., Kennedy C.J. and Jarvis M.C. Nanostructure of cellulose microfibrils in spruce wood. *Proc. Natl. Acad. Sci. U.S.A.*, 108:E1195–1203, 2011.

Fiserova J. and Goldberg M.W. Relationships at the nuclear envelope: lamins and nuclear pore complexes in animals and plants. *Biochem. Soc. Trans.*, 38:829–831, 2010.

Fujii S., Hayashi T. and Mizuno K. Sucrose synthase is an integral component of the cellulose synthesis machinery. *Plant Cell Physiol.*, 51:294–301, 2010.

Gardiner J. and Marc J. Arabidopsis thaliana, a plant model organism for the neuronal microtubule cytoskeleton? *J. Exp. Bot.*, 62:89–97, 2011.

Geisler D.A., Sampathkumar A., Mutwil M. and Persson S. Laying down the bricks: logistic aspects of cell wall biosynthesis. *Curr. Opin. Plant Biol.*, 11:647–652, 2008.

Gillmor C.S., Poindexter P., Lorieau J., Palcic M.M. and Somerville C. Alpha-glucosidase I is required for cellulose biosynthesis and morphogenesis in Arabidopsis. *J. Cell Biol.*, 156:1003–1013, 2002.

Goda H., Sasaki E., Akiyama K., Maruyama-Nakashita A., Nakabayashi K., Li W., Ogawa M., Yamauchi Y., Preston J., Aoki K., Kiba T., Takatsuto S., Fujioka S., Asami T., Nakano T., Kato H., Mizuno T., Sakakibara H., Yamaguchi S., Nambara E., Kamiya Y., Takahashi H., Hirai M.Y., Sakurai T., Shinozaki K., Saito K., Yoshida S. and Shimada Y. The AtGenExpress hormone and chemical treatment data set: experimental design, data evaluation, model data analysis and data access. *Plant J.*, 55:526–542, 2008.

Green P.B. Mechanism for Plant Cellular Morphogenesis. *Science*, 138:1404–1405, 1962.

Gu Y., Kaplinsky N., Bringmann M., Cobb A., Carroll A., Sampathkumar A., Baskin T.I., Persson S. and Somerville C.R. Identification of a cellulose synthase-associated protein required for cellulose biosynthesis. *Proc. Natl. Acad. Sci. U.S.A.*, 107:12866–12871, 2010.

Gutierrez R., Lindeboom J.J., Paredez A.R., Emons A.M. and Ehrhardt D.W. Arabidopsis cortical microtubules position cellulose synthase delivery to the plasma membrane and interact with cellulose synthase trafficking compartments. *Nat. Cell Biol.*, 11:797–806, 2009.

Hamada T. Microtubule-associated proteins in higher plants. *J. Plant Res.*, 120:79–98, 2007.

Hamant O., Heisler M.G., Jonsson H., Krupinski P., Uyttewaal M., Bokov P., Corson F., Sahlin P., Boudaoud A., Meyerowitz E.M., Couder Y. and Traas J. Developmental patterning by mechanical signals in Arabidopsis. *Science*, 322:1650–1655, 2008.

Hauser M.T., Morikami A. and Benfey P.N. Conditional root expansion mutants of Arabidopsis. *Development*, 121:1237–1252, 1995.

Hayashi T. Xyloglucans in the Primary- Cell Wall. *Annual review of plant physiology*, 40:139–168, 1989.

Heath I.B. A unified hypothesis for the role of membrane bound enzyme complexes and microtubules in plant cell wall synthesis. *J. Theor. Biol.*, 48:445–449, 1974.

Ho C.M., Hotta T., Guo F., Roberson R.W., Lee Y.R. and Liu B. Interaction of antiparallel microtubules in the phragmoplast is mediated by the microtubule-associated protein MAP65-3 in Arabidopsis. *Plant Cell*, 23:2909–2923, 2011.

Huber A.H., Nelson W.J. and Weis W.I. Three-dimensional structure of the armadillo repeat region of beta-catenin. *Cell*, 90:871–882, 1997.

Huxley H.E. The mechanism of muscular contraction. *Science*, 164:1356–1365, 1969.

Ishida T., Kaneko Y., Iwano M. and Hashimoto T. Helical microtubule arrays in a collection of twisting tubulin mutants of Arabidopsis thaliana. *Proc. Natl. Acad. Sci. U.S.A.*, 104:8544–8549, 2007.

Joshi C.P. and Mansfield S.D. The cellulose paradox–simple molecule, complex biosynthesis. *Curr. Opin. Plant Biol.*, 10:220–226, 2007.

Kawamura E. and Wasteneys G.O. MOR1, the Arabidopsis thaliana homologue of Xenopus MAP215, promotes rapid growth and shrinkage, and suppresses the pausing of microtubules in vivo. *J. Cell. Sci.*, 121:4114–4123, 2008.

Kilian J., Whitehead D., Horak J., Wanke D., Weinl S., Batistic O., D'Angelo C., Bornberg-Bauer E., Kudla J. and Harter K. The AtGenExpress global stress expression data set: protocols, evaluation and model data analysis of UV-B light, drought and cold stress responses. *Plant J.*, 50:347–363, 2007.

Kimura S., Laosinchai W., Itoh T., Cui X., Linder C.R. and Brown R.M. Immunogold labeling of rosette terminal cellulose-synthesizing complexes in the vascular plant vigna angularis. *Plant Cell*, 11:2075–2086, 1999.

Kirik V., Herrmann U., Parupalli C., Sedbrook J.C., Ehrhardt D.W. and Hlskamp M. CLASP localizes in two discrete patterns on cortical microtubules and is required for cell morphogenesis and cell division in Arabidopsis. *J. Cell. Sci.*, 120:4416–4425, 2007.

Komis G., Illes P., Beck M. and ?amaj J. Microtubules and mitogen-activated protein kinase signalling. *Curr. Opin. Plant Biol.*, 14:650–657, 2011.

Lane D.R., Wiedemeier A., Peng L., Hofte H., Vernhettes S., Desprez T., Hocart C.H., Birch R.J., Baskin T.I., Burn J.E., Arioli T., Betzner A.S. and Williamson R.E. Temperature-sensitive alleles of RSW2 link the KORRIGAN endo-1,4-beta-glucanase to cellulose synthesis and cytokinesis in Arabidopsis. *Plant Physiol.*, 126:278–288, 2001.

Ledbetter M.C. and Porter K.R. A "MICROTUBULE" IN PLANT CELL FINE STRUCTURE. *J. Cell Biol.*, 19:239–250, 1963.

Lee H.L., Chang C.K., Teng K.H. and Liang P.H. Construction and characterization of different fusion proteins between cellulases and -glucosidase to improve glucose production and thermostability. *Bioresour. Technol.*, 102:3973–3976, 2011.

Lee P.R., Cohen J.E., Tendi E.A., Farrer R., DE Vries G.H., Becker K.G. and Fields R.D. Transcriptional profiling in an MPNST-derived cell line and normal human Schwann cells. *Neuron Glia Biol.*, 1:135–147, 2004.

Li J., Xu Y. and Chong K. The novel functions of kinesin motor proteins in plants. *Protoplasma*, 2011.

Li S., Lei L., Somerville C.R. and Gu Y. Cellulose synthase interactive protein 1 (CSI1) links microtubules and cellulose synthase complexes. *Proc. Natl. Acad. Sci. U.S.A.*, 109:185–190, 2012.

Lloyd C. Plant science. Microtubules make tracks for cellulose. *Science*, 312:1482–1483, 2006.

Lloyd C. and Hussey P. Microtubule-associated proteins in plants–why we need a MAP. *Nat. Rev. Mol. Cell Biol.*, 2:40–47, 2001.

Lucas J.R., Courtney S., Hassfurder M., Dhingra S., Bryant A. and Shaw S.L. Microtubule-associated proteins MAP65-1 and MAP65-2 positively regulate axial cell growth in etiolated Arabidopsis hypocotyls. *Plant Cell*, 23:1889–1903, 2011.

Lukowitz W., Nickle T.C., Meinke D.W., Last R.L., Conklin P.L. and Somerville C.R. Arabidopsis cyt1 mutants are deficient in a mannose-1-phosphate guanylyltransferase and point to a requirement of N-linked glycosylation for cellulose biosynthesis. *Proc. Natl. Acad. Sci. U.S.A.*, 98:2262–2267, 2001.

Martens S. and McMahon H.T. Mechanisms of membrane fusion: disparate players and common principles. *Nat. Rev. Mol. Cell Biol.*, 9:543–556, 2008.

Matar D. and Catesson A. Cell plate development and delayed formation of the pectic middle lamella in root- meristems. *Protoplasma*, 146(1):10–17, 1988.

Matsui A., Ishida J., Morosawa T., Okamoto M., Kim J.M., Kurihara Y., Kawashima M., Tanaka M., To T.K., Nakaminami K., Kaminuma E., Endo T.A., Mochizuki Y., Kawaguchi S., Kobayashi N., Shinozaki K., Toyoda T. and Seki M. Arabidopsis tiling array analysis to identify the stress-responsive genes. *Methods Mol. Biol.*, 639:141–155, 2010.

Matthews J.F., Bergenstrahle M., Beckham G.T., Himmel M.E., Nimlos M.R., Brady J.W. and Crowley M.F. High-temperature behavior of cellulose I. *J Phys Chem B*, 115:2155–2166, 2011.

McMillan J.D., Jennings E.W., Mohagheghi A. and Zuccarello M. Comparative performance of precommercial cellulases hydrolyzing pretreated corn stover. *Biotechnol Biofuels*, 4:29, 2011.

McNally F.J. and Vale R.D. Identification of katanin, an ATPase that severs and disassembles stable microtubules. *Cell*, 75:419–429, 1993.

Meagher R. and Williamson R. volume 27 of *Cold Spring Harbor Monograph Series*. Cold Spring Harbor Laboratory, Cold Spring Harbor, N.Y., 1994. ISBN 978-0-87969-428-9.

Mitchison T. and Kirschner M. Dynamic instability of microtubule growth. *Nature*, 312:237–242, 1984.

Mohnen D. Pectin structure and biosynthesis. *Curr. Opin. Plant Biol.*, 11:266–277, 2008.

Mueller S.C. and Brown R.M. Evidence for an intramembrane component associated with a cellulose microfibril-synthesizing complex in higher plants. *J. Cell Biol.*, 84:315–326, 1980.

Mulder B.M. and Emons A.M. A dynamical model for plant cell wall architecture formation. *J Math Biol*, 42:261–289, 2001.

Mutwil M., Debolt S. and Persson S. Cellulose synthesis: a complex complex. *Curr. Opin. Plant Biol.*, 11:252–257, 2008a.

Mutwil M., Klie S., Tohge T., Giorgi F.M., Wilkins O., Campbell M.M., Fernie A.R., Usadel B., Nikoloski Z. and Persson S. PlaNet: combined sequence and expression comparisons across plant networks derived from seven species. *Plant Cell*, 23:895–910, 2011.

Mutwil M., Obro J., Willats W.G. and Persson S. GeneCAT–novel webtools that combine BLAST and co-expression analyses. *Nucleic Acids Res.*, 36:W320–326, 2008b.

Mutwil M., Ruprecht C., Giorgi F.M., Bringmann M., Usadel B. and Persson S. Transcriptional wiring of cell wall-related genes in Arabidopsis. *Mol Plant*, 2:1015–1024, 2009.

Mutwil M., Usadel B., Schutte M., Loraine A., Ebenhoh O. and Persson S. Assembly of an interactive correlation network for the Arabidopsis genome using a novel heuristic clustering algorithm. *Plant Physiol.*, 152:29–43, 2010.

Nakamura M., Ehrhardt D.W. and Hashimoto T. Microtubule and katanin-dependent dynamics of microtubule nucleation complexes in the acentrosomal Arabidopsis cortical array. *Nat. Cell Biol.*, 12:1064–1070, 2010.

Nicol F., His I., Jauneau A., Vernhettes S., Canut H. and Hofte H. A plasma membrane-bound putative endo-1,4-beta-D-glucanase is required for normal wall assembly and cell elongation in Arabidopsis. *EMBO J.*, 17:5563–5576, 1998.

Nusslein-Volhard C. and Wieschaus E. Mutations affecting segment number and polarity in Drosophila. *Nature*, 287:795–801, 1980.

Ochoa W.F., Garcia-Garcia J., Fita I., Corbalan-Garcia S., Verdaguer N. and Gomez-Fernandez J.C. Structure of the C2 domain from novel protein kinase Cepsilon. A membrane binding model for Ca(2+)-independent C2 domains. *J. Mol. Biol.*, 311:837–849, 2001.

Pagant S., Bichet A., Sugimoto K., Lerouxel O., Desprez T., McCann M., Lerouge P., Vernhettes S. and Hofte H. KOBITO1 encodes a novel plasma membrane protein necessary for normal synthesis of cellulose during cell expansion in Arabidopsis. *Plant Cell*, 14:2001–2013, 2002.

Paredez A.R., Somerville C.R. and Ehrhardt D.W. Visualization of cellulose synthase demonstrates functional association with microtubules. *Science*, 312:1491–1495, 2006.

Pear J.R., Kawagoe Y., Schreckengost W.E., Delmer D.P. and Stalker D.M. Higher plants contain homologs of the bacterial celA genes encoding the catalytic subunit of cellulose synthase. *Proc. Natl. Acad. Sci. U.S.A.*, 93:12637–12642, 1996.

Persson S., Paredez A., Carroll A., Palsdottir H., Doblin M., Poindexter P., Khitrov N., Auer M. and Somerville C.R. Genetic evidence for three unique components in primary cell-wall cellulose synthase complexes in Arabidopsis. *Proc. Natl. Acad. Sci. U.S.A.*, 104:15566–15571, 2007.

Persson S., Wei H., Milne J., Page G.P. and Somerville C.R. Identification of genes required for cellulose synthesis by regression analysis of public microarray data sets. *Proc. Natl. Acad. Sci. U.S.A.*, 102:8633–8638, 2005.

Pesquet E., Korolev A.V., Calder G. and Lloyd C.W. The microtubule-associated protein AtMAP70-5 regulates secondary wall patterning in Arabidopsis wood cells. *Curr. Biol.*, 20:744–749, 2010.

Pesquet E., Korolev A.V., Calder G. and Lloyd C.W. Mechanisms for shaping, orienting, positioning and patterning plant secondary cell walls. *Plant Signal Behav*, 6:843–849, 2011.

Pollard T.D., Blanchoin L. and Mullins R.D. Molecular mechanisms controlling actin filament dynamics in nonmuscle cells. *Annu Rev Biophys Biomol Struct*, 29:545–576, 2000.

Pollard T.D. and Cooper J.A. Actin and actin-binding proteins. A critical evaluation of mechanisms and functions. *Annu. Rev. Biochem.*, 55:987–1035, 1986.

Richmond T. Higher plant cellulose synthases. *Genome Biol.*, 1, 2000.

Romero S., Le Clainche C., Didry D., Egile C., Pantaloni D. and Carlier M.F. Formin is a processive motor that requires profilin to accelerate actin assembly and associated ATP hydrolysis. *Cell*, 119:419–429, 2004.

Roudier F., Fernandez A.G., Fujita M., Himmelspach R., Borner G.H., Schindelman G., Song S., Baskin T.I., Dupree P., Wasteneys G.O. and Benfey P.N. COBRA, an Arabidopsis extracellular glycosyl-phosphatidyl inositol-anchored protein, specifically controls highly anisotropic expansion through its involvement in cellulose microfibril orientation. *Plant Cell*, 17:1749–1763, 2005.

Sakai T., Honing H., Nishioka M., Uehara Y., Takahashi M., Fujisawa N., Saji K., Seki M., Shinozaki K., Jones M.A., Smirnoff N., Okada K. and Wasteneys G.O. Armadillo repeat-containing kinesins and a NIMA-related kinase are required for epidermal-cell morphogenesis in Arabidopsis. *Plant J.*, 53:157–171, 2008.

Salnikov V.V., Grimson M.J., Delmer D.P. and Haigler C.H. Sucrose synthase localizes to cellulose synthesis sites in tracheary elements. *Phytochemistry*, 57:823–833, 2001.

Sampathkumar A. *Dynamic interaction between actin filaments, microtubules and cellulose synthesis in* Arabidopsis. Ph.D. thesis, Mathematisch- Naturwissenschaftliche Fakultät I der Humboldt Universität zu Berlin., 2010.

Sampathkumar A., Lindeboom J.J., Debolt S., Gutierrez R., Ehrhardt D.W., Ketelaar T. and Persson S. Live cell imaging reveals structural associations between the actin and microtubule cytoskeleton in arabidopsis. *Plant Cell*, 23:2302–2313, 2011a.

Sampathkumar A., Neumetzler L. and Persson S. The plasma membrane and the cell wall. *The Plant Plasma Membrane*, pages 57–85, 2011b. (Murphy, A.S. and Peer, W. and Schulz, B. eds) Plant Cell Monographs.

Sanchez-Rodriguez C., Bauer S., Hematy K., Saxe F., Ibanez A.B., Vodermaier V., Konlechner C., Sampathkumar A., Ruggeberg M., Aichinger E., Neumetzler L., Burgert I., Somerville C., Hauser M.T. and Persson S. CHITINASE-LIKE1/POM-POM1 and Its Homolog CTL2 Are Glucan-Interacting Proteins Important for Cellulose Biosynthesis in Arabidopsis. *Plant Cell*, 2012.

Sasabe M., Boudolf V., De Veylder L., Inze D., Genschik P. and Machida Y. Phosphorylation of a mitotic kinesin-like protein and a MAPKKK by cyclin-dependent kinases (CDKs) is involved in the transition to cytokinesis in plants. *Proc. Natl. Acad. Sci. U.S.A.*, 108:17844–17849, 2011.

Scheller H.V. and Ulvskov P. Hemicelluloses. *Annu Rev Plant Biol*, 61:263–289, 2010.

Schindelman G., Morikami A., Jung J., Baskin T.I., Carpita N.C., Derbyshire P., McCann M.C. and Benfey P.N. COBRA encodes a putative GPI-anchored protein, which is polarly localized and necessary for oriented cell expansion in Arabidopsis. *Genes Dev.*, 15:1115–1127, 2001.

Schmid M., Davison T.S., Henz S.R., Pape U.J., Demar M., Vingron M., Scholkopf B., Weigel D. and Lohmann J.U. A gene expression map of Arabidopsis thaliana development. *Nat. Genet.*, 37:501–506, 2005.

Shaw S.L., Kamyar R. and Ehrhardt D.W. Sustained microtubule treadmilling in Arabidopsis cortical arrays. *Science*, 300:1715–1718, 2003.

Somerville C. Cellulose synthesis in higher plants. *Annu. Rev. Cell Dev. Biol.*, 22:53–78, 2006.

Somerville C., Bauer S., Brininstool G., Facette M., Hamann T., Milne J., Osborne E., Paredez A., Persson S., Raab T., Vorwerk S. and Youngs H. Toward a systems approach to understanding plant cell walls. *Science*, 306:2206–2211, 2004.

Somerville C., Youngs H., Taylor C., Davis S.C. and Long S.P. Feedstocks for lignocellulosic biofuels. *Science*, 329:790–792, 2010.

Soudham V.P., Alriksson B. and Jonsson L.J. Reducing agents improve enzymatic hydrolysis of cellulosic substrates in the presence of pretreatment liquid. *J. Biotechnol.*, 155:244–250, 2011.

Staiger C.J. and Blanchoin L. Actin dynamics: old friends with new stories. *Curr. Opin. Plant Biol.*, 9:554–562, 2006.

Taylor N.G., Laurie S. and Turner S.R. Multiple cellulose synthase catalytic subunits are required for cellulose synthesis in Arabidopsis. *Plant Cell*, 12:2529–2540, 2000.

Tewari R., Bailes E., Bunting K.A. and Coates J.C. Armadillo-repeat protein functions: questions for little creatures. *Trends Cell Biol.*, 20:470–481, 2010.

Tilman D., Socolow R., Foley J.A., Hill J., Larson E., Lynd L., Pacala S., Reilly J., Searchinger T., Somerville C. and Williams R. Energy. Beneficial biofuels–the food, energy, and environment trilemma. *Science*, 325:270–271, 2009.

Usadel B., Obayashi T., Mutwil M., Giorgi F.M., Bassel G.W., Tanimoto M., Chow A., Steinhauser D., Persson S. and Provart N.J. Co-expression tools for plant biology: opportunities for hypothesis generation and caveats. *Plant Cell Environ.*, 32:1633–1651, 2009.

Vallee R.B. On the use of heat stability as a criterion for the identification of microtubule associated proteins (MAPs). *Biochem. Biophys. Res. Commun.*, 133:128–133, 1985.

Vaughn K.C. and Harper J.D. Microtubule-organizing centers and nucleating sites in land plants. *Int. Rev. Cytol.*, 181:75–149, 1998.

Wade R.H. On and around microtubules: an overview. *Mol. Biotechnol.*, 43:177–191, 2009.

Wang J., Howles P.A., Cork A.H., Birch R.J. and Williamson R.E. Chimeric proteins suggest that the catalytic and/or C-terminal domains give CesA1 and CesA3 access to their specific sites in the cellulose synthase of primary walls. *Plant Physiol.*, 142:685–695, 2006.

Waterman-Storer C.M. and Salmon E.D. Microtubule dynamics: treadmilling comes around again. *Curr. Biol.*, 7:R369–372, 1997.

Weber M. and Huisken J. Light sheet microscopy for real-time developmental biology. *Curr. Opin. Genet. Dev.*, 21:566–572, 2011.

Whittington A.T., Vugrek O., Wei K.J., Hasenbein N.G., Sugimoto K., Rashbrooke M.C. and Wasteneys G.O. MOR1 is essential for organizing cortical microtubules in plants. *Nature*, 411:610–613, 2001.

Xu W. and Kimelman D. Mechanistic insights from structural studies of beta-catenin and its binding partners. *J. Cell. Sci.*, 120:3337–3344, 2007.

Yao J., Kwon S.E., Gaffaney J.D., Dunning F.M. and Chapman E.R. Uncoupling the roles of synaptotagmin I during endo- and exocytosis of synaptic vesicles. *Nat. Neurosci.*, 15:243–249, 2011.

Yu H., Luscombe N.M., Qian J. and Gerstein M. Genomic analysis of gene expression relationships in transcriptional regulatory networks. *Trends Genet.*, 19:422–427, 2003.

Zhong R., Kays S.J., Schroeder B.P. and Ye Z.H. Mutation of a chitinase-like gene causes ectopic deposition of lignin, aberrant cell shapes, and overproduction of ethylene. *Plant Cell*, 14:165–179, 2002.